Copyright Warning & Restrictions

The copyright law of the United States (Title 17, United States Code) governs the making of photocopies or other reproductions of copyrighted material.

Under certain conditions specified in the law, libraries and archives are authorized to furnish a photocopy or other reproduction. One of these specified conditions is that the photocopy or reproduction is not to be "used for any purpose other than private study, scholarship, or research." If a, user makes a request for, or later uses, a photocopy or reproduction for purposes in excess of "fair use" that user may be liable for copyright infringement,

This institution reserves the right to refuse to accept a copying order if, in its judgment, fulfillment of the order would involve violation of copyright law.

Please Note: The author retains the copyright while the New Jersey Institute of Technology reserves the right to distribute this thesis or dissertation

Printing note: If you do not wish to print this page, then select "Pages from: first page # to: last page #" on the print dialog screen

ABSTRACT

SEEPAGE MONITORING AND DIAGNOSIS OF DISTRESSES IN AN EARTH EMBANKMENT DAM USING PROBABILITY METHODS

by
Seyed Mohammad Reza Mousavian

Failure of embankment dams may result in catastrophic consequences. Considering seepage and internal erosion are accounted as one of the major causes of failure in earth embankment dams, it is essential to detect any concentrated seepage and sources of distress at early stages. A number of investigation and monitoring methods exist for the detection of seepage, with varying degrees of technological and implementation complexity. This research, focuses on the Electrical Resistivity Monitoring Method (ERM), and develops a condition assessment process that allows 1) the identification of potential seepage areas and progress through visual observation and flow measurement, and 2) the determination of the most likely paths where piping may have occurred.

In particular, two separate statistical studies are carried out to identify the existence of and quantify the probability of potential seepage sources in earth embankment dams. The testing and evaluation of the accuracy and reliability of the ERM method in seepage detection in earthen hydraulic structures is also undertaken as a result of the correlation of the field measurements of flow rates and ERM outputs. An earth dam suffering from seepage is studied and monitored visually and with the ERM to discover and locate the potential sources and paths of seepages, detected and observed at the downstream toe over time. A Bayesian network model is developed to evaluate the potential sources and related paths associated with the detected flows downstream. The model is completed by

developing an approach to estimate the rate of erosion and predict the potential failure time of the dam with empirical and theoretical methods.

SEEPAGE MONITORING AND DIAGNOSIS OF DISTRESSES IN AN EARTH EMBANKMENT DAM USING PROBABILITY METHODS

by
Seyed Mohammad Reza Mousavian

A Dissertation
Submitted to the Faculty of
New Jersey Institute of Technology
in Partial Fulfillment of the Requirements for the Degree of
Doctor of Philosophy in Civil Engineering

John A. Reif, JR. Department of Civil and Environmental Engineering

August 2017

APPROVAL PAGE

SEEPAGE MONITORING AND DIAGNOSIS OF DISTRESSES IN AN EARTH EMBANKMENT DAM USING PROBABILITY METHODS

Seyed Mohammad Reza Mousavian

Dr. Fadi A. Karaa, Dissertation Advisor — Date
Professor of Civil and Environmental Engineering, NJIT

Dr. Taha F. Marhaba, Committee Member — Date
Professor and Chair of Civil and Environmental Engineering, NJIT

Dr. Robert Dresnack, Committee Member — Date
Professor of Civil and Environmental Engineering, NJIT

Dr. Walter Konon, Committee Member — Date
Professor of Civil and Environmental Engineering, NJIT

Dr. Mathew P. Adams, Committee Member — Date
Professor of Civil and Environmental Engineering, NJIT

Dr. Frank Golon, Committee Member — Date
President, Davidson – Wayne Development, Newark, NJ

BIOGRAPHICAL SKETCH

Author: Seyed Mohammad Reza Mousavian

Degree: Doctor of Philosophy

Date: August 2017

Undergraduate and Graduate Education:

- Doctor of Philosophy in Civil Engineering
  New Jersey Institute of Technology, Newark, NJ, 2017

- Master of Science in Construction Management
  University of Birmingham, Birmingham, UK, 2009

- Bachelor of Science in Civil Engineering
  Isfahan University of Technology, Isfahan, Iran, 2007

Major: Civil Engineering

ACKNOWLEDGMENT

I wish to express my deepest gratitude to my advisor, Professor Fadi Karaa, for his guidance and encouragement throughout the course of this research and dissertation and Dr. Frank Golon for all his supports and assistance, without his help the progress of this research was not feasible. It was an honor to work with them on this dissertation. The author is also grateful to the members of his dissertation committee, Professor Taha Marhaba, Professor Robert Dresnack, Professor Walter Konon, and Professor Mathew Adams for their helpful evaluations and valuable suggestions.

The teacher assistantship received from the Department of Civil and Environmental Engineering is greatly appreciated during the first two years of my study and research.

Finally, I would like to deeply thank my parents, family and friends for their continuous support and understanding during all these years.

TABLE OF CONTENTS

Chapter		Page
1	PRELIMINARIES AND LITERATURE REVIEW	1
	1.1 Introduction	1
	1.2 Description of the Research	3
	1.2.1 Research Objectives	3
	1.2.2 Research Significance	4
	1.3 Literature Review	6
	1.3.1 Piping and Internal Erosion Process	6
	1.3.2 Seepage Monitoring	14
	1.3.3 Electrical Resistivity Tomography (ERT)	25
	1.3.4 Probability Methods and Bayesian Tool in Seepage Analysis	32
	1.3.5 Summary of Literature Review	45
2	STATISTICAL DATABASE	47
	2.1 Introduction	47
	2.2 Dam Seepage Zone Database	48
	2.3 Electrical Resistivity Database in Seepage Monitoring	49

TABLE OF CONTENTS
(Continued)

Chapter	Page
3 SITE INFORMATION AND DATA COLLECTION	54
3.1 Introduction	54
3.2 Site Information	54
3.3 Preliminary Assessment and Visual Inspection	54
3.3.1 Site History	54
3.3.2 Visual Inspection	56
3.3.2.1 Fall 2015	56
3.3.2.1 Spring 2016	58
3.3.2.1 Winter 2017	63
3.4 Flow Measurement	64
3.4.1 Weir #1	64
3.4.2 Weir #2	67
3.4.3 Summary of Flow Measurement	69
3.5 Electrical Resistivity Survey	69
3.5.1 Data Collection	69
3.5.2 Data Inversion	71

TABLE OF CONTENTS
(Continued)

Chapter	Page
3.5.3 Results and Discussion ….…….....	72
4 COMPITATIONAL MODEL …….…….....	76
4.1 Introduction …….....	76
4.2 Geotechnical Data …….....	77
4.3 2D Model …….....	79
4.4 3D Model …….....	81
4.5 Results and Discussion…….....	83
5 PROBABILITY ANALYSIS AND FAILURE RISK ……..	91
5.1 Introduction …….....	91
5.2 Probability Analysis of Potential Flow Paths ……	91
5.2.1 Bayesian Network Model for Detecting the Seepage Source ……..	92
5.2.2 Prior Distribution ……..	94
5.2.3 Posterior Probabilities ……...	95
5.2.4 Discussion …….....	101
5.3 Potential Failure Time and Rate of Erosion …….....	102
5.3.1 Theoretical Estimate of Failure Time …….....	103

TABLE OF CONTENTS
(Continued)

Chapter **Page**

5.3.2 Empirical Estimate of Rate of Erosion ……..... 106

5.3.3 Discussion ……..... 112

6 CONCLUSION ……..... 115

APPENDIX A STATISTICAL DATASET TO LOCATE POTENTIAL SOURCES OF SEEPAGE ……..... 118

APPENDIX B STATISTICAL DATASET TO EVALUATE ELECTRICAL RESISTIVITY METHOD IN SEEPAGE DETECTION ……. 130

APPENDIX C MATLAB SYNTAXES FOR ESTIMATING THE FAILURE TIME OF THE STUDIED DAM, DUE TO INTERNAL EROSIOIN ……... 133

REFERENCES ……..... 136

LIST OF TABLES

Table		Page
1.1	Hole Erosion Tests, Properties of Soils Samples, Critical Stress and Fell Erosion Index …….…..……	11
1.2	Summary of Different Seepage Monitoring Methods for Earth Dams …..	23
1.3	Variables Involved in Diagnosing Distressed Embankment Dams ……	43
1.4	Probability Table for The Variables Relevant to Embankment Seepage Erosion–Piping for the Studied Dam …….	45
2.1	Distribution of Seepage Source Location in Earth Dams ……..	49
2.2	Summary of Statistical Results of Applying ERT in Seepage Detection in Embankment Dams …….	51
3.1	Measured Outflow Discharge at Three Reservoir Level …….……...	69
4.1	Soil Distribution by Weight, Volumetric Water Content and Soil Conductivity Estimate ……..……..	78
4.2	Characteristic and Location of Each Soil Class in The Studied Dam for 3D Model ……..……...……...	82
4.3	Summary of Outflow Discharge Calculated with Software Model and Site Measurement For Outflow #1 And Outflow #2 ……..……	88
5.1	Calculated Model Discharge of Flow Path #1-1 for Various Flow Path Conductivity ……..…….	98
5.2	Summary of Likelihood of Each Flow Path for The Detected Outflows ...	99

LIST OF TABLES
(Continued)

Table		Page
5.3	Summary of the Posterior Probabilities of *Source_I* for Flow Path #1 and Flow Path #2 …..……	100
5.4	Estimated Discharge Values for Different Reservoir Level Over Three-Year Period ….……...……...…..	107
5.5	Discharge Mean Value And SD for Various Reservoir Level ……...…….	108
5.6	Discharge Normalized Values for Different Reservoir Levels Over Three- Year Period ……..	110
5.7	Average of Discharge Normalized Value Over Three-Year Period ……	111
A.1	List of the Studied Dams for the Statistical Analysis to Identify the Origin of Concentrated Seepage ……...……..	119
B.1	Summary of Statistical Analysis to Evaluate Accuracy of ERT Method in Seepage Detection ……..……	131

LIST OF FIGURES

Figure		Page
1.1	Generic breach flood hydrograph …….……...…….....	7
1.2	Breach size versus breach development time ……..……...……	9
1.3	Sketch of the piping erosion in a water retaining structure ……	12
1.4	Piping erosion in a water retaining structure, phases from initiation to breaching ...……..	12
1.5	Forces acting on a soil particle in seepage passage ……	13
1.6	Results of seepage monitoring using fiber optics over 1 year period …….	18
1.7	(a) Results of Seismic tomography imaging along a surveying line and (b) The final interpretational 3D isometric map showing seepage zones, for a studied dam in Nigeria.....	20
1.8	Illustration of an electrode array set up along the crest of a dam and the SP anomaly generated from downward seepage …….....	21
1.9	Detected anomaly zone (a) according to GPR results and (b) photo of the surveying line, for a dyke in northeast of Poland ...…….	23
1.10	Illustration of current and potential electrodes in soil resistivity monitoring ...……	26
1.11	Illustration of typical electrode arrays in soil ER monitoring ...…….	27
1.12	Schematic Wenner Electrode array configuration ...……...……	28

LIST OF FIGURES
(Continued)

Figure		Page
1.13	1D Electrical Resistivity data acquisition ……..…….	29
1.14	2D Electrical Resistivity data acquisition with multiple electrodes …..….	30
1.15	Pulled array system to acquire 2D Electrical Resistivity data …….…...	30
1.16	Geoelectrical image by interpreting data in electrical resistivity monitoring method …….……...……..	31
1.17	Internal erosion event-tree in Doroudzan dam, Iran ……...……	33
1.18	Bayesian Probability Network for abnormal behavior in downstream piezometer of Klimkówka Dam, Poland …….....…....	40
1.19	Forward propagation of Bayesian Probability Network for abnormal behavior in downstream piezometer of Klimkówka Dam, Poland …….	41
1.20	Backward propagation of Bayesian Probability Network for abnormal behavior in downstream piezometer of Klimkówka Dam, Poland …….	41
1.21	Summary of causal networks for diagnosing distresses associated with (a) seepage erosion–piping of homogeneous–composite dams, and (b) seepage erosion–piping of clay-core dams ……...……	42
1.22	Causal networks for diagnosing the distressed studied dam ……...	44
3.1	Detection of wet soft soil at the downstream toe …..……..	56
3.2	Standing water and seepage outflow downstream of the parapet jersey barriers ……..……..	57
3.3	Area with the fallen trees downstream of the right abutment …..……...	58
3.4	Transverse cracks along the crest …..…….	58

LIST OF FIGURES
(Continued)

Figure		Page
3.5	Location and status of observed transverse cracks along the crest …..…...	60
3.6	Detected downstream outflows ...……...…….	61
3.7	Location of blowing spring. Looking from the downstream slope towards the toe ……..	62
3.8	Location of standing water downstream of the jersey barriers at station around 2+60 ……..……..	63
3.9	Orifice weir at outflows #1 during Spring 2016 and Winter 2017 …….	66
3.10	V-Notch weir at outflow path #2 during Spring 2016 and Winter 2017	68
3.11	Electrical Resistivity survey with AEMC 6470-B device and Wenner electrode array configurations ...…...……..	70
3.12	ERT results along crest, mid-berm, and toe of the studied dam ……..…...	72
3.13	Schematic view of seepage monitoring results of the studied dam …….....	73
3.14	Schematic view of the potential flow paths for Outflow#1 and Outflow#2	74
4.1	Plan and section view of the studied dam ……..…….	76
4.2	Grain size distribution of the studied dam ……..……	77
4.3	Soil characteristics according to SPAW ……..……...	79
4.4	2D model of the studied dam in GeoStudio Seep/W software ……..….	80
4.5	Estimating graphs of (a) Hydraulic Conductivity and (b) Volumetric Water Content in GeoStudio software ……...…….	81

LIST OF FIGURES
(Continued)

Figure		Page
4.6	Results of Pressure Head and Total head of the studied dam analyzed in GeoStudio software ……...……..	83
4.7	Schematic view of measured and. analyzed water level in downstream embankment ……..……..	84
4.8	3D model and results of three potential Flow Paths of the studied dam in SVFLUX software for reservoir level at 51 ft. ……..…….	87
4.9	Outflow discharge vs. reservoir level for Outflow #1 and Outflow #2, comparing calculating discharge from 3D model for each flow path and actual site measurement ……..……	89
5.1	Causal network representing seepage incidents in the studied dam …...…	92
5.2	Discharge fluctuation over three year period for (a) Outflow #1 and (b) Outflow#2 ..……..…….	108
5.3	Seasonal outflow discharge vs. reservoir level for (a) Outflow #1 and (b) Outflow #2 …….……	109

CHAPTER 1

PRELIMINARIES AND LITERATURE REVIEW

1.1 Introduction

Failure of embankment dams may result in massive damage in the form of human casualties, destruction of property, pollution of the environment and economic loss. According to ASCE (2013), the average age of the 84,000 dams in the country is 52 years old and the overall number of high-hazard dams were estimated at nearly 14,000 in 2012. As these structures continue to age and the downstream population increases, the potential for catastrophic failure and its impact continues to grow. As Brosten et al. (2005) reported, between 1935 and 2001, a total of 205 incidents that affected USACE dams were documented.

ICOLD (1995) identified the major causes of failure in embankment dams as:

- Overtopping at high flood discharge (about 30% of the total failures);
- Internal erosion and seepage problems in the embankment (about 20%); and
- Internal erosion and seepage problems in the foundation (about 15%)

Other studies determined the source of distress in seepage and internal erosion failures. Bonala and Reddi (1998) reported in about 25% of the cases the failure was found from poor filtration design. Also Richards and Reddy (2007) reported nearly one-third of internal erosion failures may be associated with backward erosion piping, where half of them were found with erosions along conduits or internal erosions into or along foundation contacts. Foster et al. (2000) conducted a study on 11,192 embankment dam incidents with broad range of age, embankment type, construction techniques, and foundation conditions. They found 46.1% of the failures can be attributed to internal erosion where internal

erosion through embankment, foundation and from embankment into the foundation were about 30%, 15% and 1.5%, respectively. About half of the internal erosions through embankment were found along a conduit or other structures. Interagency Committee on Dam Safety (ICODS) (2015) reported a number of notable dam failures and incidents specifically related to internal erosion by identifying the mechanism of internal erosion and subsequent potential failure modes.

As the studies show, seepage and internal erosion account for a considerable portion of failure in embankment dams. In part for safety reasons, dams are regularly inspected and monitored according to regulatory codes. Supervision and regular monitoring of the tailings impoundment with suitable techniques are currently the most important requirements to obtain a high level of dam safety. However, the majority of the regular inspections are limited to annual visual inspections and evaluation of general condition of the dam. Although visual inspection may detect and address many of the potential issues, it has significant limitations and is risky when employed as the sole method of safety monitoring in dams. Hence, it is essential to establish a remedy helping anticipate the potential hazards, in order to mitigate or respond effectively and efficiently to the identified risk associated with the pre-failure scenario.

Various dam safety monitoring methods have been developed over the past few decades. Depending on site condition and limitations, purpose of inspection, parameters needing to be measured, and level of accuracy of the results, the surveying methods need to be selected and a monitoring scenario needs to be developed. It should be noted that not all the surveying methods necessarily provide exactly accurate results in all the monitoring cases. Though for each surveying method, considering the case condition and the related

limitation, the outcome needs to be within an acceptable range of accuracy and reliability that the method can be employed as a tool towards detecting sources of distress and potential seepage flow paths. Different seepage scenarios could be developed according to the potential distressed zones and seepage flow paths detected with the applied surveying methods. By creating and expanding a probability model, different scenarios are weighted and the most susceptible distressed zones and the potential flow paths for each detected seepage flow are identified. To ensure the dam is in the safe condition, it is essential to check any sign of piping and internal erosion. In the case of any occurrence of internal erosion, the rate of erosion and potential time of failure needs to be estimated as one of the major parameters in subsequent process of decision making analysis.

1.2 Description of the Research

1.2.1 Research Objectives

In the case of application of this research project, a soil dam suffering from seepage was monitored and studied for discovering the potential sources of concentrated flows detected at the downstream toe. The studied case was a concrete cored, earth embankment dam with approximate height of 60 feet and located in northern New Jersey. A probability model was developed to evaluate the potential sources of the detected seepages and rate of erosion was estimated.

Firstly, two separate statistical studies were implemented. In the first study, the accuracy and reliability of Electrical Resistivity method in seepage monitoring is evaluated by reviewing twenty two seepage monitoring cases. In the second study, the origin of the seepage incidents were classified into four regions as embankment, foundation, abutment

and embedded culverts. By studying 182 seepage incidents, the probability of each class as the source of seepage was assessed.

Secondly, the case study dam was reviewed by going over the history of the dam and previous inspection reports of the dam, prepared by others and implementing site visits and visual inspections to evaluate the condition of the dam's structure and seepage. Electrical Resistivity Tomography was performed along three surveying lines to detect low resistivity zones as potential seepage areas. Two V-Notch weirs were installed at the downstream toe to collect two detected outflows and measure the discharges.

Thirdly, potential seepage scenarios were identified based on the results of the ERT survey and site investigations. A 3D software model was developed for each identified scenario and the results were compared with the actual collected data on site. By employing Bayesian probability network, the prior probability of each identified scenario was determined. Then, the posterior probabilities were calculated as new set of data is observed.

Finally, by assuming an active erosion is occurring and approximating some flow parameters and seasonal discharge fluctuation, the potential failure time of the dam was estimated with different theoretical methods and the rate of erosion was estimated with an empirical strategy.

1.2.2 Research Significance

Embankment dams are critical infrastructures in providing water, generating energy, flood control, etc. and the failure of such infrastructures may result in catastrophic consequences. Considering seepage with internal erosion is one of the major causes of incidents, inspection of soil embankment dams with reliable methods of investigation and predicting the seepage behavior of the dams are vital to evaluate the dam's safety.

Although visual inspection provides valuable information on the general condition of a dam, it has extensive limitations especially for evaluation of seepage and underground uncertainties. Advanced technology offers various methods and tools for underground monitoring and geology investigations and these technologies have been evolved over the past few decades. There are number of studies showing applicability and effectiveness of geophysical methods in seepage monitoring. These studies mainly focus on reliability of each method, by comparing the results of observing the same case study with different methods, or by implementing guarantee observation tests.

On the other hand, as the seepage condition was monitored with any of investigation methods, an analytical model is required to evaluate the potential seepage scenarios according to the surveying results. The model needs to be updated as more sources of data are available. For this purpose, Bayesian networks serve as a powerful diagnostic tool to identify the most probable scenarios by taking into account probabilities of the events and subsequently update the results as any new observation is made. There are few researchers who have applied Bayesian networks specifically for seepage detection and the results show the applicability of this methodology.

Although numerous studies have been carried out to apply various investigation and monitoring methods in dam seepage studies as well as studies on introducing and developing analytical models in seepage and internal erosion evaluation, there is a lack of studies attempting to integrate these two approaches to develop a systematic procedure to study seepage incidents in earth embankment dams and aid to facilitate the safety decision making process.

In this study, a soil embankment dam suffering from concentrated seepage was

monitored visually and through the Electrical Resistivity method. Different seepage scenarios were identified according to the investigation results. Three-dimension software models are developed representing each identified scenario and the results were compared with the actual measurements on site. Furthermore, a Bayesian probability model was developed to analyze the probability of each identified seepage scenario according to the database, obtained from the past incidents and observed data for this case. Finally, the potential time of failure in case of when active erosion is occurring, and the rate of erosion are estimated.

1.3 Literature Review

1.3.1 Piping and Internal Erosion Process

Understanding the seepage and internal erosion process and recognizing flow-patterns are essential in seepage study of earth embankment dams. Predicting the various stages of piping and time estimating of each stage is one of the main concerns in safety monitoring of the dams as the results may lead to crucial improvement in the decision-making process for the recognition and mitigation of the pre-failure scenario. Many studies tried to develop such models based on characteristics of the dam and flow and the results were compared in some case studies. Morris (2009) offered a generic breach flood hydrograph showing the breaching process as a result of piping/erosion through an embankment. In practice, the shape and duration of the hydrograph will be determined by the type of hydraulic loading. **Figure 1.1** shows this hydrograph and different states of breach initiation and growth in typical piping process.

The following summarizes each stage of this generic breaching process:

- Time T_0: No sign of erosion and no breach initiation
- Time T_1: Start of Breach Initiation
- Time T_1–T_2: Progression of Breach Initiation
- Time T_2–T_3: Transition to Breach Formation
- Time T_3–T_5: Breach Formation
- Time T_4: Peak Discharge

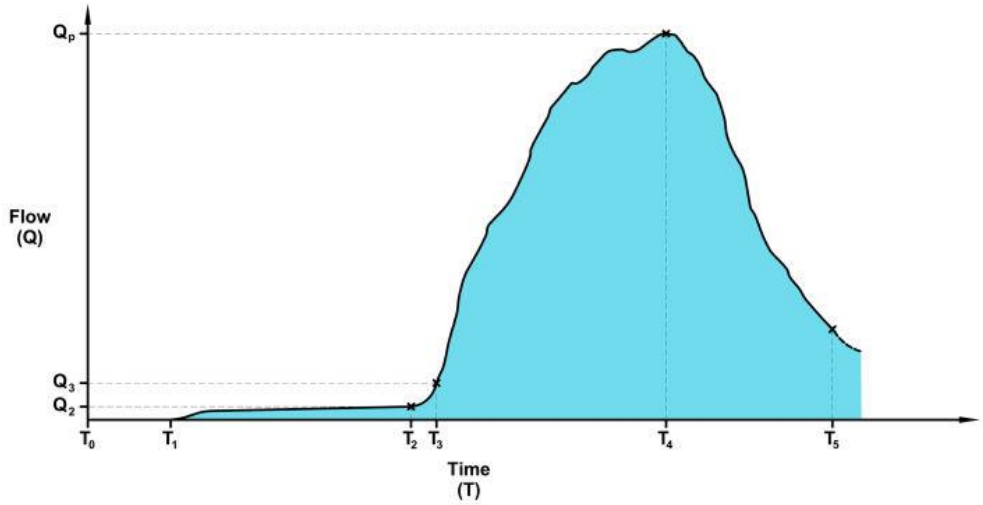

Figure 1.1 Generic breach flood hydrograph.
Source: Breaching Processes: A state of the art review (Morris, 2009).

In this hydrograph, at time of T_1, Seepage through the embankment initiates that could be detected or undetected. Here, stage Time T_1–T_2 is the most critical stage in determining the most appropriate action for maintenance, repair or emergency planning. In this stage, flow is typically small and rate of change is slow. Internal erosion and progressive material removal proceeds and breach flow increases slowly through increased loading. When piping erosion is suspected of occurring or has already been detected on the site, the rate of development is difficult to predict in order to develop the flood hydrograph. Some scholars put forward equations for prediction of time of failure according to

specifications of dams or dikes.

MacDonald and Langridge-Monopolis (1984) estimated the time of failure according to the volume of the eroded embankment material based on forty-two case histories of dam failure. Von Thun & Gillette (1990), and Froehlich (1987) estimated the failure time according to the geometry characteristics of the breach such as depth of water above breach invert at time of failure, average breach width and reservoir volume. In addition to the studies that related breach parameters merely as a function of various dam and reservoir parameters, some other studies tried to estimate the breach parameters more analytically and based on the rate of erosion for piping failure scenarios. Bonelli and Benahmed (2010) demonstrated mechanically based relations relating the time to failure and the peak flow to the two basic parameters of piping failure: the coefficient of erosion, and the maximum pipe diameter prior to roof collapse. Chen et al. (2012) proposed a numerical method to calculate the breach time, flow information and top and bottom width of the final breach. This method is developed by employing equilibrium analysis of forces in a soil element considering drag force, uplift force, friction force and effective weight of soil to estimate the rate of erosion within the seepage passage and finally calculate the desired parameters within an iterative process. Hence, employing the last two methods requires some detail flow and rate of erosion information in addition to basic dam and reservoir parameters, which calls for more comprehensive investigation and data collection. In return, they provide more accurate and reliable estimate of the failure timing and other desired flow information. Therefore, to appropriately address the dam safety, applicable and reliable monitoring methods need to be employed to detect any sign of leakage and potential erosion in a timely manner. Controlling the breach growth as it gets

into the breach formation phase (Time T_2–T_3) would be a difficult and risky practice, if not impossible. These four methods of estimating the internal erosion failure time are described in more details in this section.

- MacDonald and Langridge-Monopolis (1984)

According to 42 case histories of dam failure, plots of the maximum breach development times versus breach volumes were presented in a graph as an indicator of actual breach development times. However, since this graph is an envelope of maximums, it may still give high estimates of actual development times. **Figure 1.2** shows the chart for breach time versus breach development time:

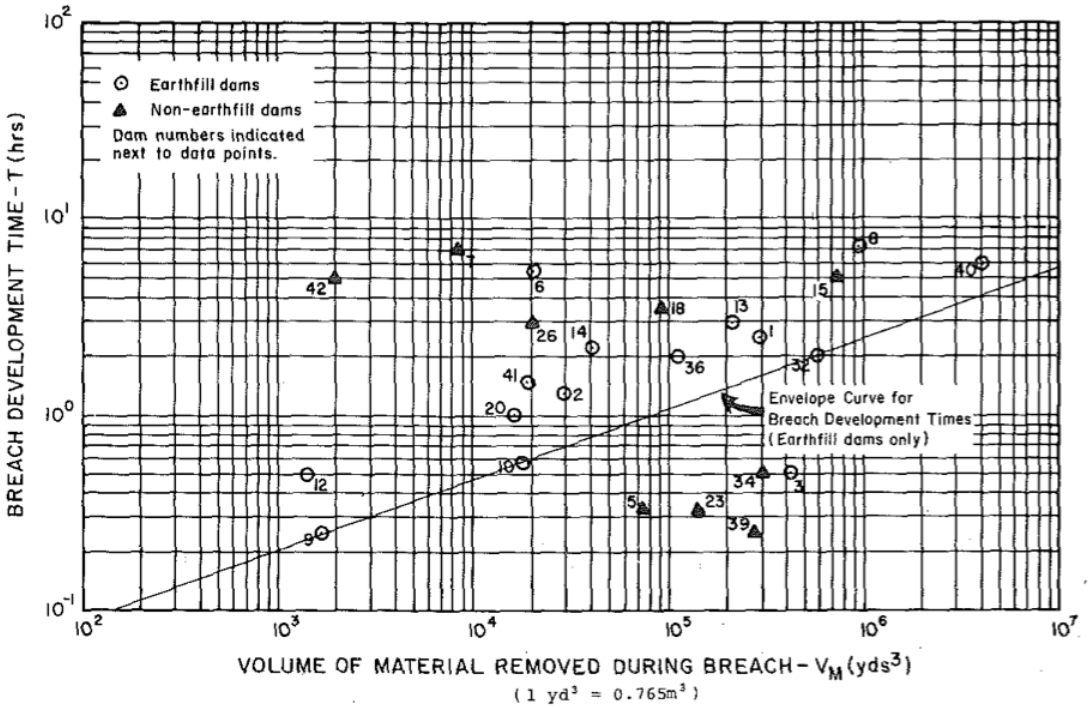

Figure 1.2 Breach size versus breach development time.
Source: Breaching characteristics of dam failures (MacDonald & Langridge-Monopolis, 1984).

$$t_f = 0.0179\ (V_{er})^{0.364}\ (hr) \tag{1.1}$$

where t_f is the failure time (h) and Ver is the volume of embankment material eroded (m3).

- Froehlich (1995)

$$t_f = 0.00254\, V_w{}^{0.53}\, h_w{}^{-0.9}\ (hr) \tag{1.2}$$

where t_f is the failure time (h), h_w is the height of the final breach (m), and V_w is the reservoir volume at the time of failure (m^3).

- Bonelli and Benahmed (2010)

Bonelli and Benahmed demonstrated new mechanically based relations relating the time to failure and the peak flow to the two basic parameters of piping failure: the coefficient of erosion, and the maximum pipe diameter prior to roof collapse. These relations make possible to infer orders of magnitude of the coefficient of erosion from field data.

They identified that piping occurs in cohesive soils if $P_0 > \tau_c$ where P_0 is the driving pressure, equal to the tangential shear stress exerted by the piping flow on the soil, and τ_c is the critical stress. The radius evolution of the pipe during erosion with constant pressure drop follows a scaling exponential law presented in equation 1.3

$$\mathrm{R(t)} = R_0 \left(\frac{\tau_C}{P_0} + \left(1 - \frac{\tau_C}{P_0}\right) \exp\left(\frac{t}{t_{er}}\right)\right) \tag{1.3}$$

$$P_0 = \frac{R_0 \Delta p}{2L}\ \text{(driving pressure)} \tag{1.4}$$

$$t_{er} = \frac{2\rho_{dry} L}{C_e \Delta p}\ \text{(characteristing time of piping)} \tag{1.5}$$

where t_{er} is the characteristic time of piping erosion, R_0 is the initial radius, Δp is the pressure drop in the hole, L is the hole length, ρ_{dry} is the dry soil density, and C_e is the Fell coefficient of soil erosion.

The rate of erosion has a significant influence on the time for progression of piping

and development of a breach in earth dams, dykes or levees. This provides an indication of the amount of warning time available to evacuate the population at risk downstream of the dam, and hence has important implications for the management of dam safety. **Table 1.1** summarizes critical stress and Fell erosion index for different types of soil based on hole erosion test.

Table 1.1 Hole Erosion Tests, Properties of Soils Samples, Critical Stress and Fell Erosion Index

Soil		% Gravel	% Sand	% Fines	% <2µm	τ_c (Pa)	I_e
Lyell	silty sand	1	70	29	13	8	2
Fattorini	medium plasticity sandy clay	3	22	75	14	6	3
Pukaki	silty sand	10	48	42	13	13	3
Jindabyne	clayey sand	0	66	34	15	6 - 72	3 - 4
Bradys	high plasticity sandy clay	1	24	75	48	50 - 76	4
Shellharbour	high plasticity clay	1	11	88	77	99 - 106	4
Waranga	low plasticity clay	0	21	79	54	106	4
Matahina	low plasticity clay	7	43	50	25	128	4
Hume	low plasticity sandy clay	0	19	81	51	66 - 92	4 - 5

Source: Piping flow erosion in water retaining structures (Bonelli & Benahmed, 2010).

$$I_e = -\log C_e \left(C_e \; given \; in \frac{S}{m}\right). \tag{1.5}$$

Given that erosion has initiated, and the filters are absent or unable to stop erosion, the hydraulics of flow in concentrated leaks are such that erosion will progress to form a continuous tunnel (the pipe). There is a consideration that the case of a straight and circular pipe, of current radius R(t) , in an embankment of height H_{dam} and base width $L_{dam} = C_L H_{dam}$ (**Figure 1.3**). The average quantities are defined as follows:

$$L(t) = c_L[H_{dam} - R(t)] \text{ (current pipe length)} \tag{1.6}$$

$$\Delta p_T(t) = \rho_w g[\Delta H_w - R(t)] \text{ (average pressure drop)} \tag{1.7}$$

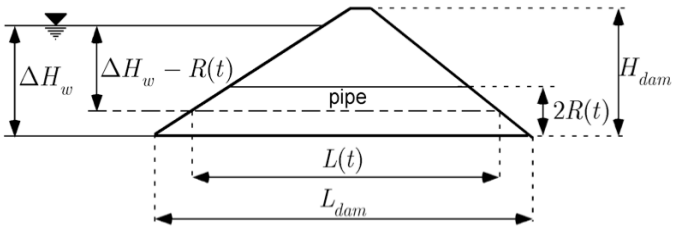

Figure 1.3: Sketch of the piping erosion in a water retaining structure.
Source: Piping flow erosion in water retaining structures (Bonelli & Benahmed, 2010).

In the next step, an expression for the remaining time for breaching is proposed. The piping process begins at time t_0 with the initial radius R_0, both unknown. A sketch of the description is represented in **Figure 1.4**. A visual inspection defines the initial time $t_d > t_0$ for detection, and can provide an estimation of the output flow rate, thus an estimation of the radius $R_d > R_0$. R_u and t_u are taken to denote the maximum radius of the pipe before roof collapse, and the collapse time, respectively.

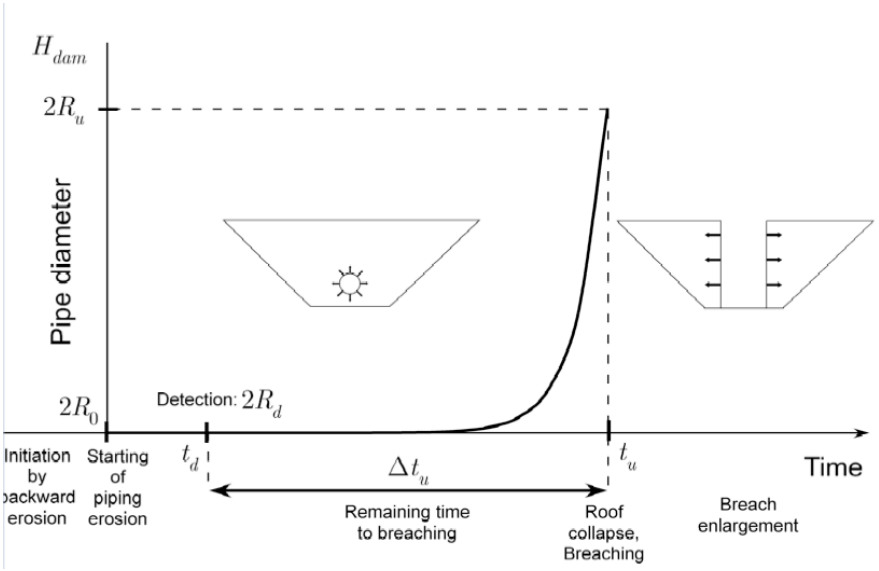

Figure 1.4 Piping erosion in a water retaining structure, phases from initiation to breaching.
Source: Piping flow erosion in water retaining structures (Bonelli & Benahmed, 2010).

$$\Delta t_u \approx t_{er} \ln\left(\frac{R_u}{R_d}\right) \tag{1.8}$$

The erosion onset radius can be neglected, as $R_d << R_u$. The remaining time prior to breach $\Delta t_u = t_u - t_d$ can therefore be estimated as follows

- Chen, Zhong and Cao (2012)

Chen et al. showed that by employing equilibrium analysis of forces in a soil element (**Figure 1.5**) considering drag force, uplift force, friction force and effective weight of soil, the critical incipient velocity (v_c) of the soil practice can be calculated. In this model, the development of the seepage passage not only depends on the hydraulic pressure within the passage, but also on the physical and mechanical properties of dam materials.

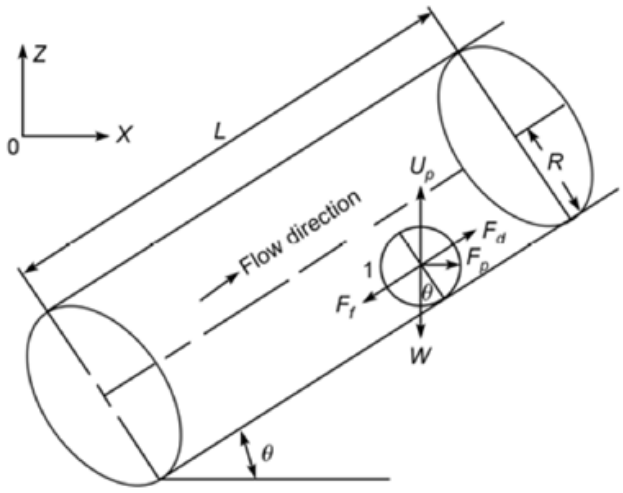

Figure 1.5 Forces acting on a soil particle in seepage passage.
Source: Breach mechanism and numerical simulation for seepage failure of earth-rock dams (Chen, Zhong and Cao, 2012).

$$v_c = \sqrt{\frac{40gd_{50}(\gamma_s - \gamma_w)(tan\,\varphi\,cos\,\theta - sin\,\theta)}{3\gamma_w\,(tan\,\varphi\,cos\,\theta - sin\,\theta + 4)} + \frac{80gC}{\gamma_w\,(tan\,\varphi\,cos\,\theta - sin\,\theta + 4)}} \tag{1.9}$$

The total erosion rate Q_s within the seepage passage is:

$$Q_s = 0.25\,(\frac{d_{90}}{d_{30}})^{0.2}\sec\theta\;P\frac{\nu_*(\nu^2-\nu_c{}^2)}{g\left(\frac{\gamma_s}{\gamma_w}-1\right)} \qquad (1.10)$$

$$= 0.5\,\pi\sec\theta\;R\;\frac{\nu_*(\nu^2-\nu_c{}^2)}{g\left(\frac{\gamma_s}{\gamma_w}-1\right)}$$

- ν_* is the velocity of erosive water flows
- ν is the velocity of water within seepage passage ($\nu=\mu\sqrt{2g\Delta h}$)
- Δh is the differential head between the upstream reservoir and the outlet zone
- μ is the velocity coefficient.

When ν is larger than ν_c the soil particles start to move until the failure of the earth-rock dam. The increment of the radius of the seepage passage within the time interval Δt_i can be predicted as:

$$\Delta R_i = \frac{\Delta t_i\,Q_s}{PL_1(1-n)} = \frac{\Delta t_i\,Q_s}{2\pi RL_1(1-n)} \qquad (1.11)$$

Where *n* is the porosity of the investigated soil and *P* denotes the perimeter of the seepage passage. And finally the accumulated increment of the radius of the seepage passage within time interval of Δt is calculated.

$$\Delta R = \sum_{i=1}^{n}\Delta R_i \qquad (1.12)$$

1.3.2 Seepage Monitoring

Concentrated seepage in earth dams is a major safety issue that, if left unchecked, may result in dam failure by various mechanisms. Implementing the remedial actions in order to reduce the risk of failure and control water loss requires not only the engineering expertise, but also adequate hydrological information to understand the problem entirely.

Otherwise, the repairs could be unsuccessful in controlling or reducing the leaks. Also, it is crucial to detect any concentrated seepage and abnormal deformation at a very early stage, especially if piping and soil erosion is occurring. If piping is not controlled and the distressed zones are not remediated at early stage of the incident, it may result in emergency condition and even final breach of the structure. Hence, appropriate seepage investigation and monitoring is essential to understand the structural condition and hydrological behavior of the dams.

The most commonly used method in dam safety and seepage monitoring is visual inspection. Detecting signs of surface discharge such as concentrated leak, boils, standing water, or wet areas, signs of surface deformation such as sinkholes, slumps, cracks, and cavities as well as using techniques in quantifying seepage parameters such as (flow rate, quantity, velocity, elevation, phreatic surface, and water quality) provide substantial information on seepage condition and safety status of the dam. Some other conventional observation tools such as piezometers and observation wells also provides valuable information about the water level at the reading points and presence of potential leaks. However, these tools had to be built-in during the construction of the structure and be in service condition to consider as a monitoring option.

In the last few decades, a series of new hydrological techniques have been developed to help in the assessment of leakage and seepage in dams. Bartholomew et al. (1987) published a technical report to introduce measuring devices of pressure, seepage, internal and surface movement, vibration and methods for data acquisition, processing, and review procedure. USBR (1983) published a technical manual for engineers and site personnel with guidelines and procedures for examination and evaluation of public and

private dams. This manual provides procedures for onsite examination and investigation. USBR (2011) provided discussion for seepage monitoring instrumentation tools such as piezometers, observation wells and thermal monitoring and key data for seepage evaluation. FEMA (2003) within an executive summary of a research workshop on seepage through embankment dams, presented the description of the most common geophysical investigation methods in seepage detection and briefly explained the advantages and limitations of each method. ASDSO (1988) in coordination with USBR, USACE, FEMA and eleven other federal agencies developed Training Aids For Dam Safety (TADS) program as an inventory guideline to identify hazard classification of the dams, effective safety inspections and analysis and implementing corrective actions. This document addressed methods of monitoring and evaluating observations for special seepage condition and subsequent field exploration and sampling. ICODS (2015) provided procedures and guidance for "best practices" concerning the evaluation and monitoring of seepage and internal erosion. In this manual, seepage detection and investigation methods were classified into three main categories as visual detection methods, non-visual detection and investigation methods, and intrusive methods. In addition, this document provided guidelines for Seepage Performance Monitoring and Seepage Collection and Measurement methods.

In addition to organizational manuals and guidelines, many researches have been implemented on applicability and accuracy of various seepage monitoring and investigation methods. Bedmar and Araguás (2002) presented different practical methods in detecting permeability, using natural and artificial traces in detecting flow paths, and surface prospecting versus well logging geophysical methods. Contreras and Hernández

also discussed different techniques for prevention and detection of leakage in dams and reservoirs.

Other studies were presenting the results of applying one or more geophysical investigating methods in detecting seepage in real case studies. Hoepffner et al. (2008), Henault et al. (2010), Artières et al. (2010), Habel (2011), Pingyu (2008), Radzicki (2014), Johnson et al. (2005), Beck et al. (2010), Perzlmaier et al. (2007) were describing applicability distributed temperature sensing and fiber optic technology for monitoring seepage and erosion processes in soil dam and dykes. Temperature measurement makes use of natural seasonal temperature variations to locate areas of preferential seepage. Generally, a constant temperature will be a sign of a small seepage, while large seasonal variations may be sign of significant seepage. Fiber optics and sensors need to be installed at the preferred locations in dam during the construction, otherwise destructive methods needs to be employed for installation of monitoring tools which is generally not a preferable practice. This method is exclusively monitoring the locations where the sensors are installed and may not provide comprehensive perspective of the dam condition. Also, it should be noted the results in this method could be sensitive to seasonal change and geothermal heat flow and special consideration is necessary to protect the equipment against freezing. On the other hand, temperature measurement method is probably the most cost effective option in long-term monitoring of seepage compare to the other geophysical monitoring methods. Also, unlike the other methods, no data interpretation or inversion is necessary for detecting and locating the seepage zones, and direct monitoring of the measuring parameter (temperature) shows the anomalies. **Figure 1.6** shows the results of monitoring of fiber optics installed along the toe of an earth embankment dam in north

France over 1 year period. The zones with anomaly behavior are showing the potential location of flow.

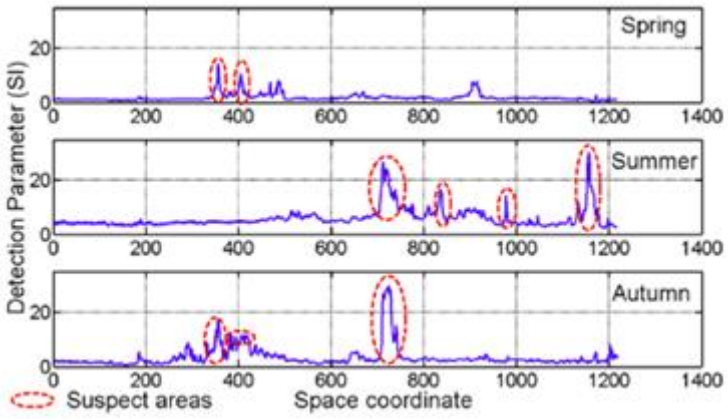

Figure 1.6 Results of seepage monitoring using fiber optics over 1 year period.
Source: Thermal Monitoring of Embankment Dams by Fiber Optics (Beck, et al., 2010).

Brosten et al. (2005), Lum et al. (2005), Osazuwa (2008), Cardarelli (2014), Bedrosian (2012), Rinehart et al. (2012), Chii (2010), Mustafa et al. (2013), Ramteke (2013), and Ikard et al. (2014) presented the applicability of Seismic method in underground seepage detection. In this method, acoustic energy is introduced into the ground at a known time and, then, by recording the reflected or refracted returning energy, the subsurface condition is mapped based on the recorded data. Results from seismic refraction methods often aid in determining the depth to competent rock for future remediation efforts. High-resolution seismic reflection methods have allowed vast improvements in data collection techniques over the past 10 years and have been used to characterize sinkholes in related seepage studies. There are two types of body waves propagating through a ground. Compressional or P-waves relate to changes in the volume of a medium. Shear or S-waves relate to the distortional changes of a medium. Generally, shorter wavelength sources provide better resolution, thus S-waves are preferred for geotechnical applications. However, S-waves tend to attenuate more rapidly than P-waves,

and it is more difficult to generate high-energy S-waves. This method can detect both lateral and depth variations in a physically relevant parameters and provide high resolution images especially in shallow surface with high permeable zones. The accuracy of the results is decreasing as the depth increase.

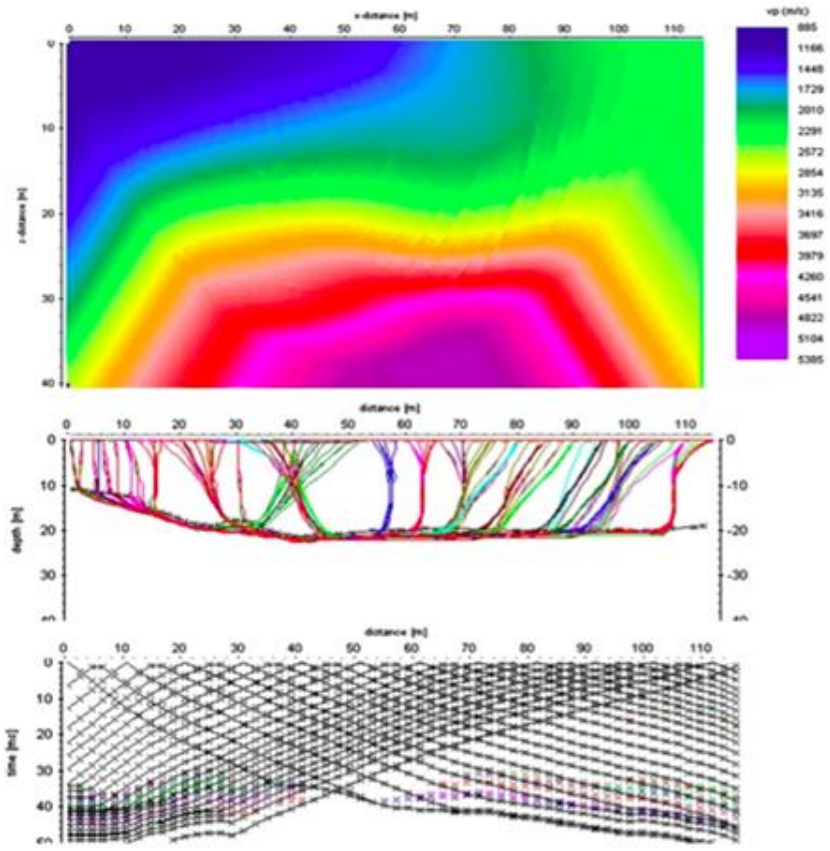

(a)

Figure 1.7 (a) Results of Seismic tomography imaging along a surveying line for a studied dam in Nigeria (Continued)

Source: Seismic refraction tomography imaging of high-permeability zones beneath an earthen dam, in Zaria area, Nigeria (Osazuwa & Chinedu, 2008).

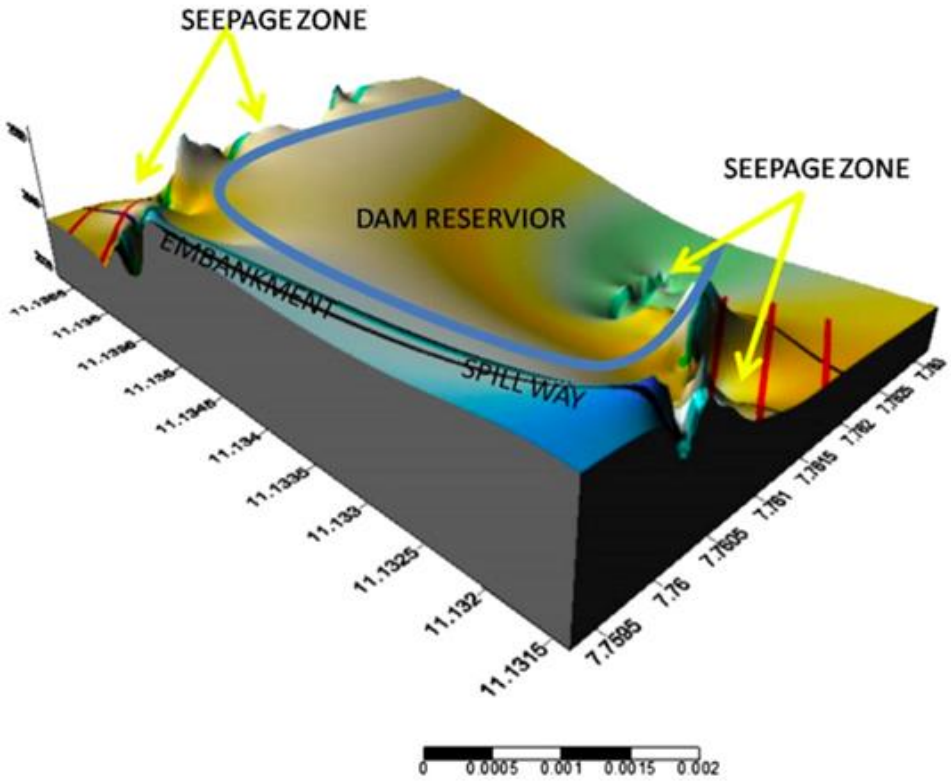

(b)

Figure 1.7 Continued (b) The final interpretational 3D isometric map showing seepage zones, for a studied dam in Nigeria.

Source: Seismic refraction tomography imaging of high-permeability zones beneath an earthen dam, in Zaria area, Nigeria (Osazuwa & Chinedu, 2008).

The seismic method is relatively more expensive compared to the other geophysical surveying methods for seepage detection. Also, data processing requires sophisticated computer hardware and is a time consuming process. **Figure 1.7** is showing the results of the Seismic monitoring method along a surveying profile and the final interpretational 3-D isometric map showing seepage zones within and around a studied dam in Nigeria.

Brosten et al. (2005), Lum et al. (2005), Bolève et al. (2012), Ikard et al. (2014), Panthulu et al. (2001), Rinehart et al. (2012), Bolève et al. (2011), Abdel Aal et al. (2004), Ikard et al. (2014), and Moore et al. (2011) applied the Self-Potential (SP) method in seepage monitoring for different case studies and presented the results. The (SP) method

is a passive technique used to measure small naturally occurring electrical potentials generated by fluid flow, mineralization, and geothermal gradients within the earth. Water flowing through the pore space of soil generates electrical current flow. SP is measured by determining the voltage across a pair of non-polarizing electrodes using a high-impedance voltmeter. This electrokinetic phenomenon is called streaming potential and gives rise to SP signals that are of primary interest in dam seepage studies. Implementation of SP method is relatively simple and the anomalies can be detected with single survey. Different resolutions and depths by changing the distance of electrodes and Cross-comparing data at different reservoir levels can reveal the potential flow paths. However, this method is sensitive to external factors like physical properties and electrical noises. Also, presence of some minerals may result in SP anomalies. **Figure 1.8** is illustrating of generic SP electrode array setup along the crest of a dam and the monitoring results, locating potential seepage zone.

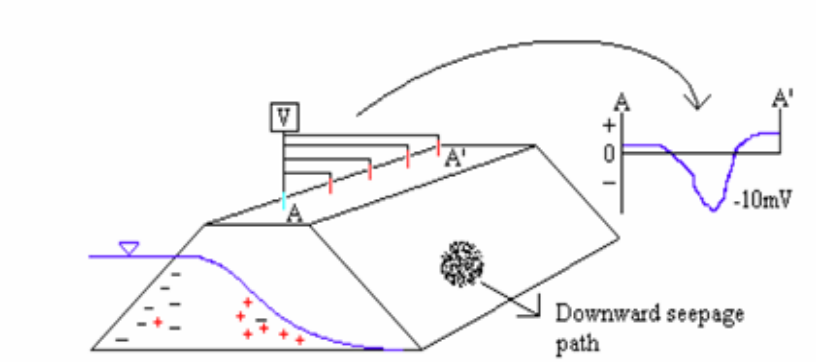

Figure 1.8 Illustration of an electrode array set up along the crest of a dam and the SP anomaly generated from downward seepage.
Source: Using Geophysics to Assess the Condition of Small Embankment Dams (Brosten, Llopis, & Kelley, 2005).

Johannson (1997), Lagmanson (2005), Ramteke (2013) and Brosten (2005) employed and evaluated the ability of Ground-penetrating radar (GPR) to provide useful and reliable information in subsurface seepage studies. GPR uses a high-frequency

electromagnetic pulse transmitted into the ground. Electromagnetic waves within a certain frequency range can propagate through rock, soil or water. The radar pulses are reflected from subsurface at boundaries where subsurface electrical properties change. These subsurface interfaces are possessing a contrast in electrical properties and are recorded by the receiving antenna. GPR can detect large zones with anomalous properties with high acquisition speed and good spatial resolution. Nevertheless, this method is extremely sensitivity to site conditions (less sensitive to seepage changes than flow dependent parameters) and relatively high energy consuming. This methods is rarely used as a sole seepage survey method usually been employed with one or more other geophysical monitoring methods for detecting the seepage zones in hydraulic structures. **Figure 1.9** shows the results of GPR monitoring method along the crest of a dyke in northeast Poland.

Walid (2011), Tigistu and Atsbaha (2014), Bedrosian et al. (2012), Aitsebaomo et al. (2013), and Ramteke (2013) reported the results of utilizing Electromagnetic survey in seepage study of the soil dams. Electromagnetic (EM) methods are used to measure conductivity differences of geologic material. In the case of seepage studies, possible seepage paths can be located through the identification of high- or low-conductivity anomalies, where water-filled or clay-filled features can produce high-conductivity anomalies and air-filled features can produce low-conductivity anomalies. By this method, data collection over large areas can be performed without ground contact with high horizontal resolution. However, the depth of investigation is limited (no greater than 5 meter) and it is highly sensitive to aboveground and buried metallic objects and alternating current electrical sources that influences the monitoring results.

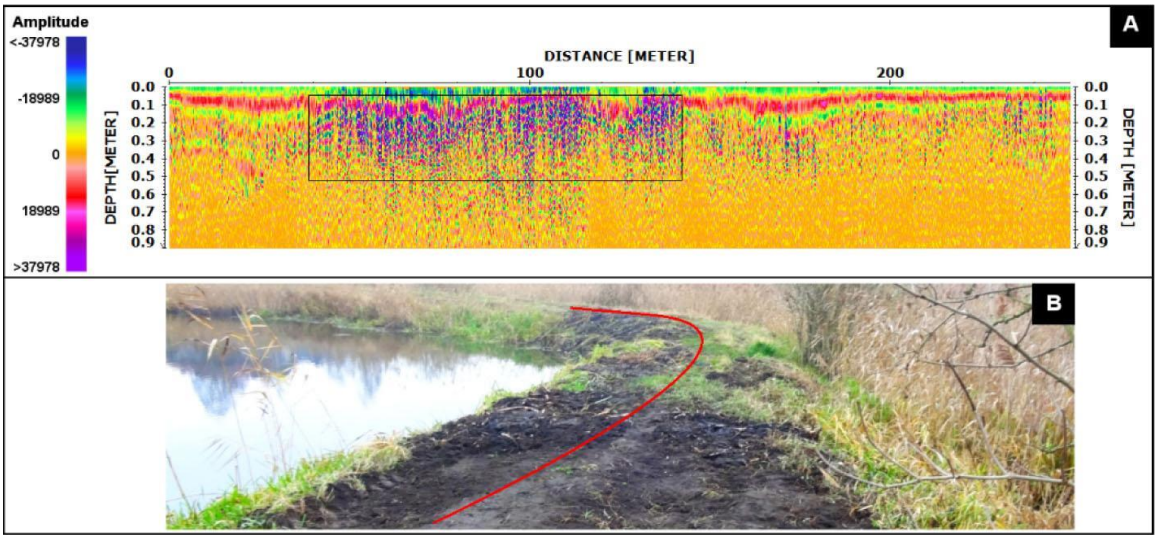

Figure 1.9 Detected anomaly zone (A) according to GPR results and (B) photo of the surveying line, for a dyke in northeast of Poland.
Source: Application of Ground Penetrating Radar Surveys and GPS Surveys for Monitoring the Condition of Levees and Dykes (Tanajewski, Bakuła, 2016).

However, among all the geophysical monitoring methods Electrical Resistivity (ER) is probably the most common and applicable one in detecting leakage zones in earthfill structures. As Samouelian et al. (2005) indicated, ground resistivity is a function of soil property such as the mineralogy, soil constituent, fluid content, porosity, temperature and degree of water saturation in the rock. A direct measure of the electrical impedance of the subsurface material can be measured by passing electrical current through the ground and recording the potential difference between the current and potential electrodes. Increasing water content and increasing salinity of the underground water will increase the electrical conductivity, which results in decreasing the measured resistivity of the soil. This hydrogeological characteristic of the soil acts as an indicator to address the potential leakage zones with the low resistivity areas in the electrical resistivity profile. Nevertheless, the site condition, geology and soil type and the limitations of this method should be taken into account when this method is applied for seepage monitoring and leak detection. The ER method is discussed more in depth in **Section 1.3.3**.

Table 1.2 Summary of Different Seepage Monitoring Methods for Earth Dams

SEEPAGE MONITORING METHODS IN EARTHEN HYDRAULIC STRUCTURES				
Monitoring Method	Measuring Parameter	Results	Pros.	Cons.
Visual Inspection	Any visual disorder	Detect external defects and abnormal behaviors	• Substantial information on structure and flow condition at minimal cost • Easy and sensible	• Not detecting any hidden flow • Not reliable to use as a sole method of monitoring
Pizometric Pressure	Pore water pressure	Piezometric level	• Easy to install and monitor • No data interpretation required • Efficient for continues long-term monitoring	• Provide data at discrete points • Instruments to be installed during construction or via destructive methods • Instruments needs to be protected agains freezing
Temperature Measurement	Natural tempreture variation	Tempreture fluctiation	• Cost effective option in long-term monitoring of seepage • No data interpretation required	• Sensors of fiber optics to be installed during construction or via destructive methods • exclusively monitoring the locations where the sensors are installed
Self-Potential	Electrical potentials of the soil	Voltage anomalies	• Single survey can show anomalies • different resolutions and depths by changing the distance of electrodes • 3D model by interpreting SP data, hydraulic pattern & geophysical data	• Sensitive to external factors and electrical noises • Presence of some minerals may result in SP anomalies
Electrical Resistivity	electrical impedance of the subsurface material	Pseudosectin of electrical resistivity along surveying profile	• 1D, 2D & 3D survey results • Horizontal and vertival resolution by modifying electrodes arrangement • Provide subsurface geology inrormation	• Special measure to improve the electrode-to-ground coupling • Decreasing the accuracy in deeper subsurface • The effects of any buried metal, pipe or any other conductive material should be taken into account
Ground Penetrating Radar	Reflected Electromagneti c ground pulses	subsurface electrical properties variation	• High data acquisition speed • Good spatial resolution	• Extremely sensitivity to site conditions (less sensitive to seepage changes than flow dependent parameters) • Relatively high energy consumption
Seismic Reflection & Refraction	Reflected or refracted acoustic energy	Image of subsurface geology with anomalous zones	• S-waves for higher resolution & P-waves for more depth • High resolution images (2D & 3D) • Detect both lateral and depth variations	• Less accurate in deep surface with low permiability • More expansive compare to the other methods • data processing requires sophisticated computer hardware and is a time consumingcprocess
Electromagnetic Profiling	Conductivity differences of geologic material	Detecting high- or low-conductivity anomalies	• Collect data without ground contact • Rapid data collection over large areas • High horizontal resolution	• Limited depth of investigation (no greater than 5m) • Sensitivity to aboveground and buried metallic objects • Sensitive to nearby alternating current electrical sources

Table 1.2 compares different geophysical methods in seepage monitoring and explains pros and cons of each method that was discussed in this section.

In addition to the geophysical methods which measure seepage-related parameters,

there are other passive methods that mainly related to displacement monitoring for slope stability, but could potentially address seepage, especially if erosion and piping is occurring. Some of these slope monitoring methods are geodetic methods like terrestrial laser scanning (TLS) and global positioning systems (GPS), geotechnical methods like time domain reflectometry (TDR), and remote sensing like synthetic aperture radar (SAR) and geographic information system (GIS). Although these methods have widely been employed in slope stability and dam safety monitoring, but seldom been utilized solely for seepage monitoring purposes.

1.3.3 Electrical Resistivity Tomography (ERT)

As discussed, Electrical Resistivity (ER) is one of the most widespread geophysical methods in seepage monitoring of earthen hydrological structures. Like other geophysical monitoring methods, ER technology has evolved during the past decades. This method has been employed in many dam seepage detections studies and the results show the effectiveness and reliability of this method. In **Chapter 2**, the results of twenty two case studies were pursued to evaluate the effectiveness and resolution of the ER method in locating leakages in soil embankment dams and dikes are presented.

In this method, surveys are conducted by laying out electrodes along a survey line. High voltage current is introduced into the ground through a pair of current electrodes (C_1 and C_2), and two potential electrodes (P_1 and P_2) measure the voltage difference. **Figure 1.10** illustrates a typical current and potential electrodes array in ER monitoring.

There are numerous array configurations for measuring ground resistivity. The best array for the survey is dependent on the type of geologic materials being investigated, the desired depth of investigation, the signal strength, the array sensitivity to vertical and

horizontal resistivity changes in the subsurface, and the probable background noise. Common arrays are Wenner, Schlumberger, pole-pole, dipole-dipole, and pole-dipole. **Figure 1.11** shows the array configuration in soil resistivity monitoring.

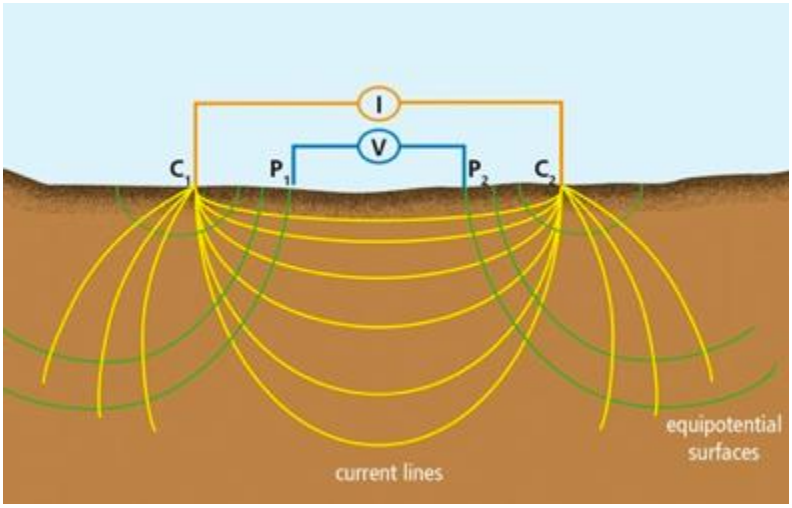

Figure 1.10 Illustration of current and potential electrodes in soil resistivity monitoring.

Wenner is the most common electrode array methods in geology and especially seepage investigation. In The Wenner array configuration, two potential electrodes are located in between the current electrodes and all the electrodes are in a same distance (called electrode a-spacing) from the adjacent electrodes. In this array configuration, the apparent resistivity value is the average measured resistivity within a block with the total length equal to the distance between the current electrodes (3a) and the depth about the distance between the adjacent electrodes (a) along the survey line. The larger distance between the electrodes (a) results in degradation of lateral resolution as the resistance is measured in a larger area and provides less accurate results. As a general rule, the accuracy of the resistivity survey diminishes as the surveying depth increases. ER results are generally more accurate near subsurface elevations.

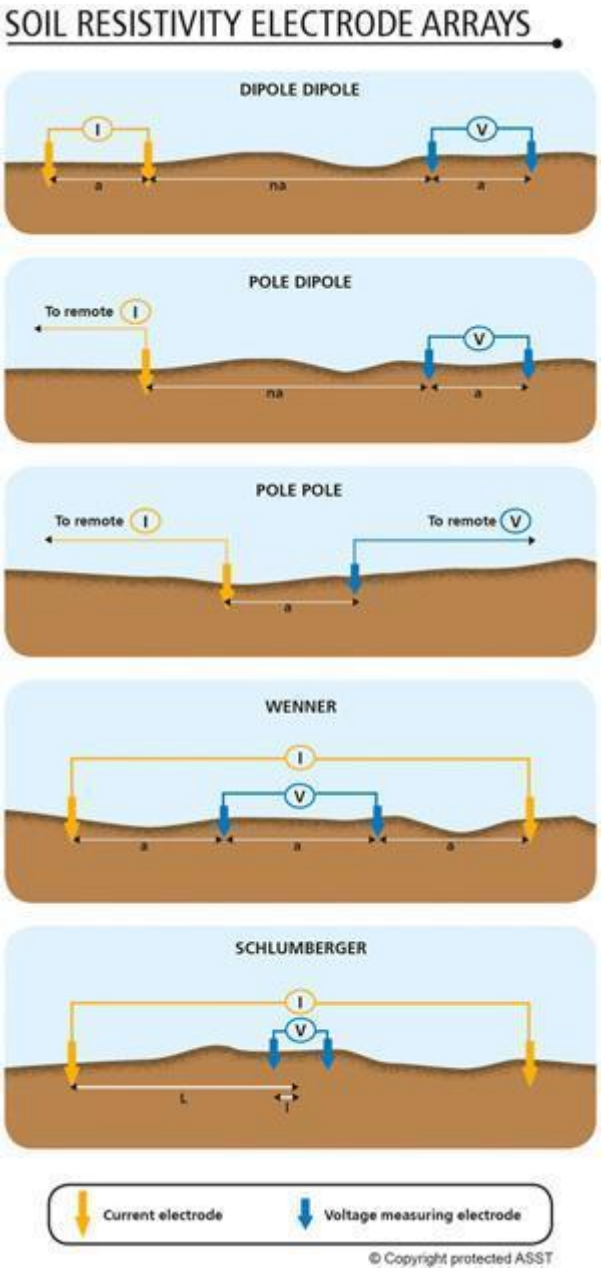

Figure 1.11 Illustration of typical electrode arrays in soil ER monitoring.
Source: http://asstgroup.com/techniques.html.

Figure 1.12 shows the schematic Wenner electrode array configuration. In this method, current (I) is introduced to the ground by the current electrodes (A and B), and the potential electrodes (M and N) measure the voltage difference to determine the resistance (R_W=V/I). The unit of resistance is ohm (Ω). Having the resistance (R_W) and electrodes

distance (a), resistivity of the surveyed block soil can be calculated with equation 1.13. If the depth of the electrodes into the ground (d) is negligible compare to electrodes distance (a), resistivity according to the Wenner method will be calculated according to equation 1.14. The unit of resistivity is ohm-meter (Ω.m).

$$\rho_E = \frac{4\,.\,\pi\,.\,a\,.\,R_W}{1 + \frac{2\,.\,a}{\sqrt{a^2 + 4\,.\,d^2}} - \frac{a}{\sqrt{a^2 + d^2}}} \tag{1.13}$$

$$\rho_E = 2\,.\pi\,.\,a\,.\,R_W \tag{1.14}$$

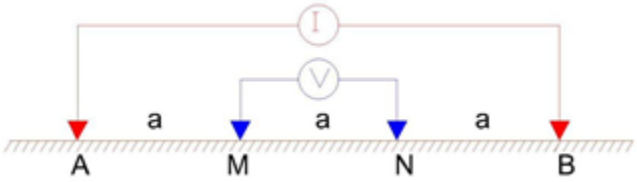

Figure 1.12 Schematic Wenner Electrode array configuration.

Electrical Resistivity survey is implemented as either one, two or three-dimensional. Dahlin (2001) and Herman (2001) described on how to perform one dimensional (1D) ER survey with Wenner method. It is carried out either as profiling or vertical electrical sounding (VES). Profiling means achieving horizontal resolutions by lateral shifting the electrodes across the surface while maintaining a constant electrode separation. VES involves achieving vertical resistivity of the subsurface by modifying the common distance between the electrodes while maintaining the location of the center point of the array. This technique for imaging the profile of subsurface structures from electrical resistivity measurements is called Electrical Resistivity Tomography (ERT) or Electrical Resistivity Imaging (ERI). **Figure 1.13** is showing the principal of ERT data acquisition in 1D.

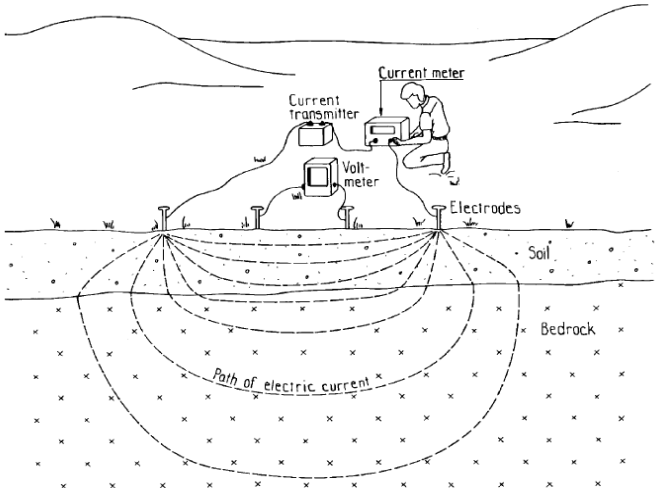

Figure 1.13 1D Electrical Resistivity data acquisition.
Source: The development of DC resistivity imaging techniques (Dahlin, 2001).

The main drawback of 1D ERT with Wenner array is the labor intensity for continuously redeploying the electrodes in group of four, as the array needs to be reconfigured to measure resistivity at different vertical and horizontal stations. However, the advent of automated data acquisition facilitates such data acquisition by employing a large number of electrodes and performing this switching automatically, while continuously reading and storing data. This method is one of the 2D techniques of resistivity data acquisition. **Figure 1.14** illustrates the procedure of procuring data with multiple electrodes. In this figure, red and green arrows represent current and potential electrodes respectively and the bold dot represents the position where apparent resistivity is measured. Here, as the distance between the electrodes increases, less number of horizontal data points are measured at the greater depth, hence the shape of the pseudo-section is usually either triangular or trapezoidal shape.

In the second 2D data acquisition method, the electrode array is being towed behind a vehicle. This concept has been developed for marine land based applications (**Figure 1.15)**. In order to obtain 3D information on the subsurface, a grid of electrodes can

be laid out, and measurements taken with the electrodes aligned in different directions. 3D technique may require large number of electrodes and the data acquisition could be a very time consuming process.

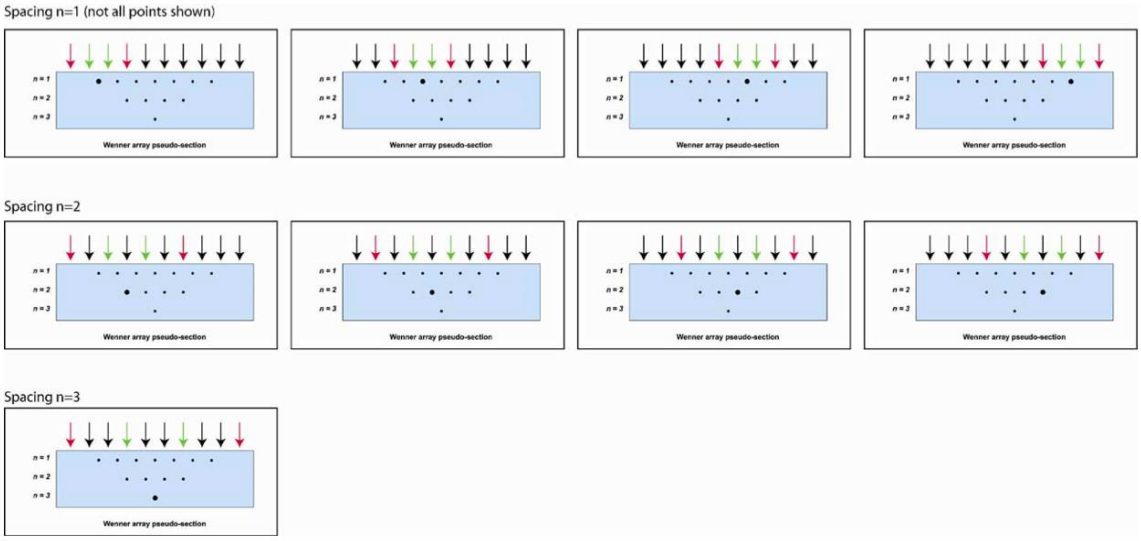

Figure 1.14 2D Electrical Resistivity data acquisition with multiple electrodes.

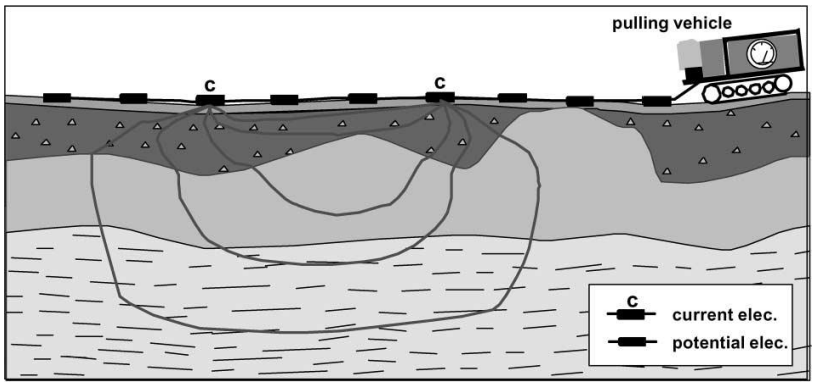

Figure 1.15 Pulled array system to acquire 2D Electrical Resistivity data.
Source: The development of DC resistivity imaging techniques (Dahlin, 2001).

In resistivity survey, since data are associated with a single depth point but in reality it is an averages over a complex current path in the survey plan, data are termed apparent resistivity. Apparent data needs to be interpreted by measuring with respect to distance between the electrodes (a) and comparing the curves from different areas and angles. As Cardimona (2002) discussed, in order to create the resistivity model, forward modeling can

be used to simulate apparent resistivity that correlate with the measured data in an iterative procedure. A starting resistivity model is chosen based on a priori information (from ground truth or averaged geophysical measurements), and apparent resistivity data are modeled for the type of field survey geometry used. These calculated data are compared with the actual data and the resistivity model is updated based on the difference between observed and calculated data. This procedure is continued until the calculated data match the actual measurements to within an interpreter-defined level of error. One of the most important results of inversion is better estimating of depth for cross-section plots, turning pseudo-sections into better approximations of the subsurface variation. This procedure is usually performed via computer programs where the software is feed with measured resistivity data, number of reading points, electrode distances (a), station of each reading, etc. and the program processes the data and estimates the resistivity profile of the soil along the surveying line.

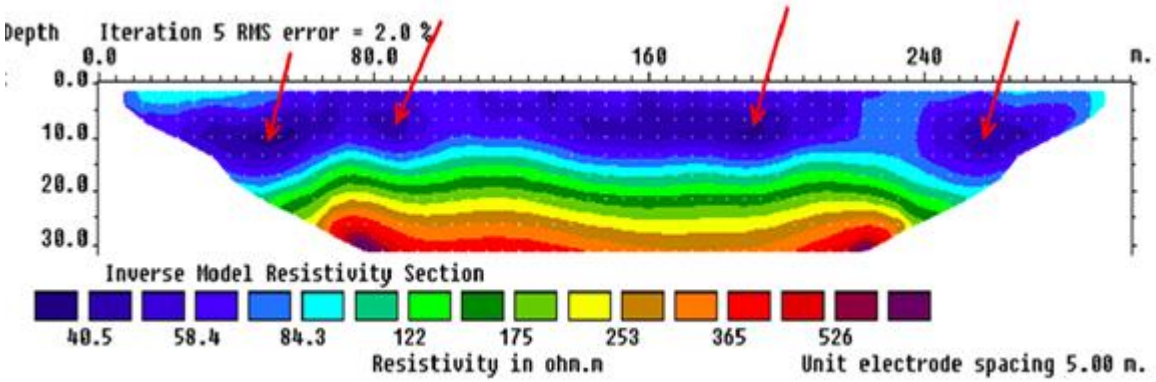

Figure 1.16 Geoelectrical image by interpreting data in electrical resistivity monitoring method.
Source: An Integrated Two-dimensional Geophysical Investigation of an Earth Dam in Zaria Area, Nigeria. (Chii , 2010)

Figure 1.16 shows the inverse model of Electrical Resistivity Tomography in a seepage monitoring of a dam in Nigeria. Arrows indicate zones of anomalously low

resistivity.

Although ER has many advantages in geophysical studies, it has some limitations as well, as Schrott and Sass (2008) noticed. Special measures needs to be taken to improve the electrode-to-ground coupling in very dry or extremely blocky substrates surfaces such as watering of the electrodes or inserting them through wet sponges. The other limitation is decreasing the accuracy in deeper subsurface. In soil ER surveying, only electrical properties of certain volume of subsurface is integrated into geoelectrical surveys and considering the extent of this volume increases in the deeper subsurface, the accuracy will diminish. Generally, the results of ER surveying is more accurate within the layers closer to the surface. In regards to the subsurface flow detection, ER may just detect the location of potential leakage or wet areas, but not any information about the flow such as hydraulic conductivity or flow velocity. The location of any buried metal, pipe or any other conductive material within the surveying line should be determined and adjusted in the ERT results. Also, the accuracy of ERT method decreases in detection of leakage zones within subsurface layers with high clay content.

1.3.4 Probability Methods and Bayesian Tool in Seepage Analysis

Various statistical methods have been used by researchers for dam safety risk analysis, predicting the dams' behavior in any specific incident and diagnose distressed zones. Peyras et al. (2006) within a study proposed qualitative methods to assess the risk of performance loss of dams with an aging functional model and by developing a historical database from dams that have experienced deterioration. Goodarzi et al. (2010) demonstrated the process of estimating risk of internal erosion for Doroudzan earth-fill dam in southern of Iran. In this study the probability of failure due to internal erosion was

estimated under two different conditions. An event-tree was developed to demonstrate the internal erosion process of the studied case and the probability of each event was determined from USBR database (**Figure 1.17**).

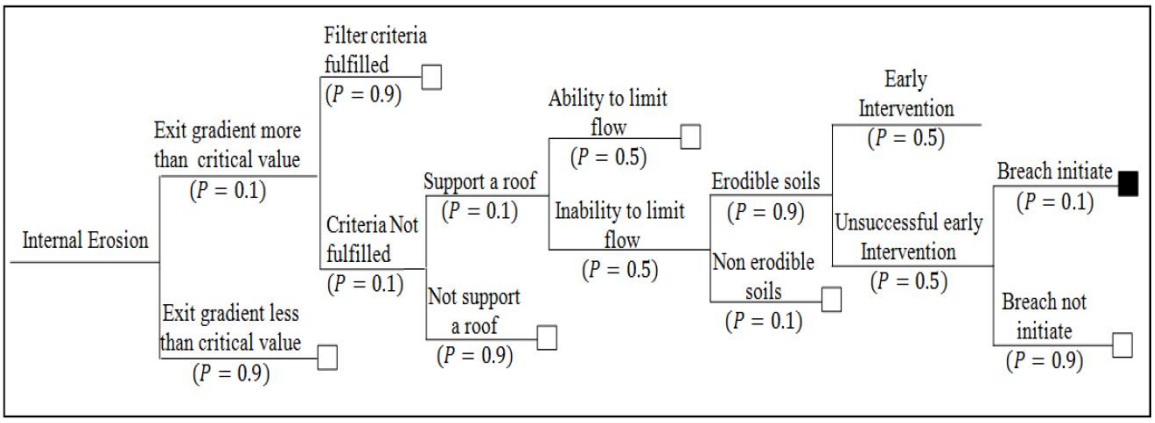

Figure 1.17 Internal erosion event-tree in Doroudzan dam, Iran.
Source: Estimating Probability of Failure Due to Internal Erosion with Event Tree (Goodarzi et al., 2010).

Different probability models have been proposed by researches to analyze dam safety and internal erosion. However, a Bayesian network is one of the most applicable methods and has been applied and developed by many scholars.

Bayesian probability theory provides a mathematical framework for performing inference, or reasoning, using probability. In the ‘Bayesian paradigm,' degrees of belief in states of nature are specified. Bayesian statistical methods start with existing 'prior' beliefs, and update these using data to give 'posterior' beliefs, which may be used as the basis for inferential decisions. The basic concept in the Bayesian treatment of uncertainty is that of conditional probability which is a measure of the probability of an event given that another event has occurred as Sakti et al. (2009) described. The conditional probability of event X, given event Y is A, written as:

$$P(X|Y) = A$$

This means that if event Y is true and everything else known is irrelevant for event

X, then the probability of event X is A. Here, each of the events X and Y have two or more states. The events are binary, if they have just two states (such as 0-1, True-False, satisfactory-unsatisfactory, etc.) or multi-state if they have more than two states.

Binary events: $X \in \{x_1, x_2\}$

$Y \in \{y_1, y_2\}$

Multi-state events: $X \in \{x_1, x_2, x_3, \ldots, x_n\}$, n = number of states for event X

$Y \in \{y_1, y_2, y_3, \ldots, y_m\}$, m = number of states for event Y

There are three axioms provide the basis for Bayesian probability calculus:

- Axiom 1: For any event X, $0 \leq P(X) \leq 1$, with $P(X) = 1$ if and only if X occurs with certainty.
- Axiom 2: For any two mutually exclusive events x and y the probability that either X or y occur is:
$$P(X \text{ or } Y) \equiv P(X \cup Y) = P(X) + P(Y).$$
- Axiom 3: For any two events x and y the probability that both x and y occur is
$$P(X \text{ and } Y) \equiv P(X \cap Y) \equiv P(X , Y) = P(Y \mid X)\, P(X) = P(X \mid Y)\, P(Y).$$

Generalizing Axiom 3 is the fundamental rule of probability calculus:

$$P(X , Y) = P(X \mid Y)\, P(Y) = P(Y \mid X)\, P(X)$$

Bayes' rule follows immediately:

$$P(Y \mid X) = \frac{P(X \mid Y)\, P(Y)}{P(X)} \tag{1.15}$$

where;

P(X , Y) is called the joint probability of events X and Y

P(Y) is the prior distribution, expresses initial belief about Y

P(Y | X) i s the posterior distribution, expresses revised belief about Y in the light of observation event X.

$P(X \mid Y) \triangleq L(Y \mid X)$ is called the likelihood for Y given X.

Generally, the main objective of Bayesian method in statistical problems is obtaining the posterior distribution of model parameters. To determine the posterior function, both sets of the parameters before data is observed (prior distribution) and parameters contained in the observed data (likelihood function) are taken into account.

The basic Bayesian method includes:

1. Formulate a probability data model

This process involves deciding on a probability distribution for the data if the parameters were known. If the n data values to be observed are $x_1, \ldots, x_n$, and the vector of unknown parameters is denoted Y, then, assuming that the observations are made independently, we are interested in choosing a probability function $P(x_i \mid Y)$ for the data (the vertical bar means "conditional on" the quantities to the right)

2. Decide on a prior distribution

Prior distribution of a parameter is the probability distribution that represents and quantifies the uncertainty about the parameter and in the values of the unknown model parameters before the current data are observed. It can be viewed as representing the current state of knowledge, or current description of uncertainty, about the model parameters prior to data being observed.

3. Observe the data, and construct the likelihood function

The likelihood function, or simply likelihood is the joint probability function of the data. Once the data has been observed, likelihood is developed based on the observed data and the formulated probability model from the first step. Posterior distribution is then determined by combining the likelihood and the prior distribution to quantify the uncertainty in the values of the unknown model parameters after the data are observed.

4. Calculate statistical outputs

Based on the posterior distribution, the summary of important features and quantities of interest are calculated.

Approaches to choosing a prior distribution divide into two main categories. Informative prior distribution and non-informative prior distribution. In informative prior distribution, the statistician uses his knowledge about the substantive problem perhaps based on other data, along with elicited expert opinion if possible, to construct a prior distribution that properly reflects his (and experts') beliefs about the unknown parameters. The notion of an informative prior distribution may seem at first to be overly subjective and unscientific.

The second main approach to choosing a prior distribution is to construct a non-informative prior distribution that represents ignorance about the model parameters. Besides non-informative, this type of distribution is also called objective, vague and diffuse, and sometimes a reference prior distribution. Choosing a non-informative prior distribution is an attempt at objectivity by acting as though no prior knowledge about the parameters exists before observing the data. This is implemented by assigning equal probability to all values of the parameter (or at least approximately equal probability over localized ranges of the parameter). The appeal of this approach is that it directly addresses the criticisms of informative prior distributions as being subjectively chosen. In some cases, there is arguably a single best non-informative prior distribution for a given data model, so that this prior distribution can be used as a default option, much like one might have default arguments in computer programs.

Once the data has been observed, the likelihood function, or simply the likelihood,

is developed. The likelihood is the joint probability function of the data, but viewed as a function of the parameters, treating the observed data as fixed quantities. Assuming that the data values, X = (x_1. . . x_n) are obtained independently, the likelihood function is given by:

$$L(Y \mid X) = P(x_1, \ldots, x_n \mid Y) = \prod_{i=1}^{n} P(x_i \mid Y) \quad (1.16)$$

In the Bayesian framework, all of the information about Y coming directly from the data is contained in the likelihood. Values of the parameters that correspond with the largest values of the likelihood are the parameters that are most supported by the data.

Li et al. (2009) employed Bayesian model averaging method in groundwater models to predict groundwater head by incorporating multiple groundwater models and multiple hydraulic conductivity estimation. In this model, the estimation of hydraulic conductivity in a groundwater model is considered as a method weight in calculating the marginal likelihood function. In this study, to determine the posterior probability of head (h) for given dataset (D), the model probability for model $M^{(p)}$, and the expectation operator (E_M) over simulation models is considered.

$$P(h \mid D) = E_M[P(h \mid M^{(p)}, D)] = \sum P(h \mid M^{(p)}, D)\, P(M^{(p)} \mid D) \quad (1.17)$$

P(h | $M^{(p)}$, D) is the posterior probability of heads for given data set D and groundwater model $M^{(p)}$ and P($M^{(p)}$ | D) is the posterior model probability for model $M^{(p)}$ or posterior model weight for model $M^{(p)}$.

$$P(M^{(p)} \mid D) = \frac{P\left(D \mid M^{(p)}\right) P(M^{(p)})}{\sum_P P(D \mid M^{(p)})\, P(M^{(p)})} \quad (1.18)$$

By assigning $\theta^{(p)}$ as a hydraulic conductivity estimation methods for model M(p),

$P(\theta^{(p)} \mid M^{(p)}, D)$ represents the method weight for $\theta^{(p)}$ in groundwater model $M^{(p)}$ given data D. It is commonly used to represent the combined BMA model weight for each combination of models and methods.

$$P(M^{(p)}, \theta^{(p)} \mid D) = P(\theta^{(p)} \mid M^{(p)}, D)\, P(M^{(p)}, D) \tag{1.19}$$

According to Bayes' rule, the method weight is

$$P(\theta^{(p)} \mid M^{(p)}, D) = \frac{P(D \mid M^{(p)}, \theta^{(p)})\, P(\theta^{(p)} \mid M^{(p)})}{\sum P(D \mid M^{(p)}, \theta^{(p)})\, P(\theta^{(p)} \mid M^{(p)})} \tag{1.20}$$

Where $P(D \mid M^{(p)}, \theta^{(p)})$ is the marginal likelihood function for a given model $M^{(p)}$ and a given method $\theta^{(p)}$ and it is commonly approximated using the Laplace approximation with the Bayesian information criterion (BIC).

$$P(D \mid M^{(p)}, \theta^{(p)}) \approx \exp[-0.5 \times BIC^{(p)}] \tag{1.21}$$

$$BIC^{(p)} = Q^{(p)} + n \ln 2\pi + m^{(p)} + \ln n \tag{1.22}$$

Where

$$Q^{(p)} = (h^{cal} - h^{obs})^T C_h^{-1} (h^{cal} - h^{obs}) \tag{1.23}$$

$Q^{(p)}$: the sum of squared weighted residuals of head

h^{obs}: the observed groundwater head

h^{cal}: the calculated groundwater head,

n: the number of the observed groundwater heads

C_h: the covariance matrix, a diagonal matrix for independent groundwater head errors. The variances in C_h are estimated by running a sufficient number of realizations of the data weighting coefficients:

$$\sigma_i^2 = \frac{1}{P \times Q \times M} \sum_{p=1}^{P} \sum_{q=1}^{Q} \sum_{m=1}^{M} \left(h_i^{cal} - h_i^{obs}\right)^2 \quad (1.23)$$

$i = 1, 2, \ldots, n$

Where *M* is the number of realizations of the data weighting coefficients, *P* is the number of simulation models, and *Q* is the number of the estimation methods.

To evaluate the applicability of Bayesian method in dam safety and seepage monitoring, some studies focused on theoretical framework and procedure of using Bayesian networks in this scope. Smith (2006) conducted dam risk analysis and considering dam risks in a more global and holistic way using Bayesian network. Li et al. (2007) evaluated the reliability of embankment dams and comparing the approach with the fault tree analysis. However, in these researches the practical uses of Bayesian networks had not been studied, either for a specific dam or a group of dams.

Mirosław-Świątek et al. (2012) developed a Bayesian Belief Nets to analyze seepage anomalies of Klimkówka Dam in Poland by using two types of information: water pressure measurements using piezometers and drainage discharge measurements using discharge flumes. In this study, the status of two seepage controlling structural elements were observed via a set of upstream and downstream piezometers and drainage discharge rate. These two seepage controlling structures are cement screen on the upstream slope and clay core. The potential causes of any abnormal behavior in piezometers or drainage discharge is either leaks through the cement screen (A_1) or clay core (A_2), or failure (plugging) of the drainage system (A_3) with state = T if the element is damaged and state = F if not. The abnormal behaviors are determined in upstream piezometers (B_1), downstream piezometer (B_2), and drainage discharge (B_3) where the water level in piezometers is high or discharge will increase with state = UP, otherwise state = DOWN.

Figure 8 shows the Bayesian Probability Network and the conditional probability table if the downstream piezometers show abnormal behavior. The probability quantities presented in the conditional probability table are the principal contribution of the expert knowledge. In **Figure 1.18**, the conditional probability table shows the probability of water level increases in downstream piezometers for different statuses of wall leakage, core leakage and drain failure.

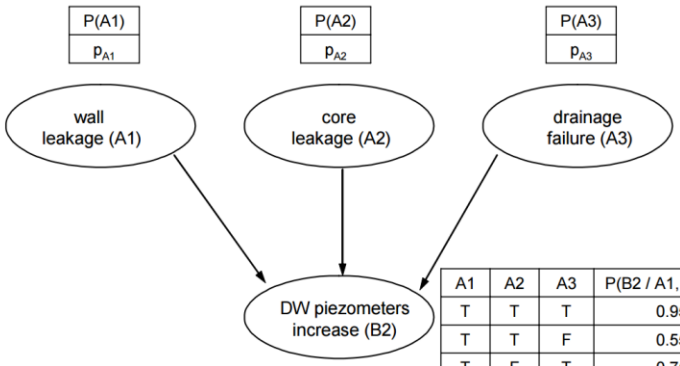

A1	A2	A3	P(B2 / A1, A2, A3)
T	T	T	0.95
T	T	F	0.55
T	F	T	0.75
F	T	T	0.85
F	F	F	0.50
F	F	T	0.80
F	T	F	0.55
T	F	F	0.55

Figure 1.18 Bayesian Probability Network for abnormal behavior in downstream piezometer of Klimkówka Dam, Poland.
Source: Application of the Bayesian Belief Nets in dam safety monitoring (Mirosław Świątek et al., 2012).

These model has been employed as the basis for both forward and backward propagations. In forward propagations, the probability of potential causing incidents (A_1, A_2, A_3) are assigned as prior information and the probability of monitoring result incidents (B_1, B_2, B_3) are calculated. **Figure 1.19** is presenting the results of forward propagation with the assumption of prior probabilities of A_1, A_2, and A_3 are equal to 0.5. For this scenario, the results show that the most likely response will be the lowering of the water level in upstream piezometer (B_1), with p = 0.75.

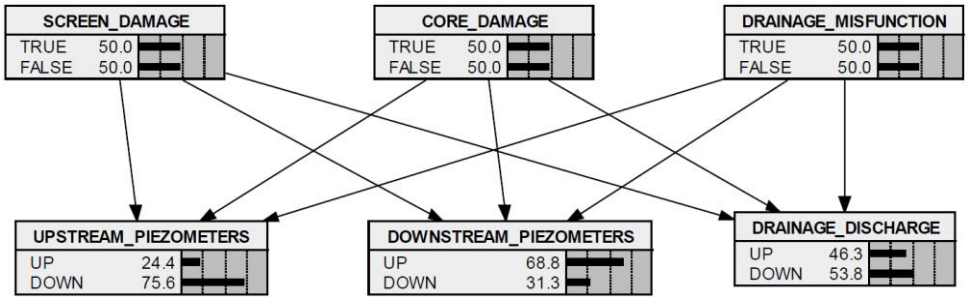

Figure 1.19 Forward propagation - P(A1) = P(A2) = P(A3) = 0.5.
Source: Application of the Bayesian Belief Nets in dam safety monitoring (Mirosław Świątek et al., 2012).

In backward propagation, the probability of the status of monitoring result incidents (B_1, B_2, B_3) are determined as prior information and the probability of the potential causing incidents (A_1, A_2, A_3) are calculated. **Figure 1.20** shows the probabilities of A_1, A_2, A_3, and B_1, if we know the water level in downstream is high and the drainage discharge is low. According to the results, the most probable cause for this scenario is malfunctioning of the drainage system with P = 82.2%.

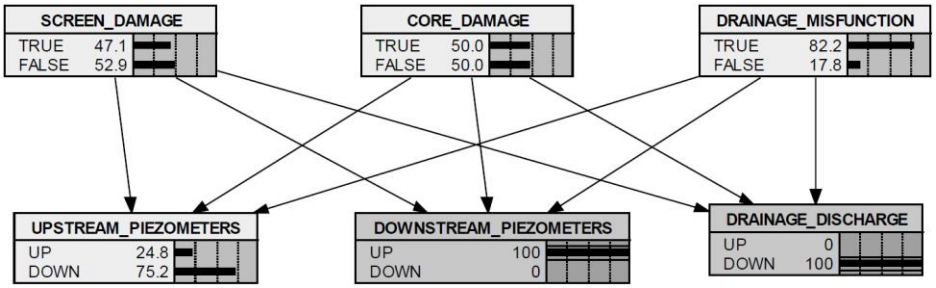

Figure 1.20 Backward propagation - P(B2) = 1, P(B3) = 0.
Source: Application of the Bayesian Belief Nets in dam safety monitoring (Mirosław Świątek et al., 2012).

Zhang et al. (2011) developed a probability-based tool by using Bayesian networks for the diagnosis of embankment dam distresses at the global level based on past performance records and conducted the diagnosis of a specific distressed dam by incorporating global-level knowledge from the database and project-specific evidence. In this research, and according to the database of 993 in-service dams in China, general

characteristics and the common patterns of distress in embankment dams were studied using Bayesian network. The interrelations among the dam distresses and their causes are quantified using conditional probabilities determined based on the historical frequencies from the dam distress database and the most important distress factors were identified through a sensitive analysis. Finally, by combining global-level performance records and project-specific evidence in a systematic structure, a specific distressed dam was studied and key distress factors was identified. **Figure 1.21** shows the summary of causal networks for diagnosing distresses associated with seepage erosion–piping of homogeneous–composite clay-core dams at global-level performance. **Table 1.3** illustrates definitions of the symbols in the causal networks.

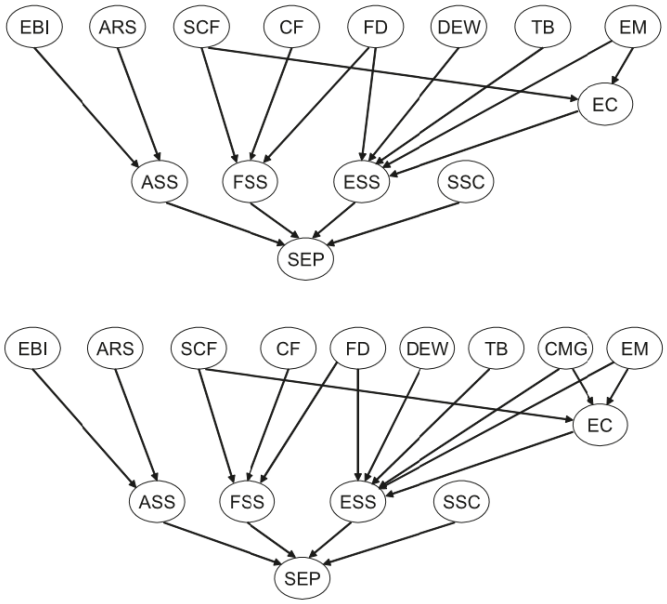

Figure 1.21 Summary of causal networks for diagnosing distresses associated with (a) seepage erosion–piping of homogeneous–composite dams, and (b) seepage erosion–piping of clay-core dams.
Source: Diagnosis of embankment dam distresses using Bayesian networks. Part I. Global-level characteristics based on a dam distress database (Zhang et al., 2011).

In this study, based on the dam distress database, an inventory of possible dam distresses and corresponding causes has been constructed. The probability of each element

is determined by judgment based on historical information and knowledge. Then, all possible distress mechanisms were identified and presented in the form of a causal network to develop a Bayesian network for diagnosing distresses of an embankment dam. By this method the probability of occurring seepage caused by any of the factors and consequently the most important distress causes by comparing the importance index relevant factors are identified. According to the result, the identified locations that is playing the predominant role for seepage erosion–piping in the clay-core dam is along embedded culverts while the second most important locations are at the foundation and in the embankment.

Table 1.3 Variables Involved in Diagnosing Distressed Embankment Dams

		State	
Node code	Variable	Number	Description
ARS	Abutment rocks or soils	2	Satisfactory, unsatisfactory
ASS	Abutment seepage situation	4	Normal, unstable, moderate leakage, serious leakage
CF	Cutoff at foundation	2	Satisfactory, unsatisfactory
CMG	Clay-core materials and geometries	2	Satisfactory, unsatisfactory
DEH	Designed embankment height	2	Satisfactory, unsatisfactory
DEW	Designed embankment width	2	Satisfactory, unsatisfactory
EBI	Embankment–abutment interface	2	Satisfactory, unsatisfactory
EC	Embankment cracking	2	Occurred, nonoccurred
ECE	Embankment crest elevation	2	Satisfactory, unsatisfactory
EM	Embankment materials	2	Satisfactory, unsatisfactory
ES	Embankment settlement	2	Normal, excessive
ESP	Emergency spillway	3	Satisfactory, moderately unsatisfactory, seriously unsatisfactory
ESS	Embankment seepage situation	4	Normal, unstable, moderate leakage, serious leakage
FD	Filtered drainage	2	Satisfactory, unsatisfactory
FDC	Flood design criteria	2	Satisfactory, unsatisfactory
FRC	Flood-releasing capacity	2	Satisfactory, unsatisfactory
FRT	Flood-releasing tunnel	3	Satisfactory, moderately unsatisfactory, seriously unsatisfactory
FSS	Foundation seepage situation	4	Normal, unstable, moderate leakage, serious leakage
GLD	Gates and lifting devices	3	Satisfactory, moderately unsatisfactory, seriously unsatisfactory
OT	Overtopping	2	Yes, no
PS	Primary spillway	4	Satisfactory, moderately unsatisfactory, seriously unsatisfactory, no spillway
PW	Parapet wall	2	Satisfactory, unsatisfactory
RBSS	Reservoir bank slope stability	2	Satisfactory, unsatisfactory
RSS	Reservoir sedimentation situation	2	Satisfactory, unsatisfactory
SCF	Sludge cleaning at foundation	2	Satisfactory, unsatisfactory
SEP	Seepage erosion or piping	2	Yes, no
SSC	Seepage situation around embedded culverts	4	Normal, unstable, moderate leakage, serious leakage
TB	Termite burrows	2	Occurred, nonoccurred
WRC	Water-retaining capacity	2	Satisfactory, unsatisfactory

Source: Diagnosis of embankment dam distresses using Bayesian networks. Part I. Global-level characteristics based on a dam distress database (Zhang et al., 2011).

In a separate study, Xu et al. (2011) attempted to extend the technique of Bayesian networks to the diagnosis of a specific distressed dam by combining global-level

knowledge from the database and project-specific evidence on the diagnosis of a distressed embankment dam, with seepage problems. In this case, the total seepage rate, seepage exit location and boundary condition of the embankment are known. The coefficients of permeability of the earthfill (K_1) and the drainage (K_3), are incorporated into the existing causal network **Figure 1.21(a)**, and a new causal network is obtained, as shown in **Figure 1.22**. K_1 and K_3 are assumed as discrete variables with two states, "satisfactory" and "unsatisfactory".

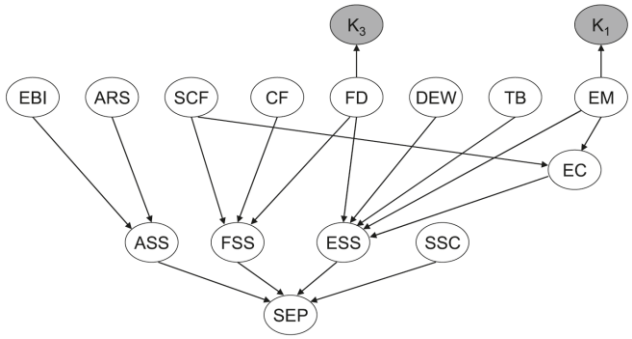

Figure 1.22 Causal networks for diagnosing the distressed studied dam.
Source: Diagnosis of embankment dam distresses using Bayesian networks. Part II. Diagnosis of a specific distressed dam (Xu et al., 2011).

The analysis of determining the distresses associated with seepage in the studied case is starting without considering the knowledge on K_1 and K_3 deduced from the project-specific evidence on the measured seepage rate. In the first step the probability of embankment seepage situation (ESS) is updated considering there are no seepage problems at the abutment (ASS), through the foundation (FSS), and along the embedded culverts (SSC). In order to combine the global-level data with the local-level evidence, the actual seepage volume was measured and by developing a software model of the dam, the value of permeability of the earth-fill and the drainage are estimated. Comparing the estimated permeability with a specified design requirement, corresponds to the two states of K_1 and K_3: "satisfactory" and "unsatisfactory". Based on the back-analysis results, the state of

nodes K_1 and K_3 are assigned and considering the states of nodes ASS, FSS, and SSC are still set to be normal based on the field evidence, the probabilities for the nodes relevant to node ESS in **Figure 1.22** is automatically updated. In this model, the observations are the field evidences of the states of nodes ASS, FSS, and SSC and the seepage volume measurement to estimate permeability. The posterior probabilities are the updated probabilities based on the observations. **Table 1.4** shows the prior and posterior probabilities for the variables relevant to embankment seepage erosion-piping.

Table 1.4 Probability Table for the Variables Relevant to Embankment Seepage Erosion–Piping for the Studied Dam

		Probability	
Variable	State	Prior	Posterior-I
Clay-core materials and geometries (CMG)	Satisfactory	—	—
	Unsatisfactory	—	—
Designed embankment width (DEW)	Satisfactory	0.9300	0.9300
	Unsatisfactory	0.0700	0.0700
Embankment cracking (EC)	Satisfactory	0.9640	0.9220
	Unsatisfactory	0.0360	0.0780
Embankment materials (EM)	Satisfactory	0.5390	0.0000
	Unsatisfactory	0.4610	1.0000
Embankment seepage situation (ESS)	Normal	0.4879	0.1324
	Unstable	0.0931	0.1730
	Moderate leakage	0.2154	0.3785
	Serious leakage	0.2036	0.3161
Filtered drainage (FD)	Satisfactory	0.8432	1.0000
	Unsatisfactory	0.1568	0.0000
Seepage erosion or piping (SEP)	Yes	0.0141	0.0223
	No	0.9859	0.9777
Termite burrows (TB)	Occurred	0.1410	0.1410
	Nonoccurred	0.8590	0.8590

Source: Diagnosis of embankment dam distresses using Bayesian networks. Part II. Diagnosis of a specific distressed dam (Xu et al., 2011).

1.3.5 Summary of Literature Review

In order to address safety, it is essential to monitor seepage and internal erosion in earth embankment dams. Various methods of monitoring and inspection have been presented by different US national organizations and scholars as guidelines, safety manuals and research studies. Visual inspection, piezometers and observing wells, temperature measurement and fiber optics, electrical resistivity, Seismic monitoring, Self-Potential, Ground Penetrating

Radar and Electromagnetic Surveying are the common methods for monitoring of seepage and internal erosion in earth dams with advantages and limitations for each method. However, among the geophysical monitoring methods, Electrical Resistivity Tomography (ERT) is probably the most popular method in seepage monitoring. Many studies have employed ERT in detecting potential seepage areas in the earth dams and confirmed the accuracy and reliability of this method.

To evaluate the seepage behavior according to the available data and observation data obtained via one or more monitoring methods, a probability method is essential to present and analyze the information in a mathematical form. Although different probability models have been proposed to analyze dam safety and internal erosion, Bayesian Probability Network is probably one of the most common and reliable methods in seepage studies of earth dams. Within two case studies implemented on real case studies, the applicability of this method has been discussed and analyzed.

CHAPTER 2

STATISTICAL DATABASE

2.1 Introduction

For better understanding of behavior of earth dams in seepage incidents and diagnosis of potential seepage and distressed zones, a database of past incident needs to be acquired to determine the possible location and probability of each source. Therefore, the seepage incidents in 182 earth dams were studied and the location of distress was identified. The sources of distressed locations were categorized into five classes labeled as: Embankment, Foundation, Abutment, Around Embedded conduits, and Unknown. This database will be employed as the global-level common patterns and causes of distresses characteristics to develop the Bayesian probability model and will be further used to update the probability model to diagnose a specific distressed studied dam at a local level by combining global-level performance records and project-specific evidence in a systematic structure.

The second set of statistical data was collected and analyzed to assess the certainty of Electrical Resistivity results in determining the location of the seepage flows. Twenty-two cases studies, where the seepage was monitored via Electrical Resistivity method were studied and the ER results were compared against the observed leakages and/or investigation results with other monitoring methods.

In this chapter, the process of collection and analysis of the data as well as some statistical reports for each set of database is presented.

2.2 Dam Seepage Zone Database

A total of 182 distressed dams suffering from concentrated seepage in the USA are

compiled into a database, including general information on the dams and the identified distressed zones. These zones were categorized into 5 classes labeled as:

- Embankment; if the source of distress was detected in the embankment
- Abutment; if the source of distress was detected in any of the abutments or the dykes
- Foundation; if the source of distress was detected in the foundation
- Around embedded conduits; if the source of distress was detected around any of the embedded conduits like culverts, pipes, spillways, etc.
- Unknown; if the source of distress was not detected or not reported

The list of the studied cases is presented in **Appendix A**. For each dam, general information and statistical data of the seepage incident is studied and analyzed.

According to the survey, out of 182 seepage incidents, in 28 cases final failure of the dams was reported, 2 unknown destiny and 152 incidents without the failure. In other word, about 15% of the seepage incidents were resulted in the final failure of the earth dams. Analyzing the distressed zones of the studied dams in the dataset revealed in 24 cases the distressed zone was located in abutments which results in 4 failures (about 17%) and 1 unknown destiny. 3 earth core dams, 1 homogeneous and 20 unknown or unreported types of dams were suffering from seepage in abutments according to the database. In 44 cases the distressed zone was detected in the embankment of the studied dams including 7 homogeneous, 2 concrete core, 1 earth core, 1 masonry core, 1 upstream facing plastic and 32 unknown or unreported types of dams. Total number of 9 failure incidents (20%) was reported for the detected seepage in embankment of the studied dams. The minimum number of incidents was reported in the foundation of the studied dams, that out of 9

incidents, only 2 failures were reported. In contrary, the maximum number or leakage distressed zones was reported around the embedded conduits. Embedded conduits are considered as all the culverts, pipes and spillways are passing through the dam and mainly where soil is in adjacent and contact with other materials such as concrete or ductile iron pipes. Total number of 63 incidents were reported for seepage around embedded conduits in the soil dams where in 8 cases it resulted in failure. According to the database, 6 homogeneous, 5 earth core, 1 metal core, 1 concrete core and 50 unknown/unreported cases were determined for this class of study. In 42 seepage incidents, the distressed zones were either not detected or reported and the source of the seepage is unknown.

By eliminating the results with unknown distressed zone and normalizing the data, the probability of seepage zone of each class can be estimated. **Table 2.1** compares the percentage of the seepage incidents within different classified zones in earth embankment dams.

Table 2.1 Distribution of Seepage Source Location in Earth Dams

Seepage location	Number of incident	% of incident	Number of failure	% failure
Abutment	24	17.1%	4	16.7%
embankment	44	31.4%	9	20.5%
Foundation	9	6.4%	2	22.2%
Around embedded culverts, pipes, spillway	63	45.0%	8	12.7%

2.3 Electrical Resistivity Database in seepage monitoring

As discussed on Chapter 1, Electrical Resistivity Tomography (ERT) is one of the most common flow detection methods in seepage monitoring of the dams. Numerous case studies showed the accuracy and reliability of this investigation method in detecting zones with anomalous behavior in dam leakage studies. In this section, twenty two case studies

were pursued to evaluate the effectiveness and resolution of the ERT method in detecting seepage distressed zones of soil dams. For this purpose, the general characteristics of each dam like location, type, size and soil type was summarized in a table. In each case study, the seepage investigation was implemented with at least two different methods including ERT and one or more other methods were explicated in Chapter 1. In many of the cases, the leakage was observed visually. However, in some incidents, visual inspection did not discover any sign of flow and instead, the other seepage monitoring tools detected symptoms of abnormal behaviors.

The applied methodology to analyze and develop the database is based on the sensitivity of ERT in locating the leakage zones which were already detected by the other monitoring methods or visual inspection. For this purpose, in each case, total number of leakage zones detected by other monitoring method but ERT are assessed and checked against the areas where anomalies were located by ERT. In the majority of the studied cases, ERT detected all the areas were addressed by the other methods or visual inspection. In some of the cases, more anomalies were detected by ERT than the other methods. But, since there was no evidence to evaluate the validity of those additional detected zones, they were excluded from sensitivity analysis of ERT accuracy evaluation. Just in two incidents ERT results were slightly off from the detected leakage zones located by the other investigation methods. According to this dataset, through the total 22 seepage monitoring case studies of soil dams, ERT method detected total number of 52 anomalies that could be indications of saturated zones and flow path inside the studied dams. Out of 52 suspicious seepage zones indicated by ERT, existence of flow was confirmed by other investigation methods also in 40 cases. ERT missed the flow zones, detected by the other

methods in two cases and in 12 other zones where just ERT detected anomalies, no other method reported whether there was a seepage or any other signs of distress. Based on the analysis, on average ERT detected 98% of the anomaly zones were already detected by the other investigation methods.

The detailed analysis of the case studies is presented in **Appendix B**. **Table 2.2** summarizes the findings of the analysis.

Table 2.2 Summary of Statistical Results of Applying ERT in Seepage Detection of Embankment Dams (Continued)

No.	Type	Location	Height	Length	Method	Anomaly Zones Detected by Other Methods (than ERT)	Anomaly Zones Detected by ERT	% precision of ERT
1	Earthfill Dam	Colorado	11 m	122 m	ERT, SP, OL	3 SP (1 was confirmed by OL)	3 (same zones as detected by other methods)	100%
2	Dam (model)	Lab model	1.5m	3.6m	ERT, OL	1 OL	1 (same zone as detected by other method)	100%
3	Dam (model)	Lab model	1.5m	3.6m	ERT, OL	2 OL	2 (same zones as detected by other method)	100%
4	Dam (model)	Lab model	1.5m	3.6m	ERT, OL	2 OL	2 (same zones as detected by other method)	100%
5	Dam Lake	Hama City, Syria	55m	2870m	ERT, OL	1 OL	1 (same zone as detected by other method)	100%
6	Saddle dam #1	India	Not Reported	550m	ERT, SP, OL	3 SP (1 was confirmed by OL)	5 (3 zone are the same as detected by other methods)	100%
7	Saddle dam #3	India	19.5m	290m	ER, SP, PP	3 SP (1 flowpath was confirmed by PP)	4 (3 zone are the same as detected by other methods)	100%
8	Earthfill Dam	California	34.5m	815m	ERT, OL	2 OL	2 (same zones as detected by other method)	100%
9	Homogeneous earth dam	Nigeria	Not Reported	300m	ERT, SR	Lower seismic velosity zone btw dpth 4-12(m)	4 low ER zones btw dpth 4-8(m)	87%

Table 2.2 (Continue) Summary of Statistical Results of Applying ERT in Seepage Detection of Embankment Dams

No.	Type	Location	Height	Length	Method	Anomaly Zones Detected by Other Methods (than ERT)	Anomaly Zones Detected by ERT	% precision of ERT
10	zoned earth dam	Taiwan	90m	280m	ERT, OL	1 OL	2 (1 zone is the same as detected by other method)	100%
11	Dam site	South of France	7m	110m	ERT, SP, OL	1 SP (Confirmed by OL)	1 (same zone as detected by other method)	100%
12	Zoned embankment	Hallby, Sweden	30m	120 (R) 200 (L)	ERT, VI, PM, TM	0 (on right dam), 1 (on left dam) VI, PM, TM	3 (on right dam), 1 (on left dam, same zone as detected by other method)	100%
13	tephra barrier across outlet of a lake	New Zealand	Not Reported	Not Reported	ERT, VI	1 VI (final collaps occurred at this location)	1 (same zone as detected by other method)	100%
14	Soil dam	Saudi Arabia	Not Reported	Not Reported	ERT, SR	2 SR	2 (same zones as detected by other method)	100%
15	Embankment dam	South Korea	20m	300m	ERT, OL	2 OL	3 (2 zones are the same as detected by other methods)	100%
16	Embankment dam	Norway	5.5m	40m	ERT	4 Built-in flow paths in embankment	3 zones were detected, 1 zone missing	75%
17	Embankment dam	Taiwan	90m	282m	ERT, PP	2 PP	2 (same zones as detected by other method)	100%
18	Homogeneous earth dam	Washington county, MO	10m	100m	ER, SP	1 SP	1 (same zone as detected by other method)	100%
19	homogeneous earth-fill dam	Colorado	4m	427m	ERT, SP, SR, PP	1 SP & SR (confirmed by PP)	1 (same zone as detected by other methods)	100%
20	Dyke	India	3.65m		ERT, SR, OL	1 SR (confirmed by OL), 1 OL	3 (2 zones are the same as detected by other methods)	100%
21	tailing dam with core	southern Sweden	27m	807m	ERT, VI	2 VI (2 sinkholes observed)	2 (same zones as detected by other method)	100%
22	Not Reported	China	Not Reported	Not Reported	ERT, OL	2 OL	4 (3 zones are in the same area addressing 1 of the leakage zone, other zone is in the same area as detected by other methods)	100%
							Average =	98%

where

- ERT: Electrical Resistivity Tomography
- OL: Observed Leakage
- SR: Seismic Reflection/Refraction
- SP: Self-Potential
- PP: Pizometer Pressure Measurement
- TM: Temperature Measurement
- VI: Visual Inspection

CHAPTER 3

SITE INFORMATION AND DATA COLLECTION

3.1 Introduction

The process of the safety investigation of the studied dam starts with preparing a profile comprises the history and initial condition evaluation of the dam. The information is mainly collected from a previous inspection report prepared by a third party and initial site visits performed by the research team. Then, based on the existing condition of the dam and available data, an investigation method and data collection procedure for the first phase of inspection is identified and implemented.

3.2 Site Information

The studied dam is an earth embankment dam with a concrete core wall, located in northern New Jersey. The height of the dam is about 60 ft. It has an ogee spillway and four low level outlets located on the gatehouse. The crest of the dam is about 20 ft. wide, paved and has two lines of guard rails along the both sides. The safety assessment of the dam is currently performed based on visual field inspection. Such inspections have been mere snapshots of the visually detected conditions performed at scheduled times that may not provide a thorough evaluation of safety condition of the dam.

3.3 Preliminary Assessment and Visual Inspections

3.3.1 Site History

The first stage of the study reviews the report of the inspection performed and prepared by

a professional third party consultant on December 2014. The summary of the inspection includes:

- The downstream toe immediately upstream and about 67 ft. from the right end of the concrete jersey barriers is soft and moist
- A spring and pool of standing water is located immediately downstream of the concrete jersey barriers along downstream toe
- Seepage at downstream toe at right abutment that was previously reported was not observed during 2014 inspection
- Standing water previously observed along upstream edge of Jersey barriers approximately 70 ft. from right of the abutment was not observed during 2014 inspection
- Concentrated leakage inside of the gatehouse chamber located behind the staircase along the right side of the gatehouse wall
- Several concentrated leaks were observed in the mortar at the bottom right chamber of gatehouse
- Small burrow was observed at the top of the upstream slope within the grass near the edge of crest pavement
- Concrete delamination of the gatehouse wall along the upstream face of the wall at normal pool level
- Some spalling of a vertical joint near the center of the gatehouse below normal pool level
- Numerous animal burrows observed throughout the downstream slope
- Some localized depressions in the main embankment where runoff crosses mid-level bench
- A 4-foot wide depression was observed along the lower portion of the slope near the center of the dam
- Two areas of significant erosion were observed along the outside of the mortared stone-wall near the downstream end of the spillway training wall
- A small spall was observed in the concrete sill at the far left side of the discharge channel apron surrounded by a circular wet area in the concrete
- Significant erosion along the top of the left outlet channel bank just upstream of the

footbridge since 2011 inspection

- 2011 and 2012 inspection reports indicated that there were seven transverse cracks were observed along the asphalt crest. Two new transverse cracks were observed during 2014 inspection. The wideness of the cracks range between 3/8" to a maximum of about 2"

- Mid-level bench is slightly irregular and not level. Some slight depressions were observed along the contact with the upper center abutment

3.3.2 Visual Inspection

Visual site investigations were performed during fall 2015, spring 2016 and winter 2017.

3.3.2.1. Fall 2015

Several site investigations were performed during fall 2015. The reservoir water level elevation was measured as 13' below the crest. The following issues were observed during the inspections.

At the downstream toe immediately upstream of the concrete jersey barriers and at station about 0+70 from the right end of the jersey barriers is a soft and moist zone. A 4 ft. metallic bar was used to check the stiffness of the soil. The bar could easily penetrate into the soil at this area and soil seems to be saturated at the larger depth (**Figure 3.1**). This zone was also reported in the 2014 inspection report.

Figure 3.1 Detection of wet soft soil at the downstream toe.

Immediately downstream of the concrete jersey barriers along downstream toe, there is a spring and pool of standing water stands. This incident was reported since 2014. However, more investigation revealed the exact location of the outflow that located at station 0+70 from right end and 10’ downstream of the of the jersey barriers (**Figure 3.2**). Standing water at this area was reported in the previous inspection reports, however this zone was not observed within the 2014 inspection.

Figure 3.2 Standing water and seepage outflow downstream of the parapet jersey barriers.

The outflow water was clear and no sign of piping/erosion was observed visually. The temperature of the outflow water was measured as 39.4° F while the water temperature at the surface of the reservoir was measured as 38.2° F, indicating the source of water with high certainty is within the reservoir rather than the underground water. Site investigation revealed an area downstream of the right abutment where large numbers of the trees were fallen. **Figure 3.3** is an aerial photo clearly shows this zone. Slight change in vegetation was also discovered in this area. The fallen trees and change in vegetation could be a sign of moist or saturated soil in this region.

Figure 3.3 Area with the fallen trees downstream of the right abutment

Several transverse cracks were observed along the crest in the pavement. Cracks were extended across the asphalt pavement (**Figure 3.4**). These cracks were reported since 2011 and the wideness of the cracks was between 3/8” and 2”.

Figure 3.4 Transverse cracks along the crest.

3.3.2.2. Spring 2016

Second series of the visual inspection was performed during May 2016 to evaluate the dam’s condition and the following cases were observed.

Eight transverse cracks were observed in the pavement along the crest. These cracks

were also observed during previous inspections. All the cracks were extended all across the pavement. The widths of the cracks were between 0.5” to 2”. **Figure 3.5** shows the locations of the cracks on the dam and statements about each one. Four of the cracks were dry (cracks #1, 2, 3, 7) whereas grass and lawns were growing out of the other four (cracks #4, 5, 6, 8). The vegetated cracks were mainly located on the east side of the dam. Growing grass through the cracks could be an indicator of existence of wet soil at these areas. Crack #7 was not observed during the previous inspection and looks like a new crack. The wideness of this crack was measured as 0.5”.

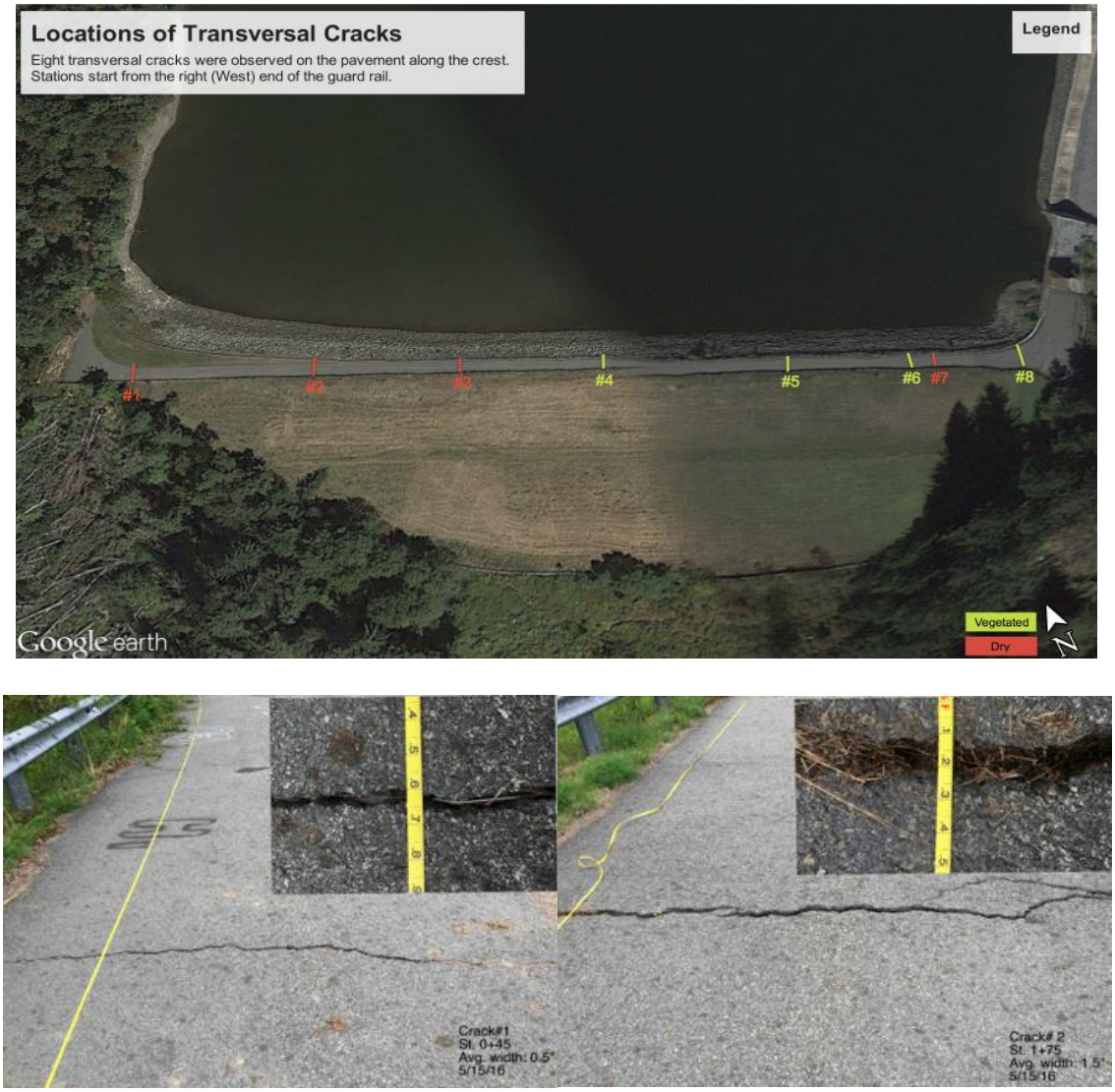

Figure 3.5 Location and status of observed transverse cracks along the crest (Continued).

Figure 3.5 (Continued) Location and status of observed transverse cracks along the crest.

The reservoir level was measured about 8.5' below the crest elevation. Water was overflowing the auxiliary spillway. Reservoir elevation was about 4’ higher than the elevation observed during fall 2015 inspection. Saturated area was observed along the toe right upstream of the concrete jersey barriers and between stations 0+40 and 1+00 from the right end of the wall. An active seepage outflow was previously observed at station 0+70

and 10' downstream of the jersey barriers during the visit in fall 2015 was not observed during this inspection. However, water is flowing out of an opening in the jersey barriers (outflow# 2) around the same station. The flowing water was clear and no sign of piping was observed visually.

Figure 3.6 Detected downstream outflows.

Additional flow (outflow #1) was observed coming out of the west corner of the toe and along the downstream of the concrete jersey barriers and merges to outflow #2 at station about 0+70 from the right end and 10' downstream of the barriers. As this flow was traced, the outflow spot was located within a pond 8' downstream of the jersey barriers and at station about 0+20 from the right end. A T-section shape barrier in this area created a pond and water is blowing out of the ground into the pond. Then water seeps below the barriers and merges to the other flow. The flowing water from the pond was clear with no

sign of piping. **Figure 3.6** shows the detected outflows at the toe of the dam. **Figure 3.7** is showing the location of the Outflow #1 from the upstream side.

For Outflow #1 although the discharge flow is clear, it is possible the washed out sediments were deposited within the pond and just clear water is flowing out. The area around the pond and along the right abutment is covered with dense bushes and fallen trees, which limited the access to these areas. As reported in 2014 inspection, some slight depressions were observed at mid-level bench along the contact with the upper center abutment. Depression could be a sign of washing out of soil materials that results in subsidence of the ground at the depressed zone.

Figure 3.7 Location of blowing spring. Looking from the downstream slope towards the toe.

An area of standing water was observed around station 2+60 from the right end and about 30’ downstream of the concrete jersey barriers. The outflow spot for this standing water was not detected via visual inspection. No sign of sinkhole or settlement was observed on the embankment and the left abutment. The standing water looks like to be contaminated. **Figure 3.8** shows the location of this swamp and contaminated water.

Figure 3.8 Location of standing water downstream of the jersey barriers at station around 2+60.

3.3.2.3. Winter 2017

Final series of site inspection was performed during winter 2017. Reservoir water elevation was measured at about 18 feet below the crest elevation, which is calculated as 42 feet from the dam’s base. Standing water at downstream toe and around station 2+60 from the right end and about 30’ downstream of the concrete jersey barriers was not observed during this

inspection. Also, no flow was observed at outflow #2 and a minor flow was measured at Outflow #1.

3.4 Flow Measurement

Two weirs were installed at downstream of the concrete jersey barriers in order to measure the discharge from Outflows #1 and 2. For each Outflow the amount of discharge was calculated via weir formulation as well as manually. Outflow discharges were measured during three seasons with different reservoir elevation. The upstream water elevation was estimated as 42 ft., 47 ft. and 51 ft. for seasons of winter, fall, and spring.

3.4.1 Weir #1

Weir #1 is an orifice weir, built from 0.5" sheetrock with dimensions of 36"(w) x 24" (h) x 36"(L) and 1" diameter orifice located 11" above the base. The weir is installed at St. 0+80 from the right end and 25' downstream of the jersey barriers. The water level in the weir was measured 15" above the base and 4" above the orifice. Weir #1 is measuring the accumulation of discharge from flows #1 and #2 at the toe. Flow #2 was independently measured with weir #2 and the difference of discharge between weirs #1 and #2 is the discharge of Outflow #1. **Figure 3.9** shows the outflow from Weir #1 at two different seasons. Two methods were employed to measure flow from the weir #1.

The first method is measuring discharge equation of a circular sharp-crested orifice (Prabhata, 2010) by unifying viscous and potential flows.

$$Q = \pi/4\, C_d\, d^2 \sqrt{2gh} \tag{4.1}$$

where Q is the discharge, C_d is the discharge coefficient, d is the orifice diameter, g is the gravitational acceleration and h the depth of orifice center below free surface. The

discharge coefficient varies with d(gh)½ /υ, where υ is the kinematic fluid viscosity. In this equation, For very large [d(gh)½ /υ] - larger than 100 - the asymptotic discharge coefficient (C_d) may be fitted to: (Prabhata, 2010)

$$C_d = 0.611 \left(1 + \frac{4.5\,\upsilon}{d\sqrt{g.h}}\right)^{0.882} \quad (4.2)$$

Discharge from weir #1 was also measured manually multiple times and the average was calculated. A 6-inch diameter container was filled with the outflow from weir #1 multiple times and the time and height of water in the container was measured for each filling.

During fall 2015 inspection, upstream head was estimated as 47 feet from the base and the elevation of water above the orifice center was measured as 2.75 inches. Therefore:

- $\upsilon = 1.21 \times 10^{-5}$ sq.ft./s at temperature 60° F
- d = 1 inches = 0.083 ft.
- g = 32.17 ft/s
- h = 2.75 inch = 0.229 ft.
- $d \times (gh)^{1/2} / \upsilon = 1.87 \times 10^4 > 1 \times 10^2$
- $C_d = 0.611$
- $Q_1 = 0.0128$ cu ft./s (Fall 2015)

The amount of discharge was also measured with an average of 0.0109 cu ft./s manually within multiple trials.

During spring 2016 inspection, upstream head was estimated as 51 feet from the base and the elevation of water above the orifice center was measured as 4 inches. Therefore:

- h = 4.5 inches = 0.375 ft.
- $d \times (gh)^{1/2} / \upsilon = 2.39 \times 10^4 > 1 \times 10^2$

- $C_d = 0.611$
- $\underline{Q_1 = 0.0164}$ cu ft/s (Spring 2016)

The amount of discharge was also measured with an average of 0.0137 cu ft/s manually within multiple trials.

(a) (b)

Figure 3.9 Orifice weir at outflows #1 during (a) Spring 2016 and (b) Winter 2017.

During winter 2017 inspection, upstream head was estimated as 42 feet from the base and the elevation of water was measured 4.5 inches below the orifice center. Since the water elevation in the weir was lower than the orifice elevation, the discharge could not be measured with the weir calculation method. Instead the flow was channelized into a dug pit and just measured manually as 0.000083 cu ft/s.

$\underline{Q_1 = 0.000083}$ cu ft/s (Winter 2017)

3.4.2 Weir #2

Weir #2 is a triangular V-notch weir, built from sheetrock with dimensions 12”(w) x 12”(h) x 18”(l) and V-notch size of 2.5”(b) x 5”(h), installed 3 ft. downstream at station 0+80 (from right end) of the barrier wall to measure the outflow #2. **Figure 3.10** shows Weir #2 at the downstream toe. Two methods were employed to measure the flow from the weir #2.

The first method is Triangular Weir Equations using Kindsvater-Shen equation.

$$Q = 4.28\, C\, tg(\theta/2)\, (h + k)^{5/2} \qquad (4.2)$$

where:

Q = discharge in cu ft/s

C = discharge coefficient calculated

θ = Notch angle in degree

h = Head in ft.

k = Head correction factor in ft.

$C = 0.607165052 - 0.000874466963\ \theta + 6.10393334 \times 10^{-6}\ \theta^2$

$k\ (ft.) = 0.0144902648 - 0.00033955535\ \theta + 3.29819003 \times 10^{-6}\ \theta^2 - 1.06215442 \times 10^{-8}\ \theta^3$

According to the dimensions of Weir #2:

- θ = 28.07 degree
- C = 0.587
- K = 0.007 ft.

During fall 2015 inspection, upstream head was estimated as 47 feet from the base and the elevation of water above the V-Notch was measured as 1.2 inches. Therefore:

- h = 0.1 ft.
- Q_2 = 0.004 cu ft/s (Fall 2015)

The amount of discharge was also measured with an average of 0.00303 cu ft/s manually within multiple trials.

(a) (b)

Figure 3.10 V-Notch weir at outflow path #2 during (a) Spring 2016 and (b) Winter 2017.

During spring 2016 inspection, upstream head was estimated as 51 feet from the base and the elevation of water above the V-Notch was measured as 1.5 inches. Therefore:

h = 0.125 ft.

Q_2 = 0.004 cu ft/s (Spring 2016)

The amount of discharge was also measured with an average of 0.00546 cu ft/s manually within multiple trials.

During winter 2017 inspection, upstream head was estimated as 42 feet from the base and the elevation no flow was observed at Outflow #2.

Q_2 = 0.00 cu ft/s (Winter 2017)

3.4.3 Summary of Flow Measurement

Discharge from the both weirs were measured with two different methods, one manually and one according to the discharge equations for weirs. For the both weirs, the calculated error between two different methods were between 10% - 15% which is within an acceptable range. Considering there is human and instrument errors in measuring discharge with manual method, quantities calculated from weir discharge equations will be addressed as reference values.

Considering Weir #1 is measuring the joint discharge of Outflows #1 and #2 and Weir #2 is measuring the sole discharge of Outflow #2, the difference between these two measurements is representing Outflow #1 discharge. **Table 3.1** is presenting the results of field measurements for the Outflows' discharge calculated with weir formulations at three reservoir level.

Table 3.1 Measured Outflow Discharge at Three Reservoir Level

Reservoir Level (ft.)	Outflow #1 (cu ft/s)	Outflow #1 (cu ft/s)
42	0.0008	0.0000
47	0.0088	0.0024
51	0.0124	0.0040

3.5 Electrical Resistivity Survey

3.5.1 Data Collection

As discussed in **Chapter 1**, and according to the statistical data provided based on the studied cases in **Chapter 2**, Electrical Resistivity survey is one of the applicable and reliable seepage monitoring methods in earthen hydraulic structures. In order to detect the possible flows in the studied dam, three ER lines were surveyed to detect the zones with

anomaly behaviors. The location of the survey lines are:

- Along the crest and 8 feet below the guard rail on the downstream embankment, starting from right (western) end of the guard rail with total length of about 700 ft.
- Along mid-level bench starting from the right (western) abutment with total length of about 600 ft.
- Along the toe and 10 ft. upstream of the concrete jersey barriers on the slope starting from the right end of the barrier wall and total length of about 100 ft.

(a) (b)

Figure 3.11 Electrical Resistivity survey with (a) AEMC 6470-B device and (b) Wenner electrode array configurations

AEMC 6470-B device with four electrodes was used to measure resistivity of about 330 points along the three surveying lines. Wenner electrode array configuration was employed with unit electrode spacing of 10 ft. and increasing the electrode distance in 10 ft. increments at each stage up to 60 ft. The applied methodology for collecting the data was similar to multi electrodes ERT survey, but instead of installing multi electrodes along

the survey line at the beginning of the survey and use automatic cable to switch between the electrodes, the electrode configuration was adjusted manually for measuring resistivity for each survey point. The apparent resistivity of each point and distance between the electrodes are recorded into the device in a consecutive order and the stations of the surveying points were recorded manually to be assigned to the recorded data for the subsequent inversion analysis. **Figure 3.11** shows AEMC 6470-B device during the resistivity data collection at the studied dam.

3.5.2 Data Inversion

For each surveying line, the recorded data is processed into a specific format to be used as input to the inversion software. The required data for the model are the title of the graph, number of the surveying points, unit distance between the electrodes, stations in the middle of the potential electrodes and apparent resistivity of each reading point. In this study, Res2vity software was employed to invert the reading data and prepare the resistivity profile along the surveying lines. **Figure 3.12** is showing the ERT profiles along three surveying lines.

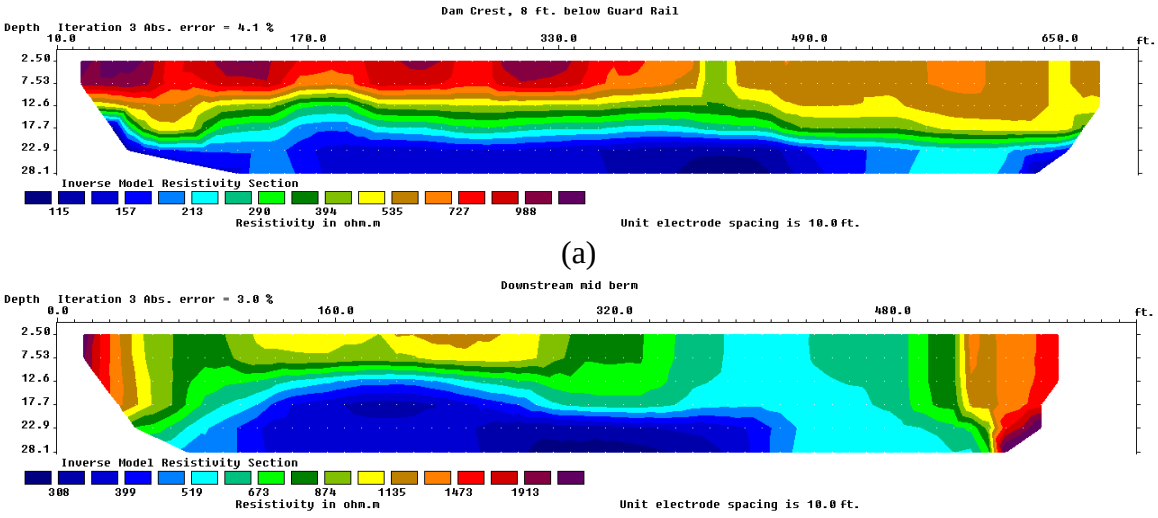

Figure 3.12 ERT results along (a) crest, (b) mid-berm of the studied dam (Continued).

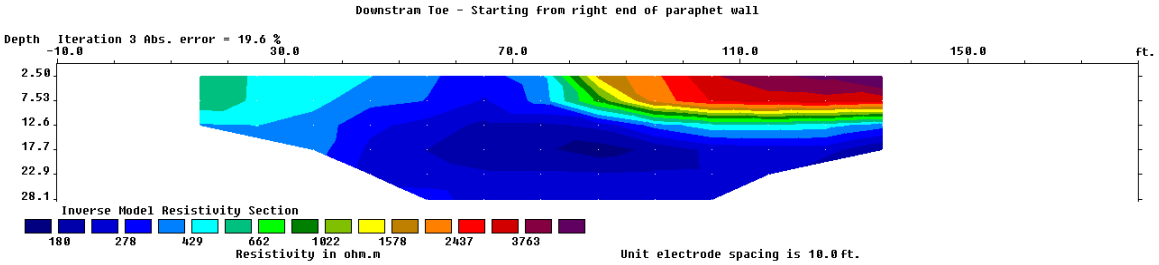

(c)

Figure 3.12 (Continued) ERT results along (c) toe of the studied dam.

3.5.3 Results and Discussion

ERT profile along the toe (**Figure 3.12(c)**) shows a low resistivity zone at station around 0+80 ft. from the right end of the concrete jersey barriers. This location with acceptable range of accuracy is addressing the outflow zone was observed at station 0+70 ft. from the right end and about 10 ft. downstream of the barriers. Detecting this outflow zone with ERT method is another example of showing the accuracy and reliability of this method in detecting seepages in soil dams.

The resistivity profile along the crest (**Figure 3.12(a)**) shows three regions with low resistivity. First point is located about 50 ft. from right end of the guard rail and at the depth of about 20 ft. adjacent to the right abutment. ERT survey could not be extended more towards the right abutment due to the limitation of access to the zone as it was covered with dense bushes and fallen trees. The second low resistant zone was detected at station around 4+30 ft. from the right end of the guard rail and at the depth about 25 ft. Large low resistant zone in this profile could be an indicator of an extensive wet zone in this area. The last low resistivity spot along the crest was detected at the right abutment and depth of about 30 ft. Due to the limitation of access, no more stations could be surveyed towards the left abutment. These three zones are estimated to be the potential entranceways into the downstream embankment.

The profile along the mid berm (**Figure 3.12(b)**) is illustrating two low resistivity zones around stations 1+80 ft. and 3+00 ft. from the right abutment. These spots are addressing potential spots of flow, passing through the surveying section. An extensive low resistant area is detected along the mid-level berm between stations 2+70 ft. and 3+50 ft. from the right abutment. This zone is expected to embed the flow towards the downstream, especially towards outflow #2. There is another comparatively small low resistant area detected at station around 1+80 ft. from the right abutment and at shallower depth along this survey line. This zone could also be considered as a spot within the potential flow pathway. No point could be surveyed near and on the abutments along this line due to access limitations.

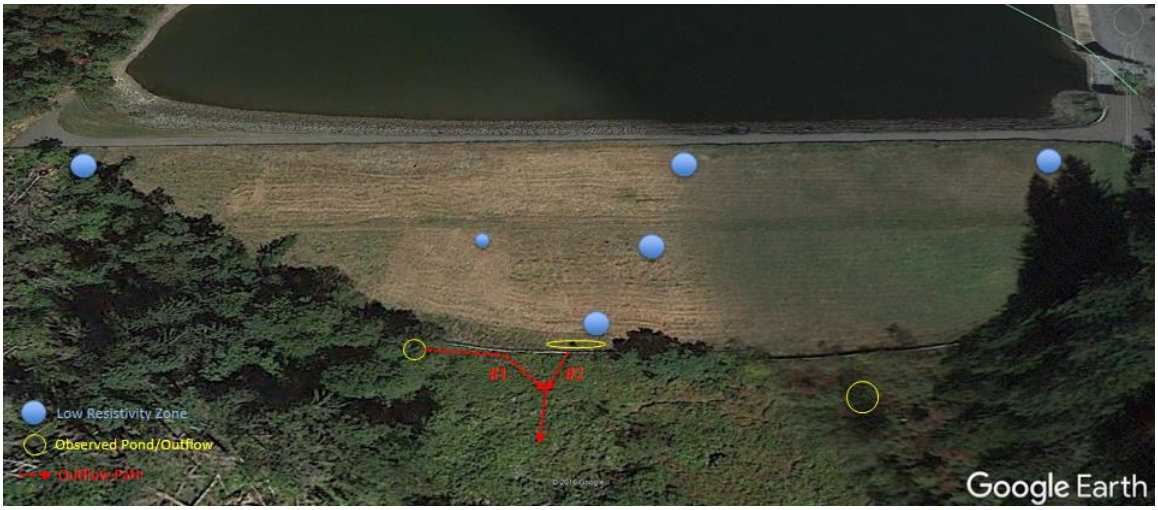

Figure 3.13 Schematic view of seepage monitoring results of the studied dam.

Figure 3.13 shows a schematic view of the findings in the first phase of seepage monitoring. In the figure, blue dots are representing the low resistivity zones which addressing potential saturated zones within the embankment detected by ER survey. Yellow circles and ovals are showing areas where water is ponded and saturated zones respectively. Red arrows are representing the observed outflow paths. Two flow paths merge together at station around 0+70 from the right end and 10' downstream of the jersey

barriers.

According to the site observations and results of the ERT survey, three potential flow paths are considered for each detected Outflow. **Figure 3.14** illustrates these potential flow paths. For each Flow Path (FP i-j), the first number (i) is the number of the origination point at the crest and the second number (j) is the Outflow number which the flow path is leading to. In C**hapter 4** the probability of each flow path is calculated according to the observed data and subsequently, the most probable scenario is identified.

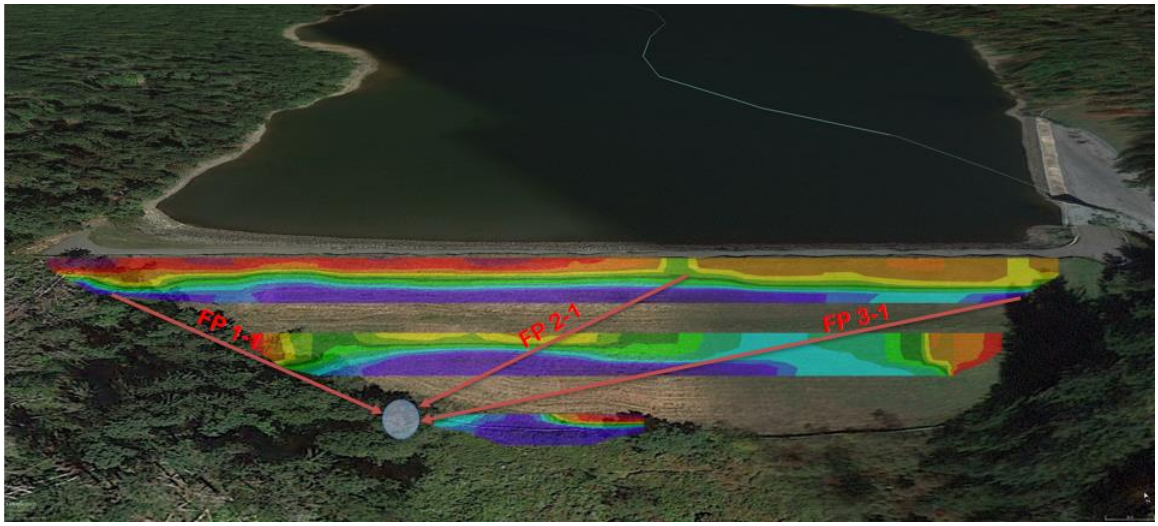

(a)

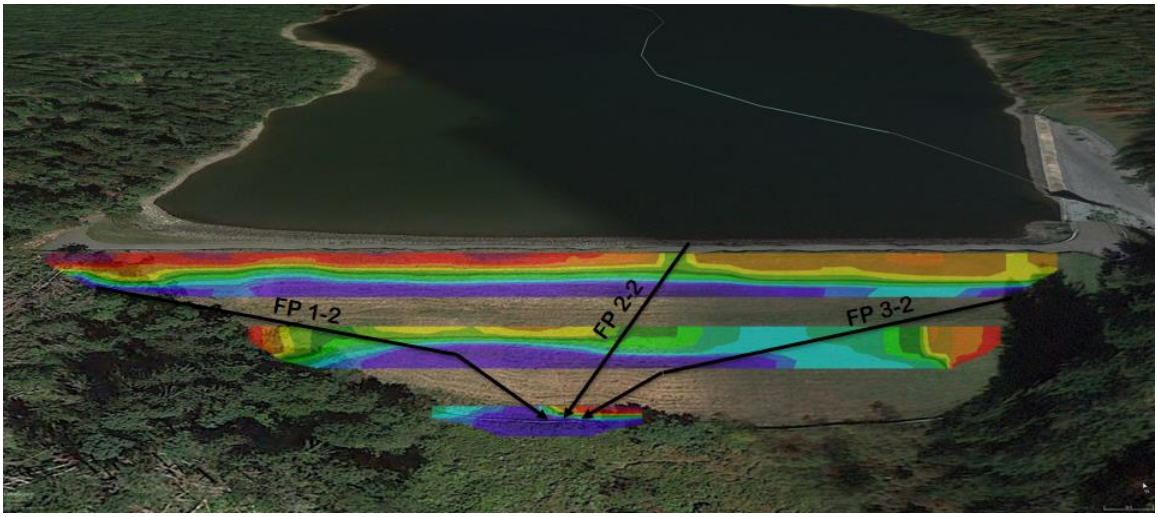

(b)

Figure 3.14 Schematic view of the potential flow paths for (a) Outflow #1 and (b) Outflow #2.

For the detected outflows at the downstream toe, the discharge flows were found clear with no visual sign of turbidity. This is an indicator the dam is not suffering from extreme active erosion under current condition. However, any change in behavior of the dam or the flow may act as a trigger. Any incident such as movement, settlements, changes in flow paths, discharge or total head, severe weather condition and precipitation, etc. may change the behavior of the seepage and the process of internal erosion could be initiated and progressed. Furthermore, there is a chance the dam is suffering from any minor and gradual erosion that can be detected visually. In this case, although no sign of turbidity is observed at the outflow spot, but in reality the soil is slowly washed out along the flow path which results in expanding the pipe diameter and increasing the discharge expand the pipe, which can eventually transform into an extreme active erosion. In **Chapter 5**, a methodology for estimating of rate of erosion is presented. Also, the potential failure time is estimated with four theoretical methods, in case of an active erosion occurs and the breach process initiates and develops. It is essential the source of the distresses are identified and remediated to avoid any subsequent catastrophic disasters.

CHAPTER 4

SOFTWARE MODEL

4.1 Introduction

In order to have a better evaluation of the studied dam's seepage behavior and have a reference to compare the field collected data against, an attempt was made to develop 2D and 3D models of the dam in GeoStudio and SVOFFICE software. In these models, the geometry of the dam, soil class, core type and boundary conditions of the dam were taken into account. The required data for the models were gathered based on field measurements, previous boring tests and inspection reports done by others and appropriate methods of estimation. **Figure 4.1** shows the plan view and a section view of the studied dam.

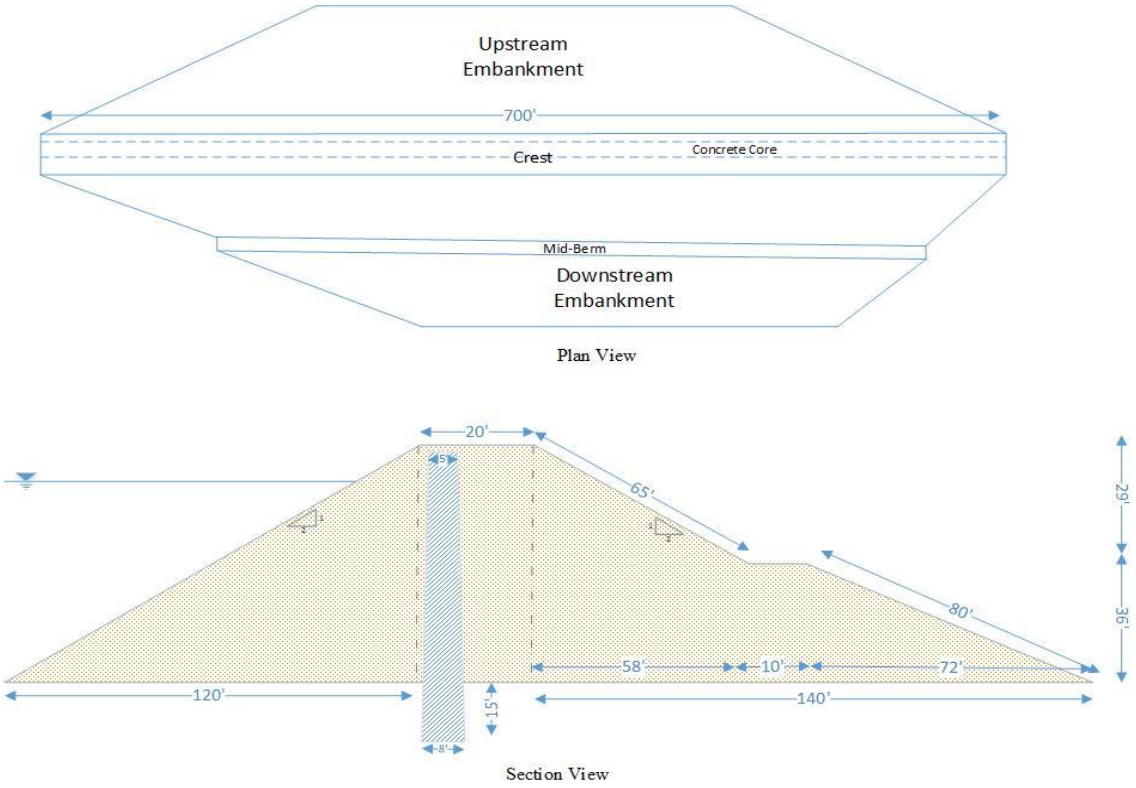

Figure 4.1 Plan and section view of the studied dam.

4.2 Geotechnical Data

Figure 4.2 is presenting the grain size distribution of the embankment according to a boring test performed by a third party on 1997. The test was carried out on the crest and to the depth of 70 feet.

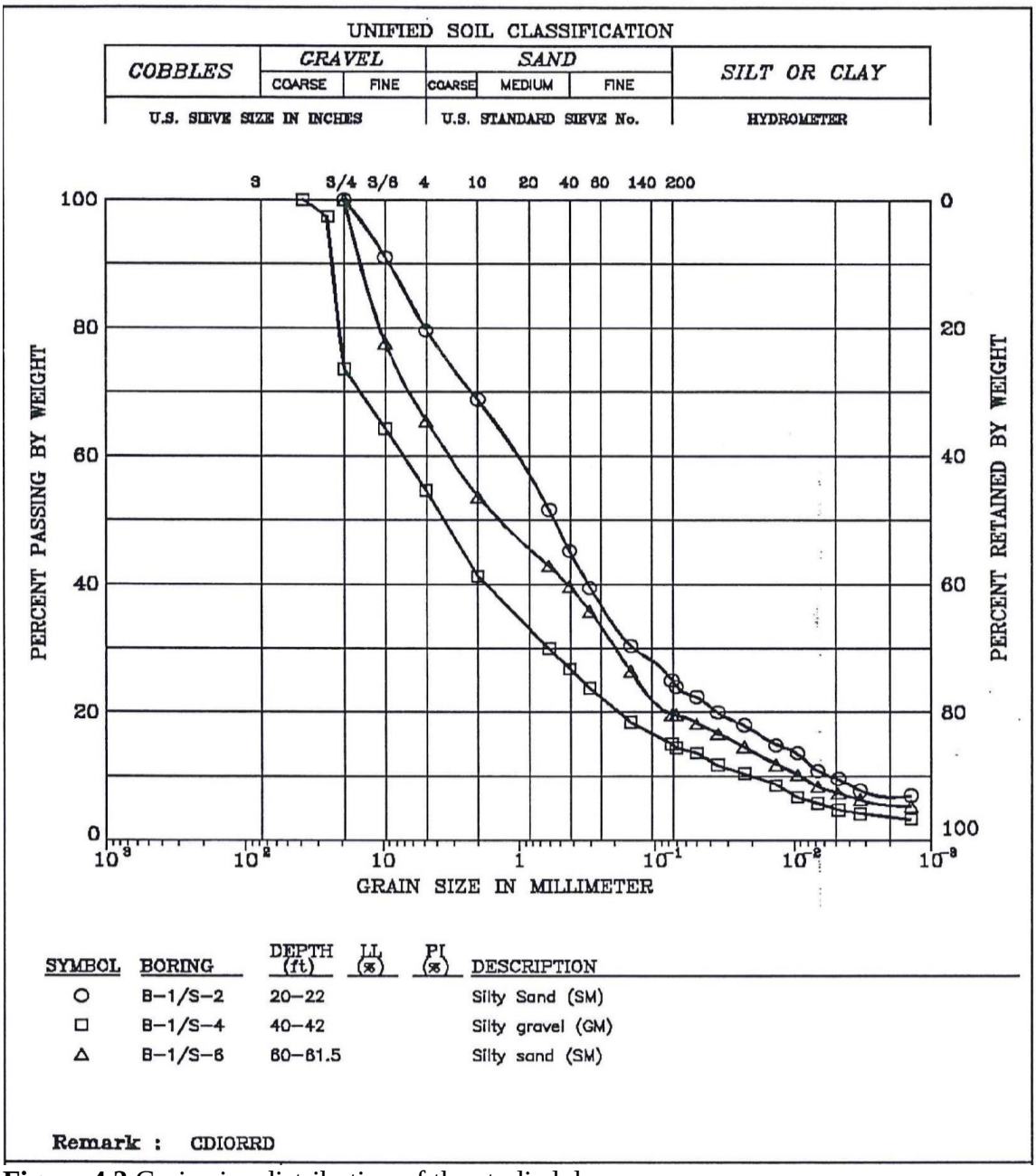

Figure 4.2 Grain size distribution of the studied dam.

Based on the boring test results, three soil distributions were identified along the boring depth. However, considering the conformity of the three distribution graphs and for simplicity, it is estimated there is a uniform soil with the average of the distributions for the entire dam. **Table 4.1** illustrates the summary of the soil distribution and estimates of the volumetric water content and soil conductivity.

Table 4.1 Soil Distribution by Weight, Volumetric Water Content and Soil Conductivity Estimate

Soil #	Boring	Depth (ft.)	Description	Gravel	Sand	Silt or Clay	K_{sat} (ft./sec)	Saturation (%Vol.)
1 O	B-1 / S-2	20-22	Silty Sand (SM)	20%	52%	28%	7.29E-08	35.60%
2 □	B-1 / S-4	40-42	Silty Gravel (GM)	46%	38%	16%	1.06E-06	32.70%
3 Δ	B-1 / S-6	60-61.5	Silty Sand (SM)	35%	45%	20%	6.39E-07	31.70%
			Average	**34%**	**45%**	**21%**	**6.02E-06**	**39.80%**

To estimate the volumetric water content (Saturation) and conductivity (K_{sat}) of each of soil classes, SPAW (Soil – Plant – Air – Water) software was employed. SPAW was developed by USDA Agricultural Research Service in cooperation with Department of Biological Systems Engineering at Washington State University. The Soil-Water Characteristics feature of this program is estimating the soil characteristics such as saturation and saturation hydraulic conductivity according to the soil distribution and compaction ratio for any studied soil. **Figure 4.3** illustrates these parameters according to the data provided in **Table 4.1** and compaction ratio of 1.1. The results show the saturated hydraulic conductivity (K_{sat}) of the soil is 0.26 in/hr. (or 6.02×10^{-6} ft/sec.) and the saturation is 39.9 %Vol.

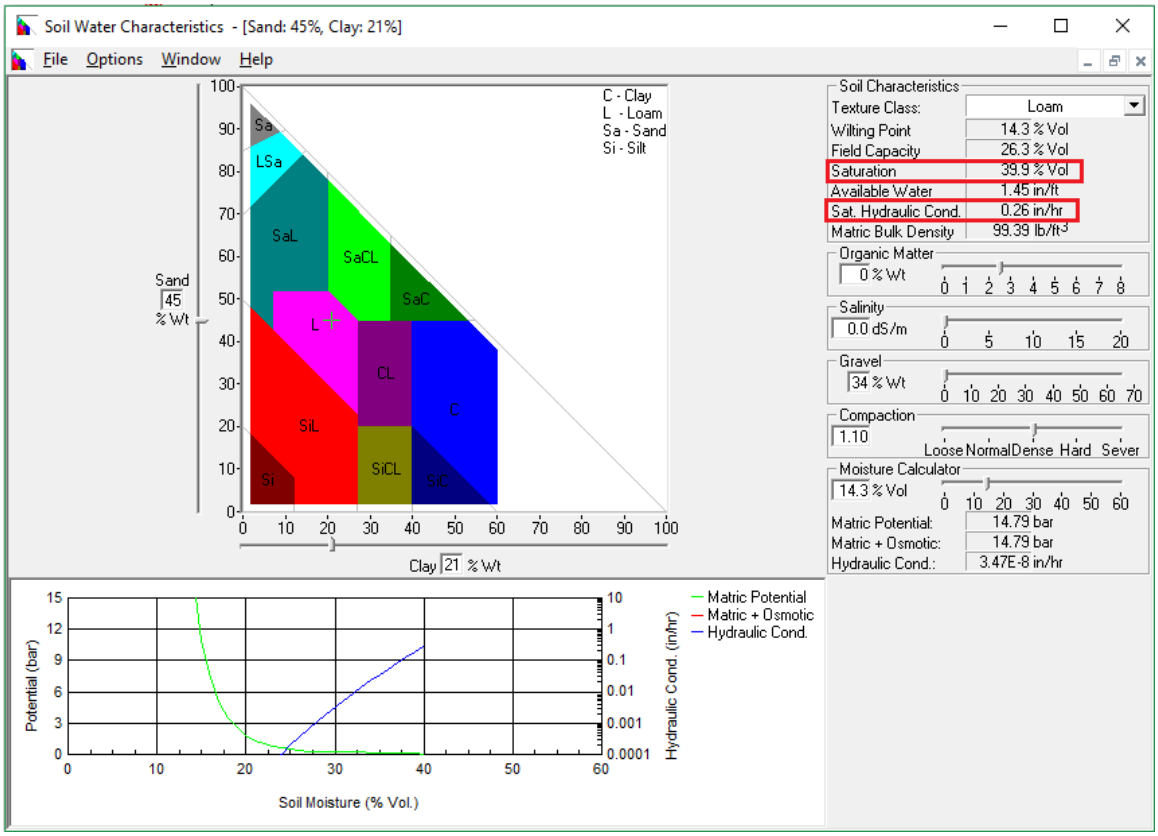

Figure 4.3 Results of soil characteristics from SPAW.

4.3 2D Model

GeoStudio 2012 software was utilized to create a 2D model of the studied dam. GeoStudio consists of 8 products for analyzing and modeling different geotechnical problems. Seep/W is the product applied for seepage modeling and analysis. **Figure 4.4** is showing the 2D model of the studied dam in Seep/W. The estimated parameters in **Table 4.1** and **Figure 4.3** are used for this model. Since the water flow inside the embankment is in unsaturated mode, the volumetric water content and hydraulic conductivity functions of the soil needs to be estimated. Seep/W has the capability to estimate the Volumetric Water Content (VWC) function according to grain size data and saturated water content of the soil for different matric suctions. To estimate the VWC for this model, the sample material was considered as “silty sand” and the saturated water content was estimated as 0.4 ft^3/ft^3.

Seep/W is also capable to estimate the hydraulic conductivity function with two different methods, Van Genutchen and Fredlund & Xing. In this model Van- Genutchen method was utilized to estimate the function with K_{sat} = 6.4×10^{-7} ft. /sec and Residual Water Content = 0.05 ft^3/ft^3. The result of this estimate is a graph showing the conductivity of the soil for a range of matric suction. In this model, the foundation material is considered as saturated loam with saturated volumetric water content of 0.317 ft^3/ft^3 and K_{sat} of 6.4x10^{-7} ft. /sec. **Figure 4.5** shows the estimated graphs in GeoStudio for Hydraulic Conductivity and Volumetric Water Content functions.

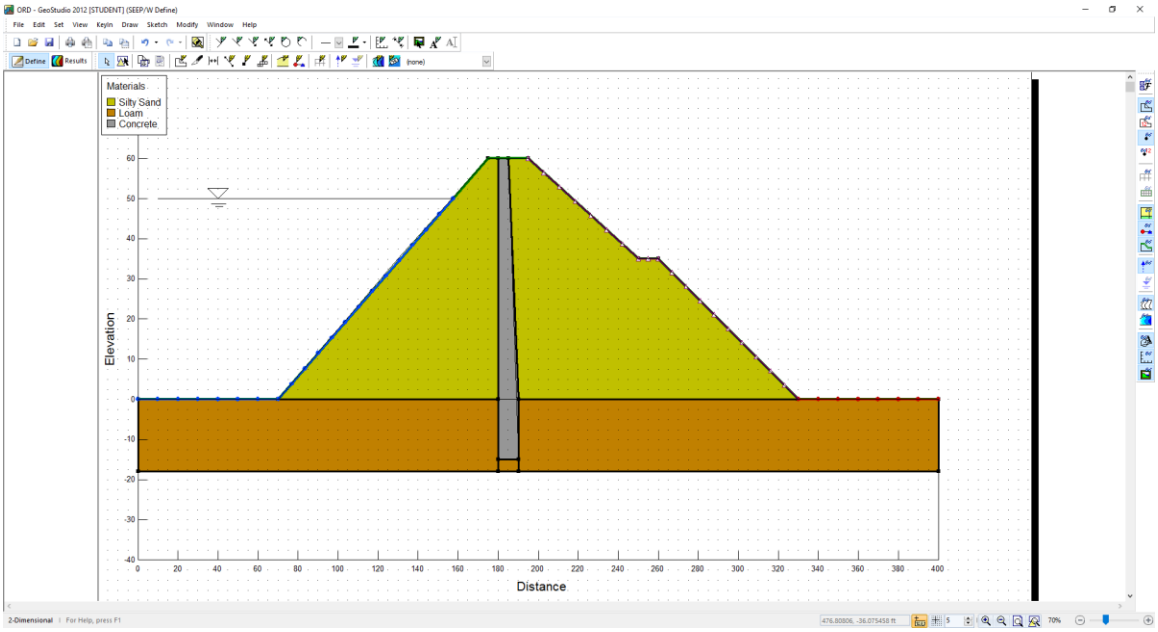

Figure 4.4 2D model of the studied dam in GeoStudio Seep/W software.

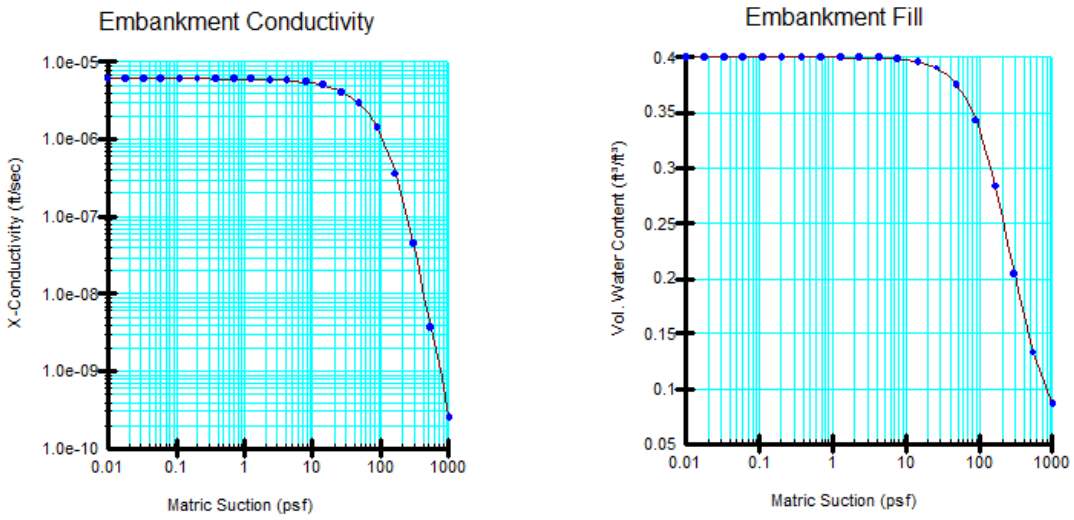

(a) (b)

Figure 4.5 Estimating graphs of (a) Hydraulic Conductivity and (b) Volumetric Water Content in GeoStudio software.

4.4 3D Model

Different 3D models were created to describe the seepage behavior for each mode reflecting potential flow paths described in Chapter 4 in SVOFFICE software. This software also has different products for various purposes in geotechnical studies. In this study, SVFLUX product was employed to model the seepage flows in the studied dam.

In this model, similar to the 2D model, unsaturated silty sand, saturated silty sand, unsaturated loose silty sand, saturated loam and concrete was assigned to embankment, flow paths, abutment, foundation and core of the model, respectively. The quantities and methods to calculate and estimate volumetric water content and hydraulic conductivity are the same as the 2D model. **Table 4.2** shows the characteristics of each material in the 3D models.

Two seepage outflows were detected at the downstream toe of the embankment and according to ER survey and field observations, three potential flow paths were identified for each detected outflow. A 3D software model is developed for each of these scenarios

for three different reservoir level by embedding the potential path within the downstream embankment, and analyzing the model to calculate the discharge value at each outflow.

Table 4.2 Characteristic and Location of Each Soil Class in the Studied Dam for 3D Model

Soil/Material Type	Location	Saturation	Saturated Hydraulic Conductivity (K_{sat})
Silty Sand	Embankment	Unsaturated	6×10^{-6} (ft/s)
Concrete	Core	Unsaturated	3.28×10^{-9} (ft/s)
Sat. Silty Sand	Flow Path	Saturated	6×10^{-3} (ft/s)
Loose Silty Sand	Abutment	Unsaturated	1×10^{-4} (ft/s)
Loam	Foundation	Saturated	6.4×10^{-6} (ft/s)

For the 3D models, the potential flow paths are modeled just within the downstream embankment with the origination points within or along the concrete core. For flow paths #1 and #3, it is assumed the origination of the paths are from the right and left ends of the concrete core and in the abutments. The origin of the flow path #2 is assumed to be a crack within the concrete core at station around 4+30 ft. from the right abutment. For the regions of the flow paths, the hydraulic conductivity of the soil is estimated relatively higher than the embankment material, and considered as saturated soil. Discharge at the two outflows are measured for three upstream reservoir elevations at 51 ft., 47 ft. and 42 ft. from the embankment base.

Outflow #1 is located at the west corner of the toe and along the downstream of the concrete jersey barriers. The potential flow paths for Outflow #1 are shown in **Figure 3.14(a)**. Flow path 1-1 is assumed to be located along the right abutment towards the downstream toe. Flow path 2-1 is originated from the concrete crack at station around 4+30 ft. from the right abutment and flows towards Outflow #1. Potential flow path 3-1 is

originating from the left abutment.

Outflow #2 was detected at station about 0+70 from the right end of downstream concrete jersey barriers. **Figure 3.14(b)** shows the potential paths are flowing to this outflow. The outflow discharge for each of the paths are measured at three different reservoir elevations from the 3D models.

4.5 Results and Discussion

Figure 4.6 is showing pressure head and total head of the 2D model analyzed by GeoStudio 2012. According to the results, the water level right downstream of the concrete core within the embankment is 12 feet above the toe elevation (48 feet below the crest elevation).

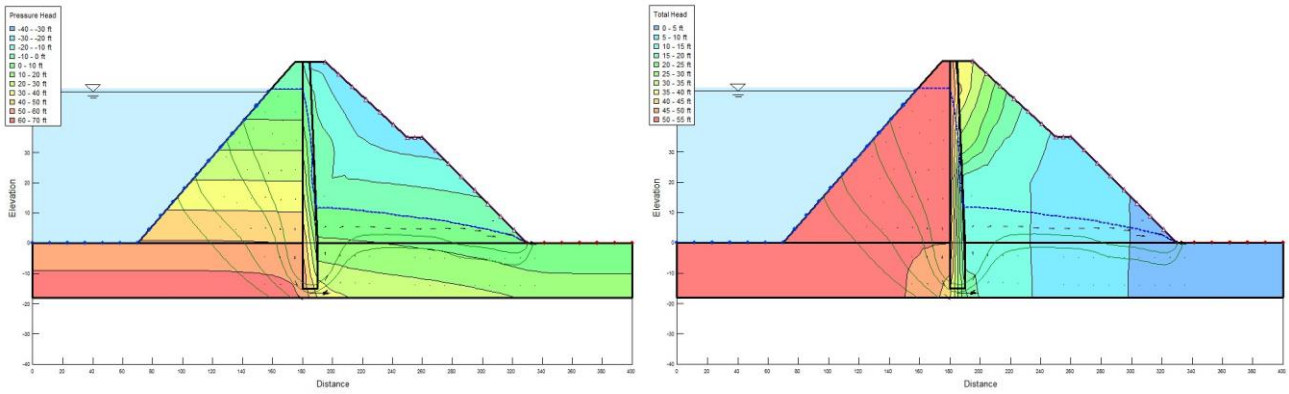

(a) (b)

Figure 4.6 Results of (a) Pressure Head and (b) Total head of the studied dam analyzed in GeoStudio software.

However, the observation well right downstream of the concrete core at St. 4+15 ft. from the right end abutment at the crest, measured water elevation 34 feet below the crest elevation (26 feet above the toe elevation). The 14 feet difference between the measured and observed water level inside the downstream embankment justifies the potential existence of uncontrolled seepage flow in this region. **Figure 4.7** is comparing this difference in water elevation in a schematic configuration.

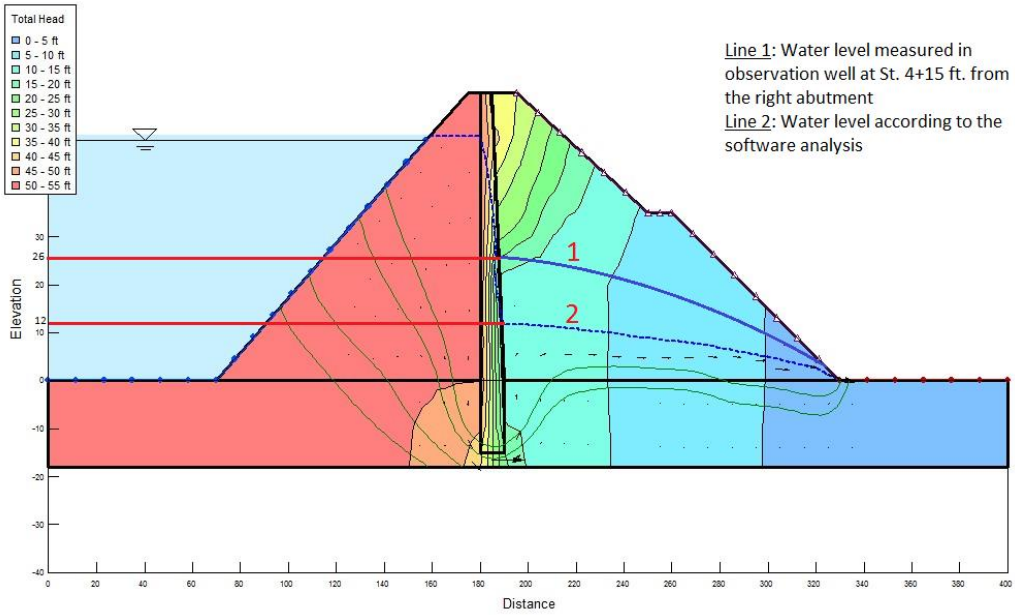

Figure 4.7 Schematic view of measured and analyzed water level in downstream embankment.

Each of the 3D models were developed and analyzed in SVFLUX software was representing a flow path towards the outflows at the downstream toe. The software provides different types of reports and contours such as pore water pressure, total head, flow velocity and flux. Total head of 51 ft., 47 ft. and 42 ft. are assigned as boundary condition for the upstream embankment and abutments, addressing three reservoir water elevation and the total head is assigned as zero at the downstream. In order to calculate the discharge, a boundary condition is assigned at the outflow side of each flow path where the flux to be measured at. **Figure 4.8** shows 3D models and analysis results for flow paths 1-1, 2-2 and 3-2 for reservoir level at 51 ft.

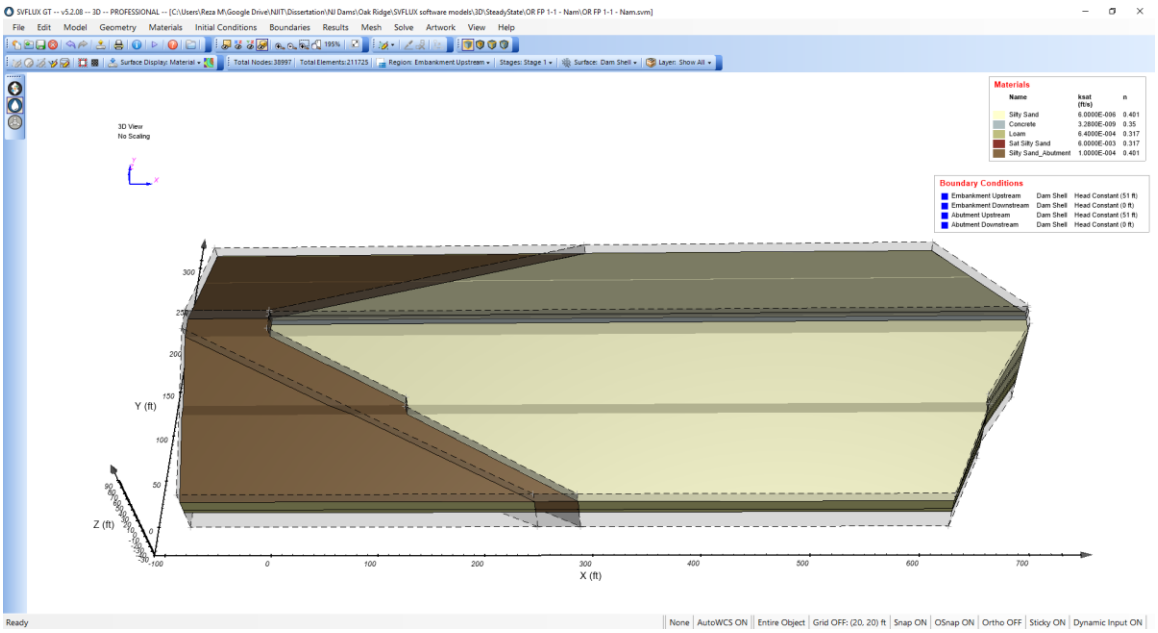

(a)

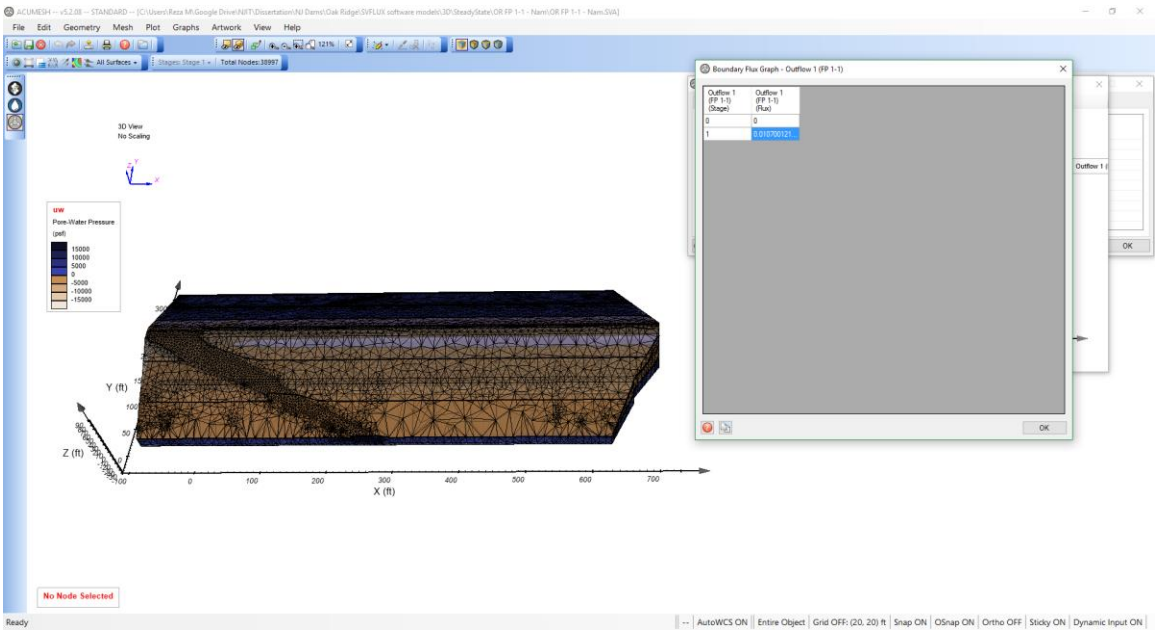

(b)

Figure 4.8 (a) 3D model of Flow path 1-1 and (b) Analysis results of Flow path 1-1 in SVFLUX software for reservoir level at 51 ft. (Continued)

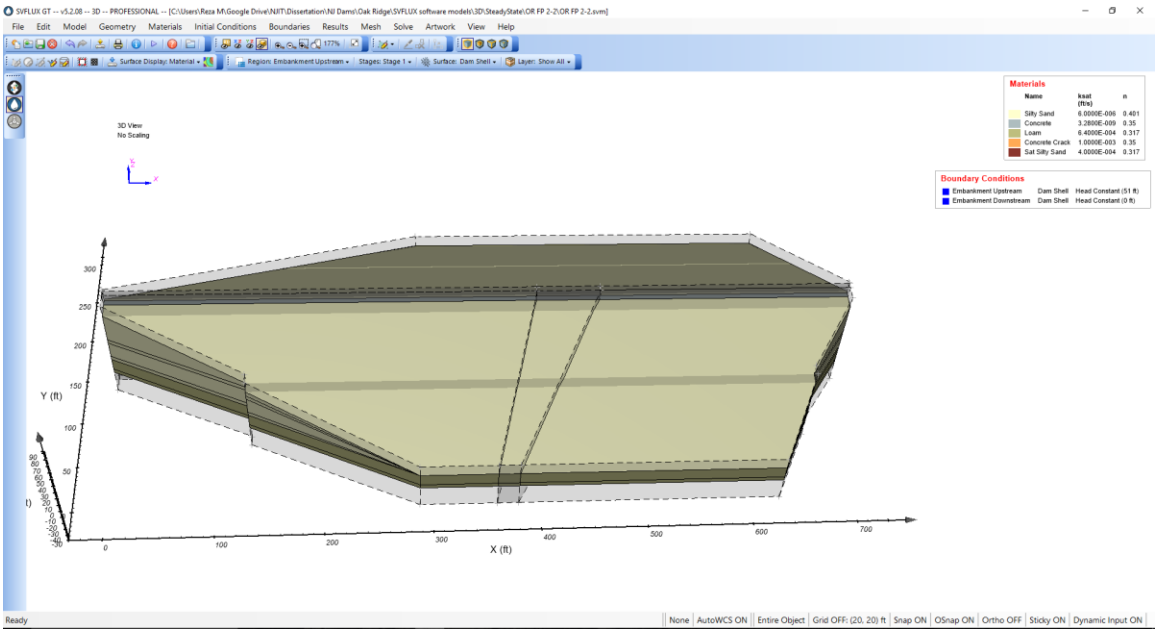

(c)

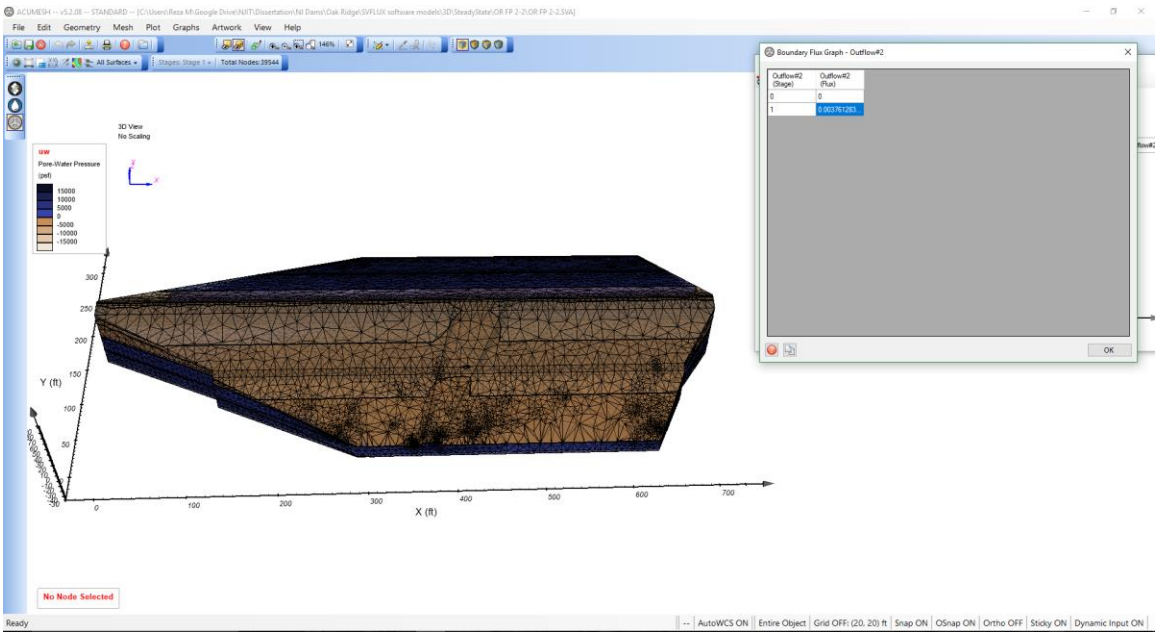

(d)

Figure 4.8 (Continued) (c) 3D model of Flow path 2-2 and (d) Analysis results of Flow path 2-2 in SVFLUX software for reservoir level at 51 ft. (Continued)

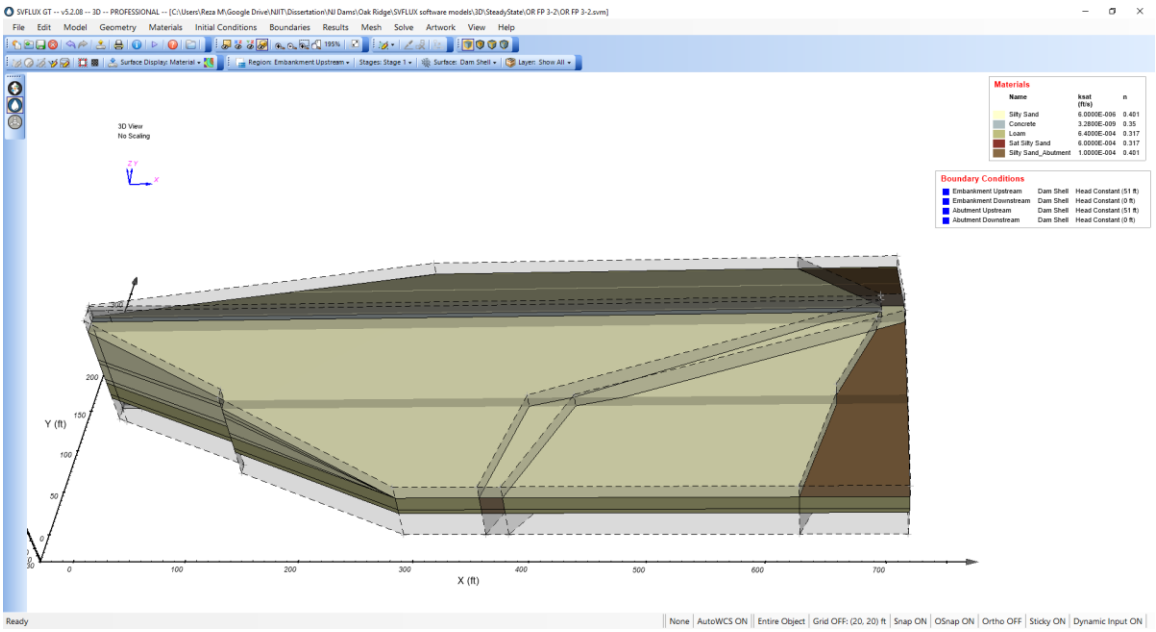

(e)

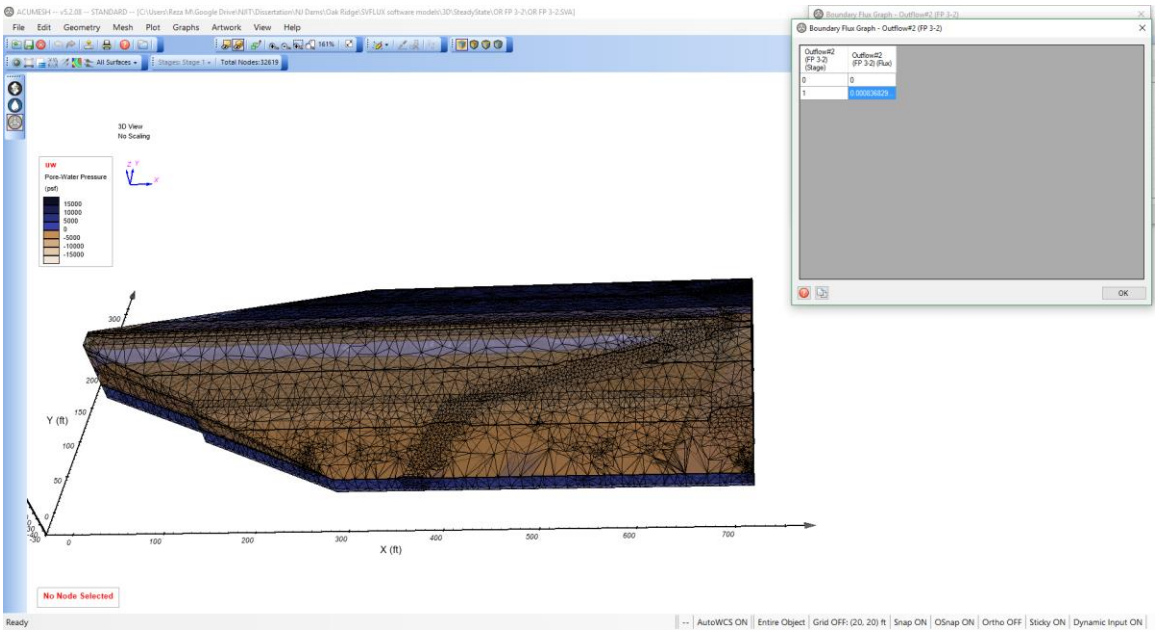

(f)

Figure 4.8 (Continued) (e) 3D model of Flow path 3-2 and (f) Analysis results of Flow path 3-2 in SVFLUX software for reservoir level at 51 ft.

Table 4.3 summarizes the results of 3D software analysis for each flow path at three different reservoir elevation and actual measurement on site.

Table 4.3 Summary of Outflow Discharge Calculated With Software Model and Site Measurement for (A) Outflow #1 and (B) Outflow #2

Outflow #1	Discharge calculated with 3D software model (cu ft/s)			Discharge measured at Field (cu ft/s)
Reservoir Elevation (ft.)	FP 1-1	FP 2-1	FP 3-1	
42	0.0015	0.0017	0.00040	0.00083
47	0.0064	0.0048	0.00192	0.00880
51	0.0107	0.0060	0.00220	0.01240

(a)

Outflow #2	Discharge calculated with 3D software model (cu ft/s)			Discharge measured at Field (cu ft/s)
Reservoir Elevation (ft.)	FP 1-2	FP 2-2	FP 3-2	
42	0.0017	0.00024	0.00002	0.0000
47	0.0043	0.00150	0.00014	0.0024
51	0.0062	0.00380	0.00084	0.0040

(b)

Figure 4.9 is comparing the outflow discharge and reservoir level of the modeled flow paths and site-measurements for two studied outflows. For each graph-line a second ordered polynomial trendline is developed and the trendline equation as well as r-squared value is calculated as follow:

- Outflow #1
    - Site measurement: $y = -7.707\times10^{-5}\,x^2 + 8.453\times10^{-3}\,x - 0.218,$ $r^2=1.0$
    - Flow path 1-1: $y = 1.053\times10^{-5}\,x^2 + 4.275\times10^{-5}\,x - 0.019,$ $r^2=1.0$
    - Flow path 2-1: $y = -3.63\times10^{-5}\,x^2 + 3.85\times10^{-3}\,x - 0.096,$ $r^2=1.0$
    - Flow path 3-1: $y = -2.635\times10^{-5}\,x^2 + 2.649\times10^{-3}\,x - 0.064,$ $r^2=1.0$

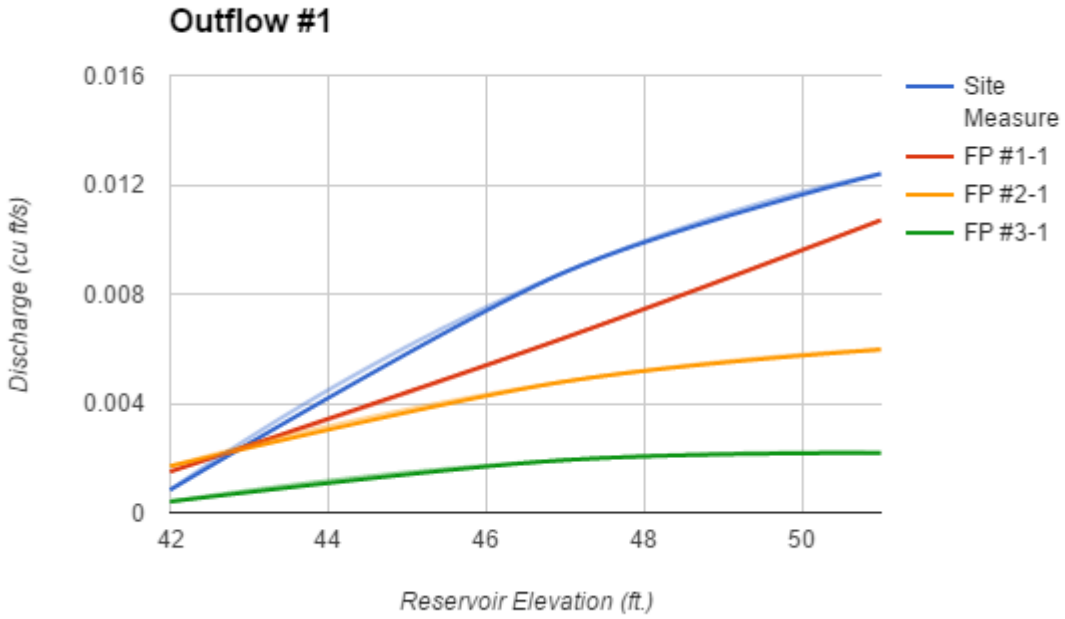

(a)

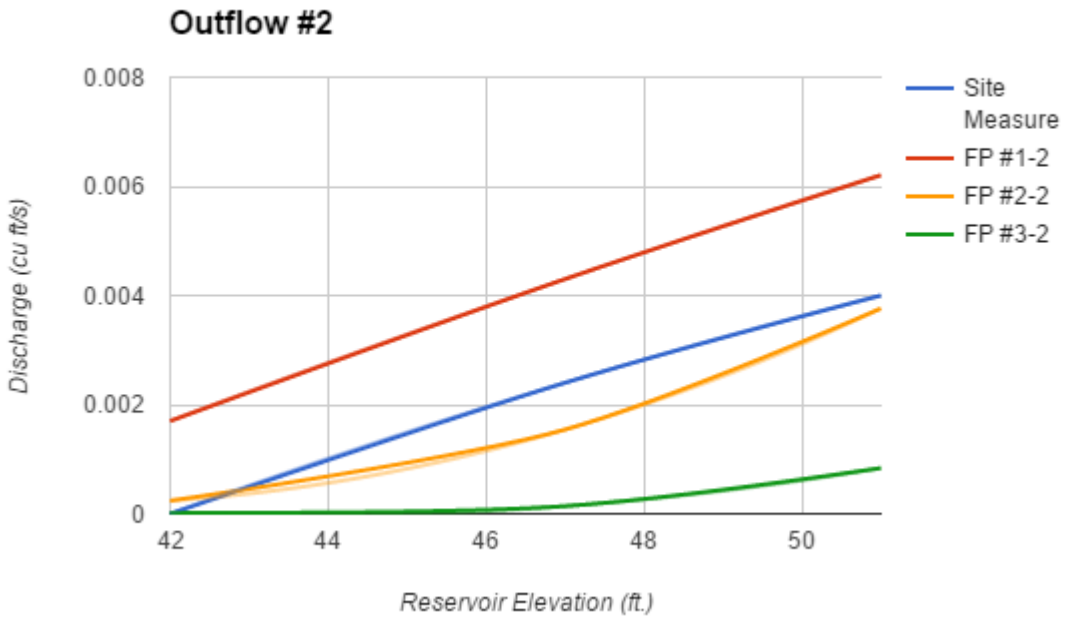

(b)

Figure 4.9 Outflow discharge vs. reservoir level for (a) Outflow #1 and (b) Outflow #2 comparing calculating discharge from 3D model for each flow path and actual site measurement

- Outflow #2
    - Site measurement: $y = -8.889\times10^{-6}\,x^2 + 1.271\times10^{-3}\,x - 0.038,$ $r^2=1.0$
    - Flow path 1-1: $y = -4.869\times10^{-4}\,x^2 + 9.533\times10^{-4}\,x - 0.03,$ $r^2=1.0$
    - Flow path 2-1: $y = 3.27\times10^{-5}\,x^2 + 2.65\times10^{-3}\,x + 0.054,$ $r^2=1.0$
    - Flow path 3-1: $y = 1.669\times10^{-5}\,x^2 - 1.461\times10^{-3}\,x + 0.032,$ $r^2=1.0$

CHAPTER 5

PROBABILITY ANALYSIS AND FAILURE RISK

5.1 Introduction

According to the results of the site investigations, ER survey and software models, different seepage scenarios were identified for each detected outflow at the downstream toe as presented in Chapter 4. In this chapter, two separate analysis are done to evaluate each of the seepage scenarios and estimate the rate of erosion in case of internal erosion incident.

In the first analysis, a Bayesian model is developed to calculate the probability of each identified scenario as a potential path of detected flows. In this model, the prior probabilities are calculated based on the generic location of seepage origination in earth embankment dams, calculated in Chapter 2, and the posterior probability will be based on the observation of software modeling results and actual data collected on site for each potential path.

In the second analysis, although no sign of erosion was detected in the studied case at the time of inspection, to evaluate the safety in extreme condition, the breach time of the dam is estimated with different methods assuming the dam is suffering from an active piping. Also, by estimating the discharge fluctuation at any outflow over three year period, the rate of erosion is assessed in a separate study.

5.2 Probability Analysis of Potential Flow Paths

In order to analyze the probability of each identified scenarios as the source of potential flow paths, a Bayesian network model is developed and updated subsequently as new

evidence was observed. In this model, the prior probabilities are calculated based on the dam seepage zone database study, presented in Chapter 2. In the next step, for each detected outflow at the downstream toe, the amount of discharge is calculated and calibrated with the 3D software models for each identified scenario and compared to the actual outflow discharge measured on site. This observation updates our belief about the status of each potential path and lead us to calculate the posterior probabilities.

5.2.1 Bayesian Network Model for Detecting the Seepage Source

According to the results of site investigation and ERT survey presented in Section 1.3.4, three potential sources of inflow were located for each outflow detected at the downstream toe. **Figure 5.1** shows the causal network representing the seepage incidents in the studied dam.

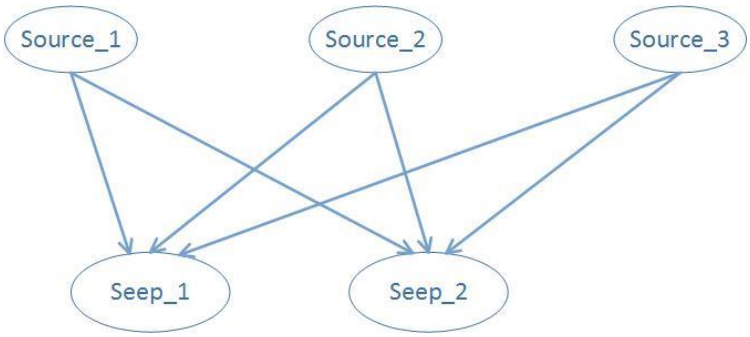

Figure 5.1 Causal network representing seepage incidents in the studied dam.

The graph consists of five nodes with two types of variables "*Source_i"* and "*Seep_j"* with subscript numbers, representing separate variables of the same name. Each variable is in one of two states: *"Pos"* and *"Neg"* for *Source_i* and "*Yes"* and *"No"* for *Seep_j*.

dom (*Source*) = {*Pos*, *Neg*} & dom (*Seep*) = {*Yes*, *No*}

The variable *Source_1* tells us this *Source* is the origin of seepage for any detected *Seep_j*, by being in state "*Pos"* and so on for variables *Source_2* and *Source_3*. Variable *Seep_1*

tells us that seepage is detected at the station allocated to this incident (St. 0+20 ft. from the right end of the jersey barriers in this case) by being in state *"Yes"*, and so on for variable *Seep_2*. In summary:

- *Source_1*: Distressed seepage zone through the right abutment at St. 0+00 ft. with domain: {*Pos, Neg*}
- *Source_2*: Distressed seepage zone through the embankment at St. 4+30 ft. from the right abutment with domain: {*Pos, Neg*}
- *Source_3*: Distressed seepage zone through the left abutment at St. 6+50 ft. with domain: {*Pos, Neg*}
- *Seep_1*: Downstream outflow seepage at St. 0+20 ft. from the right end of the concrete jersey barriers with domain: {*Yes, No*}
- *Seep_2*: Downstream outflow seepage at St. 0+70 ft. from the right end of the concrete jersey barriers with domain: {*Yes, No*}

Axioms:

1.
    a. For any event, *Source_i* $(i \in \{1, 2, 3\})$, $0 \leq P(Source\_i) \leq 1$, with $P(Source\_i) = 1$ if and only if *Source_i* is the source of the seepage of *Seep_j* $(j \in \{1, 2\})$ with certainty.

    b. For any event, *Seep_j* $(j \in \{1, 2\})$, $P(Seep\_j) = 1$ if and only if outflow seepage is detected at the surveying station. $P(Seep\_j) = 0$, otherwise.

2. For the mutually exclusive events *Source_1*, *Source_2* and *Source_3* the probability that either *Source_1* or *Source_2* or *Source_3* occur is:

$$P(Source\_1 \text{ OR } Source\_2 \text{ OR } Source\_3) = P(Source\_1) + P(Source\_2) + P(Source\_3) = 1$$

3. For any two events *Source_i* $(i \in \{1,2,3\})$ and *Seep_j* $(j \in \{1,2\})$, the probability that both *Source_i* and *Seep_j* occur is (joint probability of *Source_i* AND *Seep_j*)

$$P(Source\_i \text{ AND } Seep\_j) = P(Source\_i, Seep\_j) = P(Source\_i \mid Seep\_j)P(Seep\_j)$$

$$= P(Seep\_j \mid Source\_i)P(Source\_i)$$

Assumption:

The source of any downstream outflow seepage, *Seep_j (j ∈{1, 2}),* is not more than one distressed seepage zone, *Source_i (i ∈{1, 2, 3}).*

5.2.2 Prior Distribution

Prior distribution is an unconditional probability of an event before relevant evidence or observation is taken into account and is usually elicited by subjective assessment of an experienced expert or based on past information, such as previous experiments. If there is no prior knowledge about the variables, equal probability would be assigned to the parameters. In this case study, the prior probability of *Source_i* is determined based on the statistical data, presented in Chapter 2 and the conditions of the site.

According to this database presented in Chapter 2, in seepage incidents, the probability of concentrated seepages originating from abutment and embankment were reported as %17.1 and %31.4, respectively. These probabilities needs to be adjusted to provide the requirement of axiom 2, considering the probability of foundation and embedded culverts as sources of concentrated seepage is zero, according to the site condition. Based on the three defined scenarios, two identified sources are from the abutments and one source is from the embankment. Therefore, the adjusted prior probability for each scenario will be:

- %26.1, if the source of the concentrated seepage is through the abutment

P(*Source_1* | *Seep_j*) = P(*Source_3* | *Seep_j*) = 0.261

- %47.8, if the source of the concentrated seepage is through the embankment

P(*Source_2* | *Seep_j*) = 0.478

Accordingly,

$$P(Source\_1 \mid Seep\_j) + P(Source\_2 \mid Seep\_j) + P(Source\_3 \mid Seep\_j) = 1$$

These probabilities are considered as prior probabilities in the Bayesian Network model for determining the sources of concentrated seepage detected at the downstream toe.

Additionally, according to the results of the other study presented in chapter 2, on average, ERT method detected 98% of the anomaly zones were already discovered by the other investigation methods. In other word, this method detects seepage incidents occurring within its surveying range with 98% accuracy. **Figure 3.12** presented the results of ERT monitoring along three surveying lines which located low resistant zones, addressing potential wet areas embedding seepage flow paths. Along the crest these zones were detected at stations 0+00 ft., 4+30 ft., and 6+50 ft. from the right end of the right abutment as the sources of each potential flow paths. However, although there is an uncertainty involved for each of these detected points as the source of each path detected by ER method, for simplicity this uncertainty is not taken into account considering ER method is detecting the seepage zone with high accuracy according to the statistical study results.

5.2.3 Posterior Probability

Posterior probability of a random event is the conditional probability that is assigned after the relevant evidence or observation is taken into account. In order to diagnose the potential source of seepage distress zone, a source of project-specific variables, which reflect the behavior and performance of the structure needs to be taken into account. This set of information is updating our belief about the studied case by addressing the local-level performance records in addition to our initial belief about the source of seepage distress zones, known as global-level knowledge calculated as prior probability. According to Equation 1.15 the posterior probabilities are calculated as:

$$P(Source\_i \mid Seep\_j) = \frac{\mathrm{P}(Seep\_j \mid Source\_i)\ \mathrm{P}(Source\_i)}{\mathrm{P}(Seep\_j)} \qquad (5.1)$$

where:

- P(*Source_i* | *Seep_j*) is posterior probability of *Source_i* as source of *Seep_j* given *Seep_j* is observed
- P(*Seep_j* | *Source_i*) ≙ L(*Source_i* | *Seep_j*) is the *Likelihood* for *Source_i* as the source of *Seep_j*
- P(*Source_i*) is the prior probability of *Source_i* as source of *Seep_j*
- P(*Seep_j*) is the probability of *Seep_j*

In order to determine the posterior probability, first the Likelihood L(*Source_i* | *Seep_j*) needs to be quantified. For this purpose, the weight method of the marginal likelihood function is employed as proposed by Li et al (2009). In this model, the attempt is towards calculating the probability of *Source_i* given model $M^{(p)}$, where $M^{(p)}$ is software model of the identified flow paths and the expectation operator (E_M) over simulation models is taken into account. According to equation 1.17 we have:

$$P(Source\_i \mid Seep\_j) = E_M[\mathrm{P}(Source\_i \mid \mathrm{M}^{(p)}, Seep\_j)] \qquad (5.2)$$

$$= \sum P(Source\_i \mid \mathrm{M}^{(p)}, Seep\_j)\ P(\mathrm{M}^{(p)} \mid Seep\_j)$$

where $P(M^{(p)} \mid Seep\_j)$ is the posterior model probability for model $M^{(p)}$ or posterior model weight for model $M^{(p)}$ for any detected *Seep_j*. By replacing the parameters of the studied case in Equation 1.18 the posterior probability is calculated as:

$$P(M^{(p)} \mid Seep\_j) = \frac{P\left(Seep\_j \mid M^{(p)}\right) P(M^{(p)})}{\sum_P P(Seep\_j \mid M^{(p)})\ P(M^{(p)})} \qquad (5.3)$$

To determine combined model weight for each combination of models and methods, $\theta^{(p)}$ is assigned as a hydraulic conductivity estimation of flow paths for model

$M^{(p)}$ and $P(\theta^{(p)} \mid M^{(p)}, Seep\_j)$ represents the method weight for $\theta^{(p)}$ in software model $M^{(p)}$ for any detected *Seep_j*. According to equation 1.20, the method weight is:

$$P\left(\theta^{(p)} \mid M^{(p)}, Seep\_j\right) = \frac{P\left(Seep\_j \mid M^{(p)},\ \theta^{(p)}\right) P(\theta^{(p)} \mid M^{(p)})}{\sum P(Seep\_j \mid M^{(p)}, \theta^{(p)})\ P(\theta^{(p)} \mid M^{(p)})} \qquad (5.4)$$

where $P(Seep\_j \mid M^{(p)}, \theta^{(p)})$ is the marginal likelihood function for a given model $M^{(p)}$ and a given method $\theta^{(p)}$. According to Equations 1.21 to 1.23, the marginal likelihood function is calculated as:

$$P(Seep\_j \mid M^{(p)}, \theta^{(p)}) \approx \exp\left[-0.5 \times BIC^{(p)}\right] \qquad (5.5)$$

$$BIC^{(p)} = Q^{(p)} + n \ln 2\pi + m^{(p)} + \ln n \qquad (5.6)$$

where

$$Q^{(p)} = (q^{cal} - q^{obs})^T C_q^{-1} (q^{cal} - q^{obs}) \qquad (5.7)$$

$Q^{(p)}$: the sum of squared weighted residuals of head

q^{obs}: the observed discharge at the Outflow

q^{cal}: the calculated discharge with the software model for each flow path,

n: the number of the observed discharges

$m^{(p)}$: the number of parameters (conductivity of the flow path in this case)

C_q: the covariance matrix, a diagonal matrix for independent discharge errors. The variances in C_q are estimated by running a sufficient number of realizations of the data weighting coefficients, calculated with equation 1.23.

To determine the combined model weight, in the first step the amount of C_q needs to be determined. For this purpose, the amount of discharge was calculated for 8 different

hydraulic conductivity ($\theta^{(p)}$) of flow path regions in the software models. It is assumed the hydraulic conductivity of the flow path region is relatively lower than the surrounding soil and equivalent to conductivity of gravel, ranges between 1×10^{-3} to 1×10^{-1} ft/s. **Table 5.1** is showing the model results of the discharge (q) for different hydraulic conductivity ($\theta^{(p)}$) at three reservoir level for Flow Path 1-1. It should be noted that the hydraulic conductivity value was assigned to the main models is 6×10^{-3} ft/s.

Table 5.1 Calculated Model Discharge of Flow Path #1-1 for Various Flow Path Conductivity

FP 1-1 (*source_1*)		h_1 (42)	h_2 (47)	h_3 (51)
n	K(ft/s)	Q (cu ft/s)	Q (cu ft/s)	Q (cu ft/s)
1	1×10^{-3}	0.00079	0.0013	0.0015
2	3×10^{-3}	0.0011	0.0041	0.0052
3	6×10^{-3}	0.0015	0.0064	0.0107
4	9×10^{-3}	0.00182	0.0104	0.0147
5	2×10^{-2}	0.00242	0.0163	0.0224
6	5×10^{-2}	0.00288	0.0195	0.0286
7	8×10^{-2}	0.00351	0.0258	0.0306
8	1×10^{-1}	0.00393	0.0281	0.0313

This analysis was implemented for all the flow paths and both the outflows. According to equation 1.23 and equations 5.3 to 5.7, the likelihood of Flow Path #1 for Outflow #1 L(*Source_1*|*Seep_1*) is calculated as:

σ_1^2 (for h_1 = 42 ft.) = 3.12×10^{-6}

σ_2^2 (for h_1 = 47 ft.) = 1.15×10^{-4}

σ_3^2 (for h_1 = 51 ft.) = 1.53×10^{-4}

$Q^{(p)} = 0.212$

$n \ln 2\pi + m^{(p)} + \ln n = 6.612$

$BIC^{(p)} = 6.824$

L(*Source_1* | *Seep_1*) = 0.0330

Employing the same methodology, the likelihood for all the Flow Paths and for both the Outflows are calculated as presented in **Table 5.2**.

Table 5.2 Summary of Likelihood of Each Flow Path for the Detected Outflows

Likelihood summary	Flow Path #1 (Source_1)	Flow Path #2 (Source_2)	Flow Path #2 (Source_2)
Outflow #1 (Seep_1)	0.0330	0.0233	0.0051
Outflow #2 (Seep_2)	0.0297	0.0345	0.0090

By normalizing the likelihood values for each Outflow, the posterior probability of each *Source_i* for any *Seep_j* is calculated from equation 5.1. **Table 5.3** is summarizing the P(*Source_i* | *Seep_j*) for both of the Outflows. The joint probabilities of *Seep_j* for Outflows #1 and #2 are calculated as:

P(*Seep_1*) = 34.33%

P(*Seep_2*) = 36.34%

Table 5.3 Summary of the Posterior Probabilities of *Source_I* for (a) Flow Path #1 and (b) Flow Path #2

OUTFLOW #1 (Seep_1)				
Source	prior probability	likelihood	Likelihood (normalized)	Posterior Probability
1	26.1%	0.0330	53.8%	**40.9%**
2	47.8%	0.0233	37.9%	**52.8%**
3	26.1%	0.0051	8.3%	**6.3%**

(a)

OUTFLOW #2 (Seep_2)				
Source	prior probability	likelihood	Likelihood (normalized)	Posterior Probability
1	26.1%	0.0297	40.6%	**29.2%**
2	47.8%	0.0345	47.2%	**62.1%**
3	26.1%	0.0090	12.2%	**8.8%**

(b)

As the results of the posterior probabilities in **Table 5.3** show, *Source_2* is the most probable source of flow for both of the Outflows based on the prior beliefs on origin of the seepage flows in earth embankment dams and observation of discharge for each potential Flow Path. However, *Source_1* also has a considerable probability as the origin point of Outflow #1, especially after the observation, the probability of this source was raised significantly (from 26.1% to 40.9%). Such noticeable change is an indicator of site condition (local-level data) is recognizing this source as the most expected origin of Outflow #1, compare to the other two sources. More observations will update our belief on the probabilities and increase the accuracy and confidence over the source of flows.

For Outflow #2, the prior probability identified *Source_2* as the most probable source compare to the other two regions, after the observation was made, the probability of this origin was increased significantly and *Source_2* can be accounted as the most expected source of Outflow #2 based on the available data. Obviously, as more observations are made, our belief about these probabilities are updated. *Source_3* seems to be the least probable origin of the both Outflows #1 and #2 as its probability was decreased considerably after the first observation was made.

5.2.4 Discussion

In this section the probabilities of different scenarios, which were identified by visual inspection and ER survey of the studied dam were evaluated with Bayesian network model. In this model, the prior probabilities were calculated in a separate study presented in Chapter 2. 3D software models were developed for each potential Flow Path and the discharge values were calculated for three different reservoir levels to be compared with the actual discharge was measured on the site as presented in chapters 3 and 4. The likelihood of each source was evaluated based on the results of the discharge measurement and calculating the weighting factor based on each Flow Path conductivity distribution. According to the results, *Source_2* (potential crack in the concrete core at station about 4+30 ft. from the right end of the guard rail and at the depth about 25 ft.) is the most probable source of flow for Outflow #1 and Outflow #2. *Source_1* (Seepage through the right abutment) has also considerable probability as the origin of Outflow#1, especially after the observation was made. *Source_3* (Seepage through the left abutment) seems to have the least probability as the origin of these detected Outflows. However, it should be noted the probability of seepage source for each Outflow was evaluated independently. In

other words, in case *Source_1* is the origin of the Outflow #2 with certainty, all the probabilities for Outflow #2 needs to be updated as the new observation was made and so on and so forth. In this model, the probabilities will be updated as new source of data is available. By accepting the calculated probabilities in this step as the prior probabilities and taking into account the results of any new observation, the new posterior probabilities are calculated, which is our new belief about the sources of each detected Outflow. This process may continue until the sources are recognized with acceptable level of certainty.

5.3 Potential Failure Time and Rate of Erosion

One of the critical matters in safety studies of dams' seepage, is estimating the available time to implement essential actions. These actions range from practices such as lowering the reservoir level, implementing emergency temporary remedial operations or carrying out more site investigations to permanently fix the distressed zones. In extreme situation, even emergency evacuation of the downstream flooding regions is necessary to reduce the potential risk of loss. Although almost all the earth embankment dams are suffering from seepage to some extent, but as long as the seepage is under control and no sign of piping or erosion is detected, the condition is considered as safe. Referring to **Figure 1.1**, the dam is not necessarily in critical condition even if it is suffering from the internal erosion within the "Progression of Breach Initiation" (Time T_1–T_2) phase, but the erosion is under control and the required contingency actions were in place. However, in order to reduce the potential risk of failure and ensure the dam is performing in a safe condition, the attempt is to warrant the status of the dam will remain within "Progression of Breach Initiation" stage. As this schematic graph shows, as soon as the breach initiation stage transits into breach formation (Time T_2–T_3), the rate of erosion increases dramatically, where providing

safety of the dam could be burdensome, if not impossible.

Nevertheless, as the progress of internal erosion is suspected or already been detected in situ, it is difficult to predict the rate of erosion and estimate the time of breach as many uncertainties are involved. Many references put forward equations for prediction of time of failure according to specifications of dams or dikes. Four methods of dam seepage erosion failure time were presented in **section 1.3.1**.

For the studied case, although no sign of internal erosion was reported or observed at the time of inspection, it is assumed an active erosion is occurring and the failure time is estimated with different presented methods to evaluate the safety in more critical condition. More assumptions are made for the parameters with no available sources of data to assign. Such assumptions are described for each employed estimation method.

5.3.1 Theoretical Estimate of Failure Time

For two methods proposed by MacDonald et al. and Froehlich, a single formulation is presented, which requires to replace the parameters to estimate the time of failure. These parameters are mainly representing some basic hydraulic characteristics of the dam that were measured on site or estimated according to the characteristics of the dam and flow. On the contrary, in the methods proposed by Bonelli et al. and Chen et al., more parameters are involved and multiple equations need to be solved simultaneously and repetitively to converge the calculated quantities and measure the failure time. For this purpose, these estimation methods are programmed in MATLAB by defining the geotechnical and hydraulic parameters and calculating the final failure time within a repetitive loop. The syntaxes of these model and description of the parameters are presented in **Appendix C**. The assumptions and estimations for employing the theoretical methods in estimating the

failure time are:

- Length of the pipe is equal to the base of downstream cross section (L =140 ft. = 42.7 m)
- Diameter of the pipe before the roof collapse is equal to half of the embankment height: d = 30 ft. = 9.14 m
- Depth of water above breach invert at time of failure is equal to upstream reservoir water elevation: h_w = 51 ft. = 15.54 m
- V_w = 20,000 ac.ft. = 2.47×10^7 m^3 (reservoir volume at the time of failure)
- Silty sand soil critical stress: τ_c = 13 Pa.
- Dry soil density: ρ_{dry} = 1500 kg/m^3
- Fell coefficient of soil erosion: C_e = 0.001
- Pipe radius at the time of detection: R_d = 0.04 m
- Inclination angle of the seepage passage: θ = 30 degree
- Inter-particle friction angle of silty sand soil: φ = 32 degree
- Cohesion of silty sand soil: C = 18,000 N/m^3
- Velocity coefficient: μ = 0.97
- Porosity: n = 0.3

Therefore, the time of failure (roof collapse) with each of the theoretical methods is estimated as:

- MacDonald and Langridge-Monopolis (from equation 1.1)

  t_f = 0.32 hr ≈ 20 min

- Froehlich (from equation 1.2)

  t_f = 0.61 hr ≈ 37 min

- Bonelli and Benahmed (from equations 1.3 to 1.8)

  t_f = 1.72 hr ≈ 103 min

- Chen and Zhang (from equations 1.9 to 1.12)

  $t_f = 2.34$ hr ≈ 142 min

As the results show, the range of estimated failure time is between 20 minutes to 142 minutes. Wahl (2004) evaluated the failure time predictions suggested by MacDonald et al. and Froehlich, realizing the equations tend to conservatively underestimate actual failure times. Considering these empirical relations are mostly straightforward regression relations that give the failure time solely as a function of limited parameters of the dam and reservoir, it is not expected the calculated values are so accurate. The methods proposed by Bonelli et al. and Chen et al. seem to be more precise theoretically, as major parameters of the dam and flow are taken into account and the progression of erosion is analyzed more systematically and logically. These two methods are estimating the failure time with less than 30% difference from each other and relatively higher than the two other methods. However, it should be noted such estimates are from the time the first signs of erosion are detected and assume that soil is continuously washed out and the process of erosion develops progressively. But in reality this is not the actual behavior of internal erosion the earthen structures in most of the incidents, as the washed-out material may blocked partially or completely the evolutionary pipe and will delay or even clog the piping progress, known as self-healing. Furthermore, for the studied case, visual inspection of the existing condition of the dam did not report any sign of erosion or turbidity in the outflow seepage, indicating no active erosion is occurring at the detected outflows at the toe. Though, any change in the dam's behavior or surrounding condition may result in change of erosion progress of the dam.

5.3.2 Empirical Estimate of Rate of Erosion

In order to estimate the actual progress of erosion and increasing rate of the pipe diameter, the behavior of the dam and seepage flows need to be studied exclusively. The applied methodology to achieve this goal is monitoring the variation of discharge for each outflow over a period of time. If the outflow discharge at any spot has not been changed over the time for the same reservoir elevation, we may conclude no erosion occurred during the period of monitoring and the pipe diameter was not increased. Increasing in amount of discharge over the time for each outflow at a specific reservoir level is an indicator of expansion of pipe diameter means an internal erosion is occurring. On the other hand, decreasing in discharge could be a sign of self-healing or blockage of the pipe. Some assumptions and estimates are made to evaluate the rate of erosion in the studied dam. **Table 5.4** is presenting the estimated discharge values for different reservoir level and over 3 consecutive year.

Figures 5.2 is illustrating the discharge fluctuation over 3 years for two detected outflows. As the graphs show, the value of maximum discharge for Outflow #1 was not changed during three year period of the measurement where the maximum discharge occurred between months of July and September, depending on the reservoir level. But, Outflow #2 does not show the same behavior as the value of maximum discharge is increasing (from 0.0028 to 0.0042 cu ft. /s) during the inspection period, which could be an indicator of expanding the pipe diameter and erosion within the path.

Table 5.4 Estimated Discharge Values for Different Reservoir Level over Three-Year Period

	2014			2015			2016		
Month	Reserv. level (ft)	Q1 (cu ft/s)	Q2 (cu ft/s)	Reserv. level (ft)	Q1 (cu ft/s)	Q2 (cu ft/s)	Reserv. level (ft)	Q1 (cu ft/s)	Q2 (cu ft/s)
Jan	44	0.00112	0.00000	42	0.00126	0.00000	41	0.00093	0.00000
Feb	44	0.00305	0.00000	42	0.00098	0.00010	40	0.00071	0.00000
Mar	45	0.00523	0.00000	43	0.00184	0.00012	42	0.00104	0.00000
Apr	46	0.00647	0.00012	47	0.00743	0.00230	45	0.00369	0.00098
May	45	0.00605	0.00010	48	0.00971	0.00280	49	0.01045	0.00286
Jun	47	0.00850	0.00170	50	0.01004	0.00370	51	0.01240	0.00400
Jul	50	0.01170	0.00220	51	0.01157	0.00340	51	0.01195	0.00420
Aug	51	0.01240	0.00280	48	0.00922	0.00290	51	0.01188	0.00400
Sep	51	0.01190	0.00280	48	0.00899	0.00280	48	0.00914	0.00310
Oct	48	0.00810	0.00095	47	0.00880	0.00240	46	0.00471	0.00215
Nov	46	0.00620	0.00056	45	0.00462	0.00085	45	0.00404	0.00091
Dec	44	0.00320	0.00010	43	0.00247	0.00010	44	0.00258	0.00022

In order to study the discharge fluctuation of the outflows more accurately, the mean and standard deviation of the measured discharges for each reservoir elevation is calculated (**Table 5.5**) and seasonal discharge variations are compared along three year period. **Figure 5.3** is comparing these seasonal changes in comparison with the discharge mean value for each outflow.

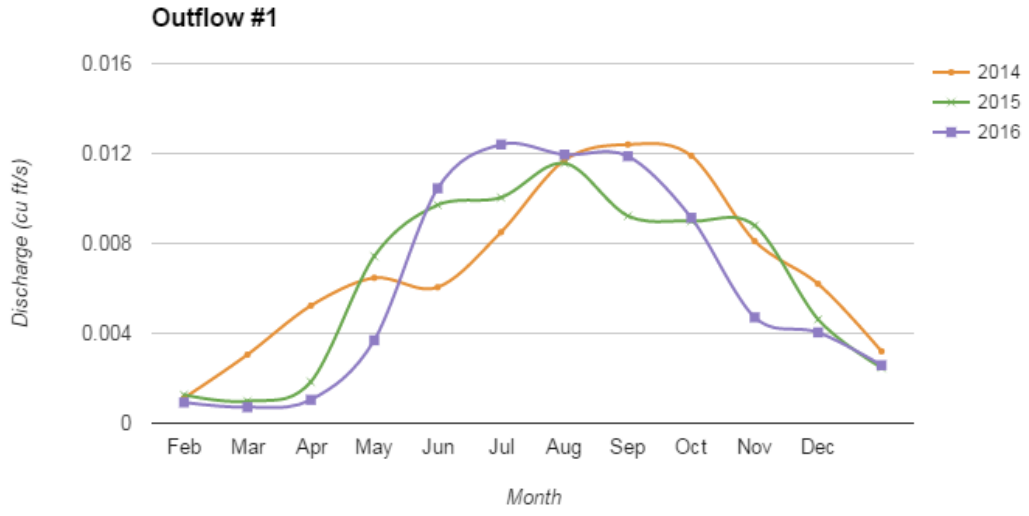

(a)

Figure 5.2 Discharge fluctuation over three year period for (a) Outflow #1 (Continued).

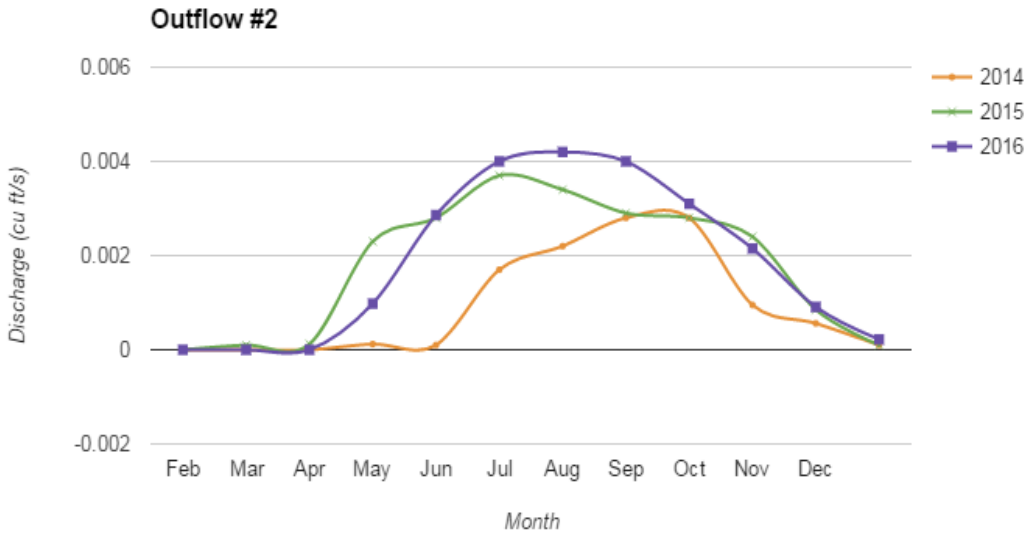

(b)

Figure 5.2 (Continued) Discharge fluctuation over three year period for (b) Outflow#2.

Table 5.5 Discharge Mean Value and SD for Various Reservoir Level

Reserv. level (ft)	Q_1 Mean (cu ft/s)	Standard deviation	Q_2 Mean (cu ft/s)	Standard deviation
40	0.000712	0.000000	0.000000	0.000000
41	0.000925	0.000000	0.000000	0.000000
42	0.001028	0.000178	0.000025	0.000050
43	0.002155	0.000445	0.000110	0.000014
44	0.002500	0.000822	0.000101	0.000101
45	0.004726	0.000944	0.000568	0.000476
46	0.005793	0.000948	0.000627	0.000543
47	0.008243	0.000720	0.002133	0.000379
48	0.009032	0.000587	0.002602	0.000682
49	0.010450	0.000000	0.002860	0.000000
50	0.010870	0.001174	0.002950	0.001061
51	0.012017	0.000326	0.003533	0.000628

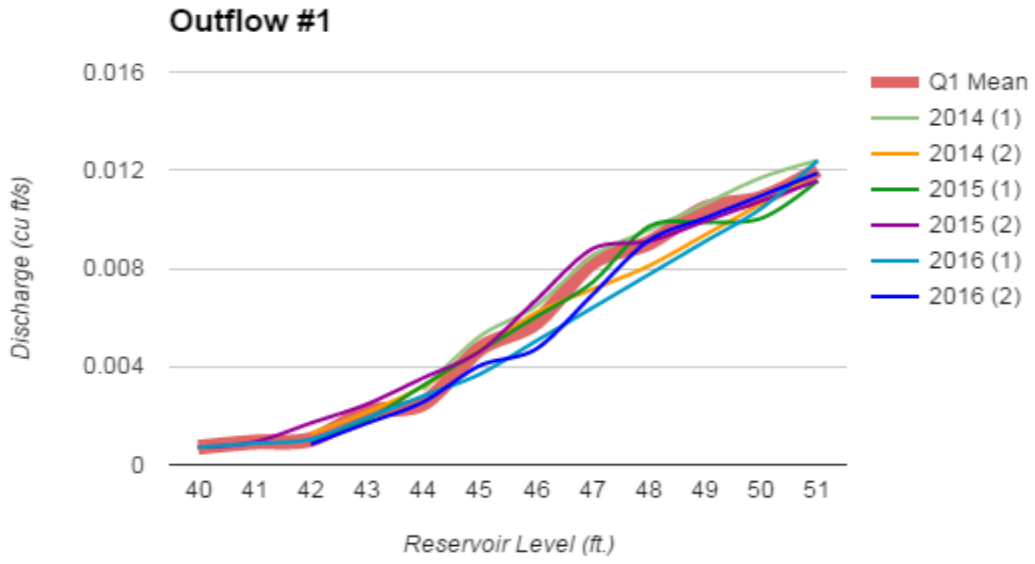

(a)

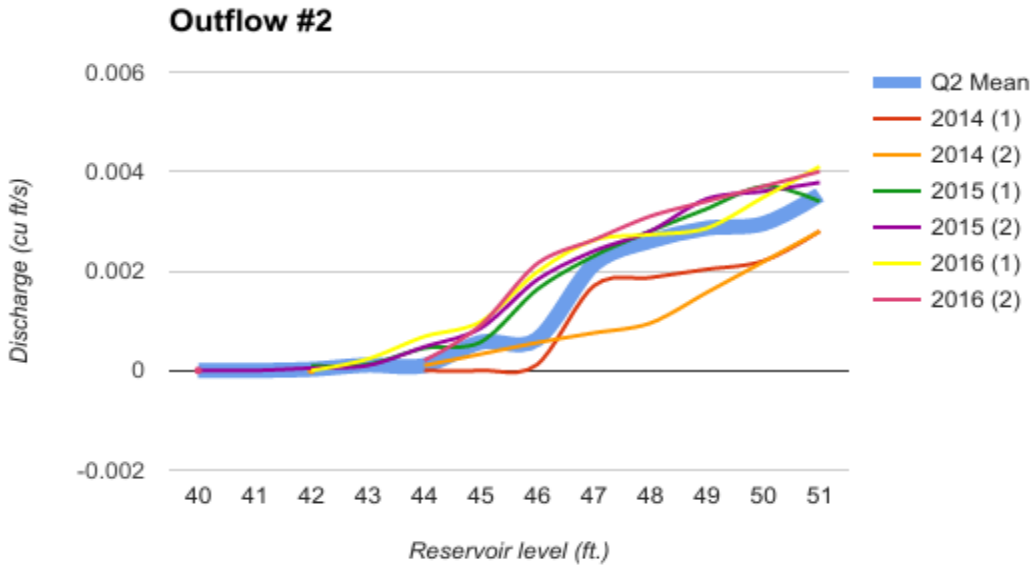

(b)

Figure 5.3 Seasonal outflow discharge vs. reservoir level for (a) Outflow #1 and (b) Outflow #2.

Table 5.6 shows the normalized value of discharge for each reservoir elevation over three year period. According to the results of the normalized values for the two outflows' discharge, it is revealed unlike Outflow #1 discharge (Q_1), the average discharge for Outflow #2 (Q_2) has been increased considerably over three year period. For better overall comparison between both of the Outflows, the average of normalized values are

presented separately in **Table 5.7**. This increase for the same level of the reservoir in Outflow #2 could be a sign of increase in size of the pipe diameter, indicating an active erosion is occurring and soil material has been washed out.

Table 5.6 Discharge Normalized Values for Different Reservoir Levels over Three-Year Period

Month	Reserv. level (ft)	Q_1 (cu ft/s)	Q_1 (cu ft/s) Normalized	Q_2 (cu ft/s)	Q_2 (cu ft/s) Normalized
Jan	44	0.00112	-1.67788	0.00000	-0.99015
Feb	44	0.00305	0.66872	0.00000	-0.99015
Mar	45	0.00523	0.53408	0.00000	-1.19224
Apr	46	0.00647	0.71389	0.00012	-0.93295
May	45	0.00605	1.40302	0.00010	-0.98234
Jun	47	0.00850	0.35640	0.00170	-1.14459
Jul	50	0.01170	0.70711	0.00220	-0.70711
Aug	51	0.01240	1.17725	0.00280	-1.16731
Sep	51	0.01190	-0.35829	0.00280	-1.16731
Oct	48	0.00810	-1.58842	0.00095	-2.41968
Nov	46	0.00620	0.42904	0.00056	-0.12276
Dec	44	0.00320	0.85110	0.00010	0.00000
		Average	0.26800		-0.98471

(2014)

Month	Reserv. level (ft)	Q_1 (cu ft/s)	Q_1 (cu ft/s) Normalized	Q_2 (cu ft/s)	Q_2 (cu ft/s) Normalized
Jan	42	0.00126	1.30587	0.00000	-0.50000
Feb	42	0.00098	-0.27018	0.00010	1.50000
Mar	43	0.00184	-0.70711	0.00012	0.70711
Apr	47	0.00743	-1.12938	0.00230	0.44023
May	48	0.00971	1.15553	0.00280	0.29329
Jun	50	0.01004	-0.70711	0.00370	0.70711
Jul	51	0.01157	-1.37175	0.00340	-0.21224
Aug	48	0.00922	0.32041	0.00290	0.43994
Sep	48	0.00899	-0.07158	0.00280	0.29329
Oct	47	0.00880	0.77297	0.00240	0.70436
Nov	45	0.00462	-0.11233	0.00085	0.59192
Dec	43	0.00247	0.70711	0.00010	-0.70711
		Average	-0.00896		0.35483

(2015)

Table 5.6 Continued Discharge Normalized Values for Different Reservoir Levels over Three-Year Period

Month	Reserv. Level (ft)	Q_1 (cu ft/s)	Q_1 (cu ft/s) Normalized	Q_2 (cu ft/s)	Q_2 (cu ft/s) Normalized
Jan	41	0.000925	0.00000	0.00000	0.00000
Feb	40	0.000712	0.00000	0.00000	0.00000
Mar	42	0.001040	0.06755	0.00000	-0.50000
Apr	45	0.003690	-1.09783	0.00098	0.86479
May	49	0.010450	0.00000	0.00286	0.00000
Jun	51	0.012400	1.17725	0.00400	0.74283
Jul	51	0.011950	-0.20474	0.00420	1.06119
Aug	51	0.011880	-0.41972	0.00400	0.74283
Sep	48	0.009140	0.18407	0.00310	1.32068
Oct	46	0.004710	-1.14293	0.00215	2.80500
Nov	45	0.004040	-0.72694	0.00091	0.71786
Dec	44	0.002580	0.09727	0.00022	1.18818
		Average	-0.17217		0.74528
			(2016)		

Table 5.7 Average of Discharge Normalized Value over Three-Year Period

Year	Q_1 (cu ft/s) Normalized	Q_2 (cu ft/s) Normalized
2014	0.26800	-0.98471
2015	-0.00896	0.35483
2016	-0.17217	0.74528

In order to have an estimate of erosion rate for Outflow #2 based on the empirical site data, some assumptions and estimates are made. The reference reservoir level for comparing the change of discharge value is considered at 51 ft. and the variation is compared over two years. The assumptions and estimates are as follow:

- Length of the Flow Path pipe (L) = 140 ft.
- Height of water head drop (h) = 40 ft.
- Pipe hydraulic conductivity (K) = 0.2 ft./s

According to **Table 5.4**:

- Q_2 (Aug 2014) = 0.0028 cu ft/s (at reservoir level = 51 ft.)
- Q_2 (Aug 2016) = 0.004 cu ft/s (at reservoir level = 51 ft.)

Therefore according to Darcy's law equation (Q = K.i.A) we have:

- Hydraulic gradient (i = h/L) = 0.29
- Initial pipe cross section area (A_1) = 0.05 SF = 7.06 sq.in.
- Initial diameter of pipe (d_1) = 3.00 in
- Final pipe cross section area (A_2) = 0.07 SF = 10.08 sq.in.
- Final diameter of pipe (d_2) = 3.59 in
- Change in Diameter (Δd) = 0.59 in (over 2 years period)
- Change in cross section (ΔA) = 0.02 SF = 3.02 sq.in.
- Amount of soil washed out (ΔV) = 2.94 cu.ft.

According to this estimate, the diameter of the pipe had been widened about 0.6 inches on average and almost 3 cubic feet of soil was washed out through the flow path pipe during two years period. As the results of the empirical analysis show, the rate of erosion may not have serious safety hazard over the short term period, if the behavior of the dam does not change. However, any incident may change the stable behavior of the flow and results in critical active erosion, where the rate of erosion raises and the breach process starts. In this case the failure time is estimated with the theoretical methods discussed earlier.

5.3.3 Discussion

Upon diagnosing initial signs of concentrated seepage and possible internal erosion, estimating the potential time of failure is essential to address the safety status of the dam

and implementing subsequent measures accordingly. Such actions vary from simple operations like lowering the reservoir to implementing emergency repairs or long-term permanent remediation, or even evacuating downstream flood zones in a critical condition to reduce the risk of loss.

However, there are many uncertainties in estimating the failure time from the time the initial signs of seepage and internal erosion is observed. Some studies have been implemented to evaluate the failure time according to the characteristics of the structure and flow. Although for the studied dam, no sign of internal erosion was observed, some assumptions were made to estimate the potential failure time with these theoretical methods, in case of any active internal erosion is occurring. According to this analysis, the theoretical time of failure was estimated between 20 to 142 minutes with different methods. However, it should be noted that these methods are considering the piping process develops progressively, assuming as soon as initial signs of erosion is detected, the soil material within the pipe is washed out and the pipe diameter expands continuously until the final roof collapse of the pipe. Although this scenario may occur, however, in reality the washed-out material may blocked partially or completely the evolutionary pipe and will delay or even clog the piping progress, known as self-healing. Therefore, these theoretical methods may underestimate the time of failure to some extent.

In a separate study, the rate of erosion was also evaluated empirically, by monitoring the variation of discharge according to the reservoir level over a period of time. In this analysis, it is considered that increasing the amount of discharge for specific reservoir level could be an indicator of material washed-out and expanding the diameter of pipe over the time. The results of discharge fluctuation monitoring at two outflows over

the 3 years period implies the amount of discharge at Outflow #1 had not been mutated over the monitoring period where the discharge at Outflow #2 was increased about 30% over two years. Considering the characteristics of the dam and the flow parameters, the increased of the pipe diameter was estimated at about 0.3 inch per year. This rate of erosion is considerably lower than the rates calculated via theoretical methods to estimate the failure time. As mentioned, no sign internal erosion or piping was observed at the studied dam and no critical active erosion is taking place, justifying the substantial difference between the theoretical and empirical estimates.

CHAPTER 6

CONCLUSION

Failure of earth embankment dam may result in catastrophic incidents. Considering concentrated seepage and internal erosion are accounted as one of the major causes of failure, it is essential the dams are regularly inspected to detect any abnormal behavior at very early stage for subsequent safety measures. Various dam safety monitoring methods have been evolved over the past few decades, each is measuring specific parameter of the structure or flow with advantages and limitations for each method. Electrical Resistivity Tomography (ERT) is one of the effective methods in seepage monitoring in earthen hydraulic structures, confirmed by scholars and experts. Many case studies confirmed the accuracy and reliability of this method. When a leak is detected with any monitoring tool, an analytical method needs to be employed to find the source of the flow and investigate for any sign of internal erosion. In case of erosion occurrence, the rate of erosion and potential failure time needs to be estimated.

In this study, first, two separate statistical studies were done. In the first study, 182 seepage incidents in earth embankment dams were studied to identify the potential sources of flow. According to this study, in 45.0% of the incidents this source was located around embedded culverts, pipes and spillways. This number was 31.4%, 17.1% and 6.4% for embankments, abutments and foundation respectively. In the second study, the accuracy of ERT method in seepage detection in earthen hydraulic structures was evaluated by reviewing 22 case studies. In these case studies, ERT and one or more other seepage monitoring methods were employed to detect the flows. According to the results, in 98% of the incidents, ERT detected the zones with anomaly behavior that already been detected by any other methods,

indicating the accuracy and reliability of ERT in earth embankment dam seepage studies.

Second, an earth embankment dam suffering from concentrated seepage was monitored visually and with ERT method. The dam is about 60 ft. high, has concrete core and is located in north New Jersey. Visual inspection found two outflows at the toe of the dam. By installing weirs, the discharge of the flows were measured during three seasons and at different reservoir levels. ER survey was implemented along three surveying lines at the crest, mid-berm and the toe and low resistant zones were detected, which were considered as the potential zone of flow at each section of survey. According to the results of the monitoring, three different seepage scenarios were identified for each of the detected outflows and the source and path of each flow was located. The recognized sources for both of the outflows were determined at the right abutment (*Source_1)*, crack in the concrete core at station about 4+30 ft. from the right abutment (*Source_2*), and the left abutment (*Source_3*). 3D software models were developed for each of the identified scenarios and the discharge was calculated for each model and at three reservoir levels.

Bayesian Model Network was employed as an analytical tool to determine the probability of each identified scenario. In this model, the prior probabilities are assessed base on the calculated probabilities that were determined in the first statistical study. These values were adjusted according to the specification of the studied case, by taking into account that the source of flows were not through the foundation and around the embedded culverts, pipes and spillways. The observation for this analysis was the error between the calculated discharges values of each identified flow path for each outflow and the actual measured values at three different reservoir levels. According to the results of the posterior probability analysis, *Source_2* has the most probability as the origin of the flow for both of the detected outflows.

For Outflow #1, *Source_1* has also a considerable probability, whilst *Source_3* has the minimum probability of acting as the origin of any of the detected outflows and based on the available data and the observation.

Although no sign of piping or internal erosion was observed at the studied dam, by assuming an active erosion is occurring, the failure time of the dam is estimated with four theoretical methods, proposed by scholars. Some assumptions and estimation were made to determine the geotechnical and hydraulic parameters. According to this analysis the failure time ranged between 20 to 142 minutes since the first signs of the erosion is detected and with the assumption the erosion is continuously progressed until the final failure of the dam. In a separate analysis, by evaluating the change of discharge rate and estimating the length of the flow pipe, change the diameter of the flow pipe and approximate volume of washed out soil was rated. Although according to available data and the general condition, the dam seems to be sick but in a stable condition, but any trigger (like settlement, earthquake, hurricane, etc.) may change the behavior and bring it to critical situation, where managing and controlling of it could be extremely difficult and costly, if not impossible.

In this research, only one geophysical monitoring method (ERT) was employed to identify potential flow path scenarios for one reservoir level. It is recommended to utilize multiple methods and over a period of time to closely monitor the behavior of the dam and quantify the results to update the probability beliefs about the potential sources of the leaks. Implementing dye test at the three potential sources were identified in this this stage of investigation is a recommended approach for the following step of monitoring.

APPENDIX A

STATISTICAL DATASET TO LOCATE POTENTIAL SOURCES OF SEEPAGE

Table A.1 is presenting the list of the studied dams for statistical analysis to identify the origin of the concentrated seepage and some generic information of each dam. The source of this assessment study is National Performance of Dams Program (NPDP) database, developed by Stanford University.

Table A.1 List of the studied dams for the statistical analysis to identify the origin of concentrated seepage (Continued)

No	NPDP ID	Dam Name	State	Incident Date	Incident Type	Dam Failure	Dam Type	Dam Height (ft)	Distress Location	Type of core
1	CA00327	Lake Almanor	CA	5/13/1997	Seepage	No	Earth	89.9	unknown	unknown
2	CA00441	Vermillion	CA	7/10/2006	Seepage	No	Earth	165	Foundation	unknown
3	CA10111	Owens Dam	CA	1914	Seepage	Yes	Earth	22.9	around outlet structure	Unkown
4	CO00167	Rist - Benson	CO	7/21/1999	Seepage;Piping	No	Earth	19	embankment	Homogeneous Earth
5	CO00347	Woodland Park	CO	12/3/1999	Seepage;Piping	No	Earth	60	unknown	unknown
6	CO00382	Jumbo	CO	1910	Seepage	Yes	Earth	70	foundation	Unkown
7	CO00434	Rampart	CO	6/14/1995	Seepage;Piping	No	Earth	230	unknown	earth core
8	CO00483	Balman Reservoir	CO	10/28/1996	Seepage;Piping	No	Earth	26.9	embankment	unknown
9	CO00513	Wahatoya Lake	CO	4/2/2001	Seepage	No	Earth	24	Embankment	unknown
10	CO00544	North Lake	CO	2/18/2000	Seepage	No	Earth	94	Unknown	unknown
11	CO00677	Consolidated	CO	6/7/1995	Seepage	No	Earth	40	embankment	Homogeneous Earth
12	CO00684	Spring Park	CO	2/10/1999	Seepage	No	Earth	20	from joint in outlet conduit	Homogeneous Earth
13	CO00689	Jones	CO	9/26/1995	Seepage; Embankment Slide	No	Earth	29.8	embankment	Homogeneous Earth
14	CO00701	Matheson Reservoir	CO	9/12/2000	Seepage;Piping	No	Earth	63	Foundation	Upstream Facing Earth
15	CO00712	Little King Ranch	CO	8/2/1995	Seepage;Piping	No	Earth	50.1	unknown	earth core
16	CO00716	Scholl	CO	8/19/1998	Seepage;Piping	No	Earth	50.84	abutment	earth core
17	CO00720	Granby #11	CO	6/6/2000	Seepage;Piping	No	Earth	31	Embankment	Homogeneous Earth
18	CO00760	G.W. Verhoeff	CO	6/13/1995	Seepage;Piping	No	Earth	18	embankment	unknown
19	CO00790	Sanchez	CO	6/29/2000	Seepage;Piping	No	Earth	137	Foundation	unknown
20	CO00962	Big Beaver	CO	7/10/1997	Seepage	No	Earth	89.9	10 feet below spillway	unknown
21	CO01046	Horse Creek	CO	2/25/1999	Seepage	No	Earth	23	unknown	unknown
22	CO01116	Lake Henry	CO	6/9/1995	Seepage;Piping	No	Earth	18	embankment	unknown

Table A.1 (Continue) List of the studied dams for the statistical analysis to identify the origin of concentrated seepage (Continued)

No	NPDP ID	Dam Name	State	Incident Date	Incident Type	Dam Failure	Dam Type	Dam Height (ft)	Distress Location	Type of core
23	CO01164	Elder	CO	4/1/1999	Seepage;Piping	No	Earth	21	adjacent to the outlet	unknown
24	CO01194	Ryan Gulch	CO	8/27/1996	Seepage	No	Earth	36.1	at the toe over over outlet	unknown
25	CO01236	Oligarchy #1	CO	5/13/1999	Seepage	No	Earth	18	Embankment	Homogeneous Earth
26	CO01899	Milton Lake	CO	6/27/1995	Seepage;Piping	No	Earth	49.9	over toe drain pipe	unknown
27	CO02033	No Name 1-1 #1	CO	10/5/2000	Seepage;Piping	No	Earth	18.5	Embankment	unknown
28	CO02795	Regulating Reservoir	CO	10/29/1996	Seepage;Piping	No	Earth	96.1	embankment	Upstream Facing Plastic
29	CO02804	Western Hillside Reservoir	CO	10/11/1997	Seepage;Piping	No	Earth	45.9	foundation	Upstream Facing Plastic
30	CO83006	Clear Lake	CO	5/28/1997	Seepage;Piping	No	Earth	19	outlet works	Metal
31	FL00176	Lake Grady Dam	FL	1/25/2000	Seepage;Piping	No	Earth	25	Spillway	unknown
32	GA00113	Walkers Lake Dam	GA	2001	Seepage	No	Earth	21	Spillway pipe	unknown
33	GA00795	Lake Toccoa Dam	GA	1/31/2001	Seepage	No	Earth	22.7	Spillway pipe	unknown
34	GA03958	Plant Bowen Ash Pond	GA	7/28/2002	Seepage	No	Earth	44.9	Unknown	unknown
35	GA04598	Lake Nora Dam	GA	8/10/2001	Seepage;Piping	No	Earth	60.2	Unknown	unknown
36	GA04975	Forsyth Reservoir	GA	12/24/1997	Inflow Flood - Hydrologic Event;Seepage;Piping;Concrete Deterioration	Yes	Earth	20	concrete shell spillway	unknown
37	ID00039	Magic Dam	ID	7/24/1996	Seepage	No	Earth	4.9	beneath flashboard spillway	unknown
38	ID00105	Little Canyon (Morrow)	ID	5/16/1995	Seepage;Piping	No	Earth	25.6	above outlet	unknown
39	ID00123	Jussila Bow	ID	8/16/1993	Seepage	No	Earth	18.4	above the outlet pipe	unknown

Table A.1 (Continue) List of the studied dams for the statistical analysis to identify the origin of concentrated seepage (Continued)

No	NPDP ID	Dam Name	State	Incident Date	Incident Type	Dam Failure	Dam Type	Dam Height (ft)	Distress Location	Type of core
40	ID00151	Troy	ID	2/5/1995	Seepage;Piping	Yes	Earth	37.4	abutment	unknown
41	ID83069	Horseshoe Bend Canal	ID	3/12/1998	Seepage	No	Earth	24.9	power canal	unknown
42	IL00201	Big Four Reservoir Dam	IL	3/25/1999	Seepage	No	Earth	27	Embankment	unknown
43	IL00421	Lake Rice Dam	IL	3/23/1992	Seepage	No	Earth	10.7	abutment	unknown
44	IL00712	Riverview Dam	IL	11/21/1985	Seepage	Yes	Earth	8.8	spillway chute	unknown
45	IL00739	Pine Lake Dam	IL	1/18/1995	Seepage;Piping;Concrete Deterioration	No	Earth	25	concrete chute spillway	unknown
46	IL50396	Pittsfield Dredge Disposal Pond Dam	IL	4/29/1999	Seepage;Piping	Yes	Earth	35	Conduit	unknown
47	KS01251	Larson, Dr. O.M.	KS	1/22/2001	Piping;Seepage	No	Earth	20	Unknown	unknown
48	KS01253	Demaranville, Don, Sarcoxie Lake Dam	KS	7/25/2001	Seepage;Headcut in the emergency spillway	No	Earth	35	Spillway	unknown
49	KS02987	Ksnoname 2987	KS	3/6/2002	Seepage	No	Earth	45	Primary Spillway	unknown
50	KS03730	Yeager, Yeager Lakes Dam	KS	1/7/2002	Seepage	No	Earth	22	Spillway	unknown
51	KY00137	Caulk Lake Dam	KY	12/16/1973	Seepage	Yes	Earth	20.1	Embankment	unknown
52	KY00174	Hematite	KY	6/11/1998	Not Known; Seepage; Piping	Yes	Earth	12.1	unknown	unknown
53	MAS00001	Williamsburg	MA	5/16/1874	Seepage	Yes	Earth	13.1	Embankment	Masonary
54	MES00001	Mountjoy Hill Reservoir	ME	8/6/1893	Seepage	Yes	Earth	13.7	Around embeded pipe	None
55	MO10135	Holiday Acres Lake Dam	MO	1/3/1994	Seepage;Embankment Slide	No	Earth	44.9	abutment	earth core
56	MO10660	City Of Higbee Dam	MO	6/18/1993	Seepage	No	Earth	44.9	Embankment	none

Table A.1 (Continue) List of the studied dams for the statistical analysis to identify the origin of concentrated seepage (Continued)

No	NPDP ID	Dam Name	State	Incident Date	Incident Type	Dam Failure	Dam Type	Dam Height (ft)	Distress Location	Type of core
57	MO11241	Lake Flamingo Dam	MO	6/6/2001	Seepage/Piping	No	Earth	20	Spillway	unknown
58	MO20164	Lake Venita Dam	MO	2/21/1997	Seepage;Piping	Yes	Earth	29.8	embankment	unknown
59	MO20237	Sunny Shores Dam	MO	6/21/1995	Seepage	No	Earth	19.7	beneath concrete weir	unknown
60	MO30541	Las Brisas Lake Dam	MO	5/24/1993	Seepage;Embankment Erosion	No	Earth	45.9	along the outside of the principal spillway pipe	earth core
61	MO31374	Richardet Dam	MO	12/1/1985	Seepage;Embankment Slide	Yes	Earth	6.7	Embankment	unknown
62	MS00503	Lake Hazel	MS	9/27/2004	Animal Attack;Seepage	No	Earth	25	Unknown	unknown
63	MS00709	Lake Beaver	MS	5/24/2004	Seepage;Piping	No	Earth	24	Unknown	Homogeneous Earth
64	MS01716	Dennery Lake	MS	4/2/2005	Seepage; Piping; Biological growth	Yes	Earth	22	Unknown	Earth Core
65	MS02674	Faulkner Lake	MS	5/1/2004	Seepage;Piping	No	Earth	30	under primary spillway slab	Earth Core
66	MS03334	Lake Gary Dam	MS	9/1/1995	Seepage;Piping	Yes	Earth	40	embankment	unknown
67	MS03357	Bridgefield Lake Dam	MS	7/6/2001	Seepage/Piping	No	Earth	25	Embankment	Earth Core
68	MT00014	Nilan East Dam	MT	4/6/1999	Seepage;Piping	No	Earth	51	Embankment	unknown
69	MT00577	Willow Creek	MT	6/27/1996	Seepage;Piping	No	Earth	92.8	embankment	Bituminous Concrete
70	MT00850	Tin Cup Lake	MT	5/20/1998	Seepage;Piping	No	Earth	22.6	embankment	unknown
71	MTS00004	Anaconda	MT	7/28/1938	Seepage	Yes	Earth	21.9	Unknown	concrete
72	NC00002	Woodlake Dam	NC	11/10/1998	Seepage;Piping	No	Earth	23	the primary spillway	unknown
73	NC00092	Broughton Hospital Dam	NC	12/22/1999	Seepage/Piping	No	Earth	70	Spillway	unknown

Table A.1 (Continue) List of the studied dams for the statistical analysis to identify the origin of concentrated seepage (Continued)

No	NPDP ID	Dam Name	State	Incident Date	Incident Type	Dam Failure	Dam Type	Dam Height (ft)	Distress Location	Type of core
74	NC00114	Lake Montonia Dam	NC	2/21/1995	Seepage;Piping;Concrete Deterioration	No	Earth	45	bottom drain pipe/ abutment	unknown
75	NC00171	Osage Lake Dam	NC	10/31/2000	Seepage	No	Earth	36	Unknown	unknown
76	NC00189	High Rock Lake Dam	NC	2/17/1995	Seepage;Embankment Erosion	No	Earth	37.1	under the concrete spillway channel	unknown
77	NC00196	Mother Earth Dam Lower	NC	10/1/1999	Seepage;Piping	No	Earth	20.5	Drain Barrel	unknown
78	NC00202	Young Dam	NC	2/8/1996	Seepage	No	Earth	36.1	unknown	unknown
79	NC00242	Roaring Gap Lake Dam	NC	10/19/2000	Seepage	No	Earth	68.9	Embankment	unknown
80	NC00286	Echo Lake Dam	NC	3/30/1995	Seepage;Concrete Deterioration	No	Earth	43	vicinity of the first joint of the pipe	unknown
81	NC00504	Little Lake Dam	NC	1/11/2001	Seepage	No	Earth	18	Spillway	unknown
82	NC00508	White Store Lake Dam	NC	1/11/2001	Seepage	No	Earth	20	Unknown	unknown
83	NC00633	Bland Lake Dam	NC	4/17/2001	Piping;Seepage;Lack of maintenance	No	Earth	18	Spillway	unknown
84	NC00636	Boyd Lake Dam	NC	4/6/2000	Seepage/Piping	No	Earth	15	Spillway	unknown
85	NC01033	Lake Unity Dam	NC	8/30/2000	Seepage	No	Earth	20	Abutment	unknown
86	NC01091	X Way Millpond Dam	NC	1/23/1996	Seepage;Piping	No	Earth	15.1	principal spillway sidewalls	unknown
87	NC01096	Hannas Lake Dam	NC	1/31/1995	Seepage	No	Earth	20	unknown	unknown
88	NC01153	Country Club Lake Dam	NC	1994	Seepage	Unknown	Earth	9.8	foundation	unknown
89	NC01220	Linville Lake Dam	NC	2/14/1995	Seepage;Embankment Erosion	No	Earth	24.9	emergency spillway	unknown
90	NC01298	Hogback Dam	NC	7/3/2000	Seepage	No	Earth	42.5	Spillway	unknown
91	NC01358	Fraternal Order Of Eagles	NC	12/1/1994	Animal Attack;Seepage;Embankment Erosion	No	Earth	30.8	embankment	unknown

Table A.1 (Continue) List of the studied dams for the statistical analysis to identify the origin of concentrated seepage (Continued)

No	NPDP ID	Dam Name	State	Incident Date	Incident Type	Dam Failure	Dam Type	Dam Height (ft)	Distress Location	Type of core
92	NC01404	Moravian Camp Lake Dam	NC	2/14/1995	Seepage	No	Earth	42	at the outlet of the barrel pipe, below the dam	unknown
93	NC01558	White Lake Dam	NC	1/24/1995	Seepage;Piping	No	Earth	49.9	unknown	unknown
94	NC01793	Davis Pond Dam	NC	4/4/1994	Seepage;Concrete Deterioration	No	Earth	22	embankment	unknown
95	NC01843	Flat Rock Pond Dam	NC	2/14/1995	Seepage;Embankment Erosion	No	Earth	22	embankment	unknown
96	NC02144	Points East Dam	NC	10/6/1999	Seepage;Piping	No	Earth	17	Unknown	
97	NC02611	Dobbs Pond Dam #2	NC	1/12/1995	Seepage	No	Earth	20	unknown	unknown
98	NC02833	Lakeview Farm Dam	NC	12/7/2000	Animal Attack/Damage; Seepage; Biological growth	No	Earth	21	Unknown	unknown
99	NC02974	Blanchard Dam #4	NC	3/12/1998	Seepage	No	Earth	37.1	embankment	unknown
100	NC03001	Cataloochee Ranch Dam	NC	11/15/1994	Seepage;Embankment Slide	No	Earth	22.6	left of the bottom drain outlet	unknown
101	NC03056	Winkler Lake Dam Lower(Flat Rock Lakes)	NC	4/20/1999	Seepage	Yes	Earth	25	Outlet pipe	unknown
102	NC03064	Shealy Lake Dam Upper	NC	12/16/1999	Seepage/Piping	No	Earth	18	Embankment	unknown
103	NC03071	Wilkes Dam	NC	1/13/1999	Seepage	No	Earth	25	Embankment	unknown
104	NC03077	Delorenzo Dam	NC	3/2/1995	Seepage	No	Earth	48.9	abutment	unknown
105	NC03107	New Hope Fishing Lake East	NC	12/16/1998	Seepage/Piping	No	Earth	23.9	embankment	unknown
106	NC03427	Jordan Business Forms Lake Dam	NC	4/29/1994	Seepage	No	Earth	29.8	embankment	unknown
107	NC03453	University Place Dam	NC	1/25/1995	Seepage	No	Earth	44.9	bottom drain conduit pipe	unknown

Table A.1 (Continue) List of the studied dams for the statistical analysis to identify the origin of concentrated seepage (Continued)

No	NPDP ID	Dam Name	State	Incident Date	Incident Type	Dam Failure	Dam Type	Dam Height (ft)	Distress Location	Type of core
108	NC03470	Raintree Dam #4	NC	N/A	Seepage	No	Earth	19	abutment	unknown
109	NC03578	Pinehurst Unit 15 Dam	NC	4/16/1999	Hole (Seepage/Piping?)	No	Earth	28	Unknown	unknown
110	NC03868	Sanford Knight Dam	NC	10/7/1997	Seepage	No	Earth	unknown	foundation	unknown
111	NC04095	John W. Bennett	NC	1/7/1999	Seepage	No	Earth	22	Spillway	unknown
112	NC04254	City Lake	NC	11/20/2002	Seepage; Biological growth; Embankment Erosion	No	Earth	22.8	Abutment	unknown
113	NC04338	Brevard Music Camp Lower	NC	1/4/2001	Seepage	No	Earth	23	Spillway Wall	unknown
114	NC04658	Applachian Crest Dam	NC	9/1/2002	Seepage; Embankment Erosion; Modification without permit	No	Earth	35	Embankment	unknown
115	NC04843	Melva Brook Pond "Lower"	NC	12/17/2002	Seepage; Biological growth; Embankment Erosion	No	Earth	18.3	Embankment	unknown
116	NC04920	Goforth Dam # 1	NC	6/27/1995	Seepage	No	Earth	20	abutment	unknown
117	NC04921	Goforth Dam # 2	NC	3/16/1995	Seepage	No	Earth	29.8	abutment	unknown
118	NC05189	Ratliff Pond Dam	NC	12/3/2002	Seepage	No	Earth	22	Unknown	unknown
119	ND00005	Mount Carmel Dam	ND	N/A	Seepage	No	Earth	54	under concrete chute spillway and drop inlet	Earth Core
120	ND00426	Simpson Dam; Alvin	ND	7/17/1986	Inflow Flood - Hydrologic Event; Seepage; Piping	Yes	Earth	4.9	around embeded pipe	unknown
121	NE00963	Bear Cr Dam 7-D	NE	6/11/1999	Seepage	No	Earth	36	Conduit	Homogeneous Earth
122	NE01875	Hurt Dam	NE	6/19/1995	Seepage;Piping	No	Earth	29.8	under the downstream end of the pipe	Homogeneous Earth

Table A.1 (Continue) List of the studied dams for the statistical analysis to identify the origin of concentrated seepage (Continued)

No	NPDP ID	Dam Name	State	Incident Date	Incident Type	Dam Failure	Dam Type	Dam Height (ft)	Distress Location	Type of core
123	NE02363	Timperley Wildlife Res	NE	6/1/1999	Seepage	Yes	Earth	11	Spillway conduit	Homogeneous Earth
124	NH00749	Pond	NH	7/31/2001	Seepage	No	Earth	14	Pond Drain	unknown
125	NH01364	Mountain Lake	NH	9/7/2000	Deterioration;Seepage	No	Earth	13	Spillway	unknown
126	NV00076	Mill Creek No 2	NV	7/6/1995	Seepage;Piping	No	Earth	55.1	unknown	earth core
127	NYS00020	Fred Trick Dam No. 1357	NY	11/19/1974	Seepage; Structural Failure	Yes	Earth	4.6	Embankment	concrete
128	OH00023	Caldwell Lake Dam	OH	5/4/1994	Seepage;Piping;Concrete Deterioration	No	Earth	35.4	along the spillway conduit	unknown
129	OH00093	Sellers Lake Dam	OH	3/15/2000	Seepage	No	Earth	29.6	Abutment	unknown
130	OH00094	Jacobs Lake Dam	OH	6/28/2000	Seepage/Piping	No	Earth	25	Unknown	unknown
131	OH00120	Jefferson Sportsman'S Lake No. 1 Dam	OH	11/1/2000	Seepage/Piping/Inadequate Spillway Capacity	No	Earth	39.5	Unknown	unknown
132	OH00123	Friendship Park Lake Dam	OH	10/20/1999	Seepage	No	Earth	94.4	Abutment	unknown
133	OH00139	Foster'S Lake Dam	OH	1/29/1994	Inflow Flood - Hydrologic Event; Seepage; Embankment Slide	No	Earth	26.2	embankment	unknown
134	OH00290	Elks Country Club Lake Dam	OH	3/13/1995	Seepage;Piping;Concrete Deterioration	No	Earth	27.9	embankment	unknown
135	OH00382	Lake Seneca Dam	OH	9/27/1996	Seepage;Piping	No	Earth	36.1	drain outlet	unknown
136	OH00470	Lake Otto Dam	OH	N/A	Seepage	No	Earth	24.9	Conduit and outlet aera	unknown
137	OH00495	Crystal Lake Dam	OH	8/30/1995	Not Known; Seepage; Concrete Deterioration	No	Earth	14.4	unknown	unknown
138	OH00506	Di-Or Lake Dam	OH	2/28/1995	Seepage;Concrete Deterioration	No	Earth	32.1	along spillway pipe	Homogeneous Earth

Table A.1 (Continue) List of the studied dams for the statistical analysis to identify the origin of concentrated seepage (Continued)

No	NPDP ID	Dam Name	State	Incident Date	Incident Type	Dam Failure	Dam Type	Dam Height (ft)	Distress Location	Type of core
139	OH00516	Decker Lake Dam	OH	2/2/1998	Inadequate Spillway Capacity/Seepage	No	Earth	16.1	unknown	unknown
140	OH00676	Aurora Pond Dam	OH	8/22/2000	Seepage/Piping/Inadequate Spillway Capacity	No	Earth	9.2	Spillway	unknown
141	OH00757	Bellevue Upground Reservoir No. 5	OH	7/29/1998	Seepage	No	Earth	27.9	unknown	unknown
142	OH00780	New Washington Reservoir No. 2 (West)	OH	12/14/1998	Seepage	No	Earth	14.8	unknown	unknown
143	OH00861	Robins Ridge Golf Club Lake No. 2 Dam	OH	5/23/1996	Seepage;Piping	No	Earth	27.9	abutment	unknown
144	OH00866	Columbus And Southern Pond Dam	OH	5/10/2000	Seepage	No	Earth	37	Unknown	unknown
145	OH00898	Jeffco Pond Dam	OH	3/23/1999	Seepage/Slide/Inadequate Spillway Ca	No	Earth	37	Embankment	unknown
146	OH00903	Mader Pond Dam	OH	1/17/2001	Seepage	No	Earth	28.9	Unknown	unknown
147	OH01017	Plymouth Wastewater Lagoon	OH	12/4/1996	Seepage	No	Earth	10.2	embankment	unknown
148	OH01045	Olivito Lake Dam	OH	3/27/1999	Seepage;Piping	No	Earth	31.8	Abutment	unknown
149	OH01114	Pine Lake Dam	OH	9/13/2000	Seepage/Deterioration	No	Earth	16	Unknown	unknown
150	OH01310	Gravis Lake Dam	OH	6/21/2000	Seepage/Piping/Inadequate Spillway Capacity	No	Earth	33.6	Unknown	unknown
151	OH02258	Thomas Lake Dam	OH	2/13/1996	Seepage	No	Earth	25.3	foundation	unknown
152	OH02281	Paint Creek Coon Hunters Club, Inc. Dam	OH	12/8/1999	Seepage/Piping/Inadequate Spillway Capacity	No	Earth	20.6	Unknown	unknown
153	OH02387	Scioto County Sludge Lagoon	OH	3/13/1995	Seepage	No	Earth	45.9	embankment	unknown

Table A.1 (Continue) List of the studied dams for the statistical analysis to identify the origin of concentrated seepage (Continued)

No	NPDP ID	Dam Name	State	Incident Date	Incident Type	Dam Failure	Dam Type	Dam Height (ft)	Distress Location	Type of core
154	OH02431	Shady Hollow Pond Dam	OH	2/3/1997	Seepage	No	Earth	14.4	abutment	unknown
155	OH02658	Bud Lake Dam	OH	2/29/2000	Seepage/Piping/Dam Operations	No	Earth	26	Abutment	unknown
156	OH02707	Crawford Fitting Company Pond Dam	OH	12/8/1995	Seepage;Piping	No	Earth	13.8	embankment	unknown
157	OH02753	New Washington Reservoir No. 1 (East)	OH	12/14/1998	Seepage	No	Earth	11.5	unknown	unknown
158	OK00566	Sahoma Lake	OK	6/26/1997	Seepage;Piping	No	Earth	44.9	around outlet box at downstream toe	soil
159	OK00663	Scs-Upper Red Rock Creek Site-20	OK	10/3/1986	Seepage;Piping	Yes	Earth	9.4	Embankment	unknown
160	OK11001	Knight	OK	7/6/1999	Seepage/Piping	No	Earth	15	Unknown	unknown
161	OK11073	Cedar Lake	OK	11/8/1986	Not Known;Seepage;Piping	Yes	Earth	13.7	abutment	unknown
162	OR83056	Frog Lake Dam B	OR	5/31/1996	Seepage	No	Earth	69.9	unknown	unknown
163	PA00283	Hemlock	PA	7/22/1996	Deterioration/Seepage/Piping	No	Earth	43	unknown	unknown
164	PA00394	Warren H. Ohl	PA	1/18/1995	Seepage;Piping	No	Earth	59	around spillway channel	unknown
165	PA00595	Rexmont No. 1	PA	2/18/2000	Seepage/Piping/Erosion	No	Earth	30	Spillway	unknown
166	PA00782	Bradys Lake	PA	N/A	Seepage/Piping/Inadequate Spillway Capacity	No	Earth	18	Unknown	unknown
167	RIS00017	Little Round Top	RI	6/6/2002	Seepage	No	Earth		Spillway	unknown
168	SD00011	Newell	SD	5/14/1997	Seepage	No	Earth	27.9	abutment	Soil
169	SD02205	Prince Irrigation Dam #2	SD	10/5/2000	Seepage/Piping	No	Earth	46	Spillway	Bituminous Concrete

Table A.1 (Continue) List of the studied dams for the statistical analysis to identify the origin of concentrated seepage

No	NPDP ID	Dam Name	State	Incident Date	Incident Type	Dam Failure	Dam Type	Dam Height (ft)	Distress Location	Type of core
170	TN01102	Hoskins	TN	2/7/2000	Seepage;Piping	No	Earth	18	Embankment	Homogeneous Earth
171	TX00954	Big Woods Spring Lake Dam	TX	10/31/1996	Seepage;Piping	No	Earth	27.9	unknown	unknown
172	UT00114	Fool Creek No 1	UT	2/5/1974	Seepage	Yes	Earth	7.3	dike	unknown
173	UT00301	Trial Lake	UT	6/7/1986	Seepage;Piping	Yes	Earth	9.4	dike	unknown
174	UT00328	Willow Creek	UT	6/12/1942	Seepage	Yes	Earth	7.6	Abutment	Unkown
175	UT00514	Quail Creek	UT	12/31/1988	Seepage;Piping;Embankment Erosion	Yes	Earth	63.7	Embankment	unknown
176	UT10113	Steinaker	UT	12/1/1962	Seepage	Unknown	Earth	49.4	Abutment	unknown
177	WA00547	Swano Lake Dam	Wa	12/27/1994	Inflow Flood - Hydrologic Event;Seepage;Embankment Erosion	No	Earth	20	at an open pipe joint sluiced	earth core
178	WA83006	Swift No 2 Hydroelectric Project	Wa	4/21/2002	Seepage;Piping	Yes	Earth	83	Foundation	unknown
179	WAS00014	Sid White	Wa	5/20/1971	Seepage	Yes	Earth	4.3	Embankment	unknown
180	WI00410	Bad Axe Structure No. 24	WI	6/1/2000	Seepage/Piping	No	Earth	40	Abutment	Homogeneous Earth
181	WI00503	Dam	WI	4/23/1997	Seepage;Piping	No	Earth	17.1	principal spillway	unknown
182	WI01167	Coon Creek 41	WI	1978	Seepage	Yes	Earth	11.9	abutment	unknown

APPENDIX B

STATISTICAL DATASET TO EVALUATE ELECTRICAL RESISTIVITY METHOD IN SEEPAGE DETECTION

Table B.1 is presenting the list of the studied dams for statistical analysis to evaluate the accuracy of Electrical Resistivity method in detecting subsurface flows in earthen hydraulic structures.

Table B.1 Summary of statistical analysis to evaluate accuracy of ERT method in seepage detection (Continued)

No.	Type	Location	Material	Height	Length	Method	Anomaly Zones Detected by Other Methods (than ERT)	Anomaly Zones Detected by ERT	% precision of ERT	Reference
1	Earthfill Dam	Colorado	Homogeneous earthfill composed of silty clay material	11 m	122 m	ERT, SP, OL	3 SP (1 was confirmed by OL)	3 (same zones as detected by other methods)	100%	Ikard, Revil, Schmutz, Karaoulis, Jardani, Mooney (2013)
2	Dam (model)	Lab model	Homogeneous - soil, sand & gravel	1.5m	3.6m	ERT, OL	1 OL	1 (same zone as detected by other method)	100%	Zhao, Wang, Sun, Zhang (2011)
3	Dam (model)	Lab model	Concrete Core - soil, sand & gravel	1.5m	3.6m	ERT, OL	2 OL	2 (same zones as detected by other method)	100%	Zhao, Wang, Sun, Zhang (2011)
4	Dam (model)	Lab model	clay & gravel (core), sand (cover), gravel (embank)	1.5m	3.6m	ERT, OL	2 OL	2 (same zones as detected by other method)	100%	Zhao, Wang, Sun, Zhang (2011)
5	Dam Lake	Hama City, Syria	Syncline covered by continentals sediments	55m	2870m	ERT, OL	1 OL	1 (same zone as detected by other method)	100%	Al-Fares (2011)
6	Saddle dam #1	India	ohyllitic quartzites, quartzites, quartz-mica-schist	Not Reported	550m	ERT, SP, OL	3 SP (1 was confirmed by OL)	5 (3 zone are the same as detected by other methods)	100%	Panthulu, Krishnaiah, Shirke (2001)
7	Saddle dam #3	India	Micaceous schist & quartzites	19.5m	290m	ER, SP, PP	3 SP (1 flowpath was confirmed by PP)	4 (3 zone are the same as detected by other methods)	100%	Panthulu, Krishnaiah, Shirke (2001)
8	Earthfill Dam	California	Prosser Creek aluvium	34.5m	815m	ERT, OL	2 OL	2 (same zones as detected by other method)	100%	Bedrosian, Burton, Powers, Minsley, Phillips, Hunter (2012)
9	Homogeneous earth dam	Nigeria	Biotite gneiss beneath the reservoir and drainage basin	Not Reported	300m	ERT, SR	Lower seismic velosity zone btw dpth 4-12(m)	4 low ER zones btw dpth 4-8(m)	87%	Chii (2010)
10	zoned earth dam	Taiwan	med to coarse massive sandstone	90m	280m	ERT, OL	1 OL	2 (1 zone is the same as detected by other method)	100%	Lin, Hung, Yu,Wu (2013)
11	Dam site	South of France	site is composed by two basins separated by a dyke	7m	110m	ERT, SP, OL	1 SP (Confirmed by OL)	1 (same zone as detected by other method)	100%	Bolève, Janod, Revil, Lafon (2011)
12	Zoned embankment	Hallby, Sweden	Two (left & right) part dams - low permeable central core of till surronded by filter zones of sand on each side & coarse rockfill	30m	120 (R) 200 (L)	ERT, VI, PM, TM	0 (on right dam), 1 (on left dam) VI, PM, TM	3 (on right dam), 1 (on left dam, same zone as detected by other method)	100%	Sjödahl, Dahlin, Johansson, Loke (2008)
13	tephra barrier across outlet of a lake	New Zealand	7.6m of tephra in alternating unconsolidated layers of sand and silt sized material	Not Reported	Tephra barrier 8m above lake level	ERT, VI	1 VI (final collaps occurred at this location)	1 (same zone as detected by other method)	100%	Turner, Ingham, Bibby, Keys (2011)
14	Soil dam	Saudi Arabia	Alluvium deposits underlay by Wadi infill alluvium & highly fractured rock	Not Reported	Not Reporte	ERT, SR	2 SR	2 (same zones as detected by other method)	100%	Moustafa, Ibrahim, Elawadi, Metwaly, Al Agami,(2013)

Table B.1 (Continue) Summary of statistical analysis to evaluate accuracy of ERT method in seepage detection

No.	Type	Location	Material	Height	Length	Method	Anomaly Zones Detected by Other Methods (than ERT)	Anomaly Zones Detected by ERT	% precision of ERT	Reference
15	Embankment dam	South Korea	Not Reported	20m	300m	ERT, OL	2 OL	3 (2 zones are the same as detected by other methods)	100%	Kim, K., & Cho, I. (2011)
16	Embankment dam	Norway	Not Reported	5.5m	40m	ERT	4 Built-in flow paths in embankment	3 zones were detected, 1 zone missing	75%	Sjödahl, Dahlin, Johansson (2010)
17	Embankment dam	Taiwan	medium to coarse massive sandstones	90m	282m	ERT, PP	2 PP	2 (same zones as detected by other method)	100%	Lin, Hung, Yu, Wu (2013)
18	Homogeneous earth dam	Washington county, MO	Silty clay embankemnt with dolomite bedrock	10m	100m	ER, SP	1 SP	1 (same zone as detected by other method)	100%	Aal, Ismail, Anderson, Atekwana (2004)
19	homogeneous earth-fill dam	Colorado	Sandy clay and gravel	4m	427m	ERT, SP, SR, PP	1 SP & SR (confirmed by PP)	1 (same zone as detected by other methods)	100%	Ikard, Rittgers, Revil, Mooney (2014)
20	Dyke	India	Not Reported	3.65m		ERT, SR, OL	1 SR (confirmed by OL), 1 OL	3 (2 zones are the same as detected by other methods)	100%	Ramteke (2013)
21	tailing dam with core	southern Sweden	mixed fractions of crushed rock from the mining	27m	807m	ERT, VI	2 VI (2 sinkholes observed)	2 (same zones as detected by other method)	100%	Sjödahl, Dahlin, Johansson (2005)
22	Not Reported	China	Cenazoic sediments, diorite, limestone. karstic area beneath the dam	Not Reported	Not Reported	ERT, OL	2 OL	4 (3 zones are in the same area addressing 1 of the leakage zone, other zone is in the same area as detected by other methods)	100%	Di, Wang (2009)
								Averagre=	**98%**	

ERT: Electrical Resistivity Tomography
OL: Observed Leakage
SR: Seismic Reflection/Refraction
SP: Self-Potential
PP: Pizometer Pressure Measurement

TM: Temperature Measurement
VI: Visual Inspection

APPENDIX C

MATLAB SYNTAXES FOR Estimating THE FAILURE TIME OF THE STUDIED DAM, DUE TO INTERNAL EROSIOIN

In Appendix C, MATLAB programing syntaxes for estimating the failure time of the studied dam with two methods proposed by Bonelli and Benahmed, and Chen, Zhong and Cao are presented. Some parameters are estimated.

```
%Time of failure based on Bonelli and Benahmed method%

Tc = 13;              %Soil critical stress, Silty Sand (pa)%
L0=42.7;              %initial length of the pipe (m)%
Rho_s=1500;           %dry soil density (kg/m^3)%
Ie=3;                 %Fell erosion index (s/m)%
Ce=10^(-Ie);          %Fell coefficient of soil erosion)
Hdam=18.3;            %height of the dam (m)%
Hw=15.54;             %water level from the base (m)%
Rd=0.04;              %pipe radius at the time of detection (m)%
Rho_w=1000;           %water density (kg/m^3)%
g=9.8;                %gravity (m/s^2)%

Cl=L0/Hdam;
Lt=L0;      %current pipe length (m)%
delta_Pt=98333;       %average pressure drop (Pa)%
Rt=Rd;                %radius evolution of pipe (m)%
P0=Rd*delta_Pt/(2*Lt);  %driving pressure (Pa)%
ter=2*Rho_s*Lt/(Ce*delta_Pt);  %characteristing time of piping%

Ru=Hdam/2;            %maximum radius of piping before roof collapse (m)%
td=0;                 %time of detection (s)
tf=0;                 %time of failure (s);

 while Rt<Ru

     Rt=Rd*(Tc/P0+(1-Tc/P0)*exp(td/ter));
     P0=Rd*delta_Pt/(2*Lt);
     ter=2*Rho_s*Lt/(Ce*delta_Pt);
     tf=ter*log(Ru/Rd);

     Lt=Cl*(Hdam-Rt);
     delta_Pt=Rho_w*g*(Hw-Rt);

     td=td+1;

 end

     disp(tf/3600);
```

```
%Time of failure based on Chen and Zhang method%

theta=30;           %inclination angle of the seepage passage (degree)%
phi=32;             %inter-particle friction angle of silty sand soil (degree)%
C=1.80E4;           %Cohesion (N/m^2)%
d50=1.5E-3;         %median diameter of dam materials (m)%
gamma_s=1.47E4;         %specified weight of soil (N/m^3)%
gamma_w=9.80E3;         %specified weight of water (N/m^3)%
g=9.8;                  %gravity (m/s^2)%
mu=0.97;                %velocity coefficient%
h=15.5;                 %reservoir water elevation (m)%
Rd=0.04;                %initial radius of the seepage pipe (m)%
L=42.7;                 %length of seepage path (m)%
n=0.3;                  %porosity%
Hdam=18.3;              %height of the dam (m)%


v=mu*(2*g*h)^0.5;       %seepage velocity (m/s)%

vc=((40*g*d50*(gamma_s-gamma_w)*(tan(phi)*cos(theta)-
sin(theta))/(3*gamma_w*(tan(phi)*cos(theta)-
sin(theta)+4))+80*g*C/(gamma_w*(tan(phi)*cos(theta)-sin(theta)+4))^0.5;
                        %critical incipient velocity (m/s)%

Rt=Rd;                  %radius of pipe at time of t (m)%
t=0;                    %time (hr)%
delta_R=0;              %increment of seepage radius (m)%

while Rt<Hdam/2

        vf=(g*Rt*h/(2*L))^0.5;      %friction velocity (m/s)%

        Qs=0.5*pi/cos(theta)*Rt*vf*(v^2-vc^2)/(g*(gamma_s/gamms_w-1));
        %seepage erosion within seepage passage (m^3/s)%

        Qb=pi*Rt^2*mu*(2*g*h)^0.5;      %flux within seepage passage (m^3/s)%

        delta_R=t*Qs/(2*pi*Rt*L*(1-n));
        Rt=Rt+delta_R;
        t=t+0.02;
end;

disp( t)
```

REFERENCES

Aal, G. Z. A., Ismail, A. M., Anderson, N. L., & Atekwana, E. A. (2004). Geophysical Investigation of Seepage from an Earth Fill Dam, Washington County, MO. *Journal of Applied Geophysics*, *44*, 167-180.

Aitsebaomo, F. O., Adeyemi, O. A., & Quadri, H. A. (2013) Electromagnetic Survey of Erosion in Awba, Ibadan, Nigeria Embankment Dam. *International Journal Of Engineering And Science*, Vol.3, Issue 3, PP 01-05.

Al-Fares, W. (2011). Contribution of the geophysical methods in characterizing the water leakage in Afamia B dam, Syria. *Journal of Applied Geophysics, 75*(3), 464-471.

Artières, O., Beck, Y. L., Khan, A. A., Cunat, P., Fry, J. J., Courivaud, J. R., ... & Pinettes, P. (2010). Assessment of dams and dikes behavior with a fiber optics based monitoring solution. *Dam Maintenance and Rehabilitation II*, 79.

Bartholomew, C. L., Murray, B. C., & Goins, D. L. (1987). Embankment dam instrumentation manual. In *Embankment dam instrumentation manual*. Department of the Interior.

Beck, Y. L., Khan, A. A., Cunat, P., Guidoux, C., Artières, O., Mars, J., & Fry, J. J. (2010, September). Thermal monitoring of embankment dams by fiber optics. In *8th ICOLD European Club Symposium* (pp. 444-448).

Bedmar, A. P., & Araguás, L. A. (2002). Detection and prevention of leaks from dams. *CRC Press*.

Bedrosian, P. A., Burton, B. L., Powers, M. H., Minsley, B. J., Phillips, J. D., & Hunter, L. E. (2012). Geophysical investigations of geology and structure at the Martis Creek Dam, Truckee, California. *Journal of Applied Geophysics, 77*, 7-20.

Bolève, A., Vandemeulebrouck, J., & Grangeon, J. (2012). Dyke leakage localization and hydraulic permeability estimation through self-potential and hydro-acoustic measurements: Self-potential 'abacus' diagram for hydraulic permeability estimation and uncertainty computation. *Journal of Applied Geophysics, 86*, 17-28.

Bolève, A., Janod, F., Revil, A., Lafon, A., & Fry, J. (2011). Localization and quantification of leakages in dams using time-lapse self-potential measurements associated with salt tracer injection. *Journal of Hydrology, 403*(3-4), 242-252.

Bonelli, S., & Benahmed, N. (2011). Piping flow erosion in water retaining structures. *International Journal on Hydropower and Dams*, *18*(3), 94.

Brosten, T. R., Llopis, J. L., & Kelley, J. R. (2005). *Using geophysics to assess the condition of small embankment dams*. Vicksburg, MS: US Army Corps of Engineers, Engineer Research and Development Center, Geotechnical and Structures Laboratory.

Bureau of Reclamation (1988) *Training aids for dam safety: Module, instrumentation for embankment and concrete dams*. Denver, CO.

Cardarelli, E., Cercato, M., & Donno, G. D. (2014). Characterization of an earth-filled dam through the combined use of electrical resistivity tomography, P- and SH-wave seismic tomography and surface wave data. *Journal of Applied Geophysics, 106*, 87-95.

Cardimona, S. (2002). Electrical resistivity techniques for subsurface investigation. *Department of Geophysics, university of Missouri Rolla-Mo*.

Chen, S., Zhong, Q., & Cao, W. (2012, 04). Breach mechanism and numerical simulation for seepage failure of earth-rock dams. *Science China Technological Sciences, 55*(6), 1757-1764.

Chii, C. E. (2010). An Integrated Two-Dimensional Geophysical Investigation of an Earth Dam in Zaria Area Nigeria. *Nature and Science, 8*(10), 358-368.

Contreras, I. A., & Hernández, S. H. *Techniques for prevention and detection of leakage in dams and reservoirs.* Retrieved on 09.15.2013 from http://ussdams.com/proceedings/2010Proc/785-814.pdf

Dahlin, T. (2001). The development of DC resistivity imaging techniques. *Computers & Geosciences, 27*(9), 1019-1029.

Di, Q., & Wang, M. (2009). Determining areas of leakage in the Da Ye Dam using multi-electrode resistivity. *Bulletin of Engineering Geology and the Environment, 69*(1), 105-109.

FEMA (2003), *The National Dam Safety Program. Research Needs Workshop:*
Seepage through Embankment Dams. Federal Emergency Management Agency. Workshop was held on October 17-19, 2000, Denver, Colorado.

Foster, M., Spannagle, M., & Fell, R. (1998). *Analysis of embankment dam incidents*. Sydney: University of New South Wales, School of Civil Engineering.

Foster, M., Fell, R., & Spannagle, M. (2000). The statistics of embankment dam failures and accidents. *Canadian Geotechnical Journal, 37*(5), 1000-1024.

Froehlich, D. C. (1987). Embankment-dam breach parameters. In *Hydraulic Engineering, Proceedings of the 1987 National Conference.* (pp. 570-575).

Goodarzi, E., Shui, L. T., Ziaei, M., & Haghizadeh, A. (2010). Estimating probability of failure due to internal erosion with event tree analysis. *European Journal of Geotechnical Engineering*, 935-948.

Habel, W. R., & Krebber, K. (2011). Fiber-optic sensor applications in civil and geotechnical engineering. *Photonic Sensors, 1*(3), 268-280.

Haile, T., & Atsbaha, S. (2014). Electrical resistivity tomography, VES and magnetic surveys for dam site characterization, Wukro, Northern Ethiopia. *Journal of African Earth Sciences, 97*, 67-77.

Henault, J., Moreau, G., Blairon, S., Salin, J., Courivaud, J., Taillade, F., Delepine-Lesoille, S. (2010). Truly Distributed Optical Fiber Sensors for Structural Health Monitoring: From the Telecommunication Optical Fiber Drawling Tower to Water Leakage Detection in Dikes and Concrete Structure Strain Monitoring. *Advances in Civil Engineering, 2010*, 1-13.

Herman, R. (2001). An introduction to electrical resistivity in geophysics. *American Journal of Physics, 69*(9), 943-952.

Herrmann, A. W. (2013). ASCE 2013 Report Card for America's Infrastructure. *IABSE Symposium Report, 99*(33), 9-10.

Hoepffner, R., Singer, J., Thuro, K., & Aufleger, M. (2008). Development of an integral system for dam and landslide monitoring based on distributed fiber optic technology. *Ensuring Reservoir Safety into the Future*, 177-189.

ICODS (2015). Evaluation and Monitoring of Seepage and Internal Erosion. *FEMA P-1032*. Federal Emergency Management Agency.

ICOLD (1995), Dam Failures – Statistical Analysis. Ruptures de barrages – Analyse statistique, Paris, *ICOLD/CIGB.*

Ikard, S., Rittgers, J., Revil, A., & Mooney, M. (2014). Geophysical Investigation of Seepage beneath an Earthen Dam. *Groundwater, 53*(2), 238-250.

Ikard, S. J., Revil, A., Schmutz, M., Karaoulis, M., Jardani, A., & Mooney, M. (2013). Characterization of Focused Seepage through an Earthfill Dam Using Geoelectrical Methods. *Groundwater, 52*(6), 952-965.

Johansson, S. (1997). *Seepage monitoring in embankment dams* (Doctoral dissertation, Institutionen för anläggning och miljö). ISBN: 91-7170-792-1

Lagmanson, M. (2005). *Electrical Resistivity Imaging.* Retrieved February 17, 2015, from https://quicksilver.epa.gov/work/HQ/175896.pdf

Li, X., & Tsai, F. T. (2009). Bayesian model averaging for groundwater head prediction and uncertainty analysis using multimodel and multimethod. *Water Resources Research, 45*(9).

Li, D.Q., Yan, L.L., and Shao, D.G. (2007). Reliability evaluation of embankment dams using Bayesian network. *Engineering Journal of Wuhan University, 40*(6): 24–29.

Lin, C. P., Hung, Y. C., Yu, Z. H., & Wu, P. L. (2013). Investigation of abnormal seepages in an earth dam using resistivity tomography. *Journal of GeoEngineering*, *8*(2), 61-70.

Lum, K. Y., & Sheffer, M. R. (2005). Dam safety: Review of geophysical methods to detect seepage and internal erosion in embankment dams. *Hydro-Review*, *29*.

MacDonald, T. C., & Langridge-Monopolis, J. (1984). Breaching characteristics of dam failures. *Journal of Hydraulic Engineering*, *110*(5), 567-586.

Mirosław-Świątek, D., Kembłowski, M., & Jankowski, W. (2012). Application of the Bayesian Belief Nets in dam safety monitoring. *Annals of Warsaw University of Life Sciences - SGGW. Land Reclamation, 44*(1).

Moore, J. R., Boleve, A., Sanders, J. W., & Glaser, S. D. (2011). Self-potential investigation of moraine dam seepage. *Journal of Applied Geophysics*, *74*(4), 277-286.

Morris, M. (2009). *Breaching processes: A state of the art review*. HR Wallingford.

Moustafa, S. S., Ibrahim, E. H., Elawadi, E., Metwaly, M., & Al Agami, N. (2013). Seismic refraction and resistivity imaging for assessment of groundwater seepage under a Dam site, Southwest of Saudi Arabia. *International Journal of Physical Sciences*, *7*(48), 6230-6239.

Osazuwa, I., & Chinedu, A. (2008). Seismic refraction tomography imaging of high-permeability zones beneath an earthen dam, in Zaria area, Nigeria. *Journal of Applied Geophysics*, *66*(1-2), 44-58.

Panthulu, T., Krishnaiah, C., & Shirke, J. (2001). Detection of seepage paths in earth dams using self-potential and electrical resistivity methods. *Engineering Geology, 59*(3-4), 281-295.

Perzlmaier, S., Aufleger, M., & Donstadter, J. (2007). Active and passive defences against internal erosion in assessment of the risk insternal erosion of water retaining structures: dams, dykes and levees. *Intermediate report of the European Working Group in Internal Erosion of ICOLD* (pp. 194-207).

Peyras, L., Royet, P., & Boissier, D. (2006). Dam ageing diagnosis and risk analysis: Development of methods to support expert judgment. *Canadian Geotechnical Journal, 43*(2), 169-186.

Radzicki, K. (2014). The thermal monitoring method–a quality change in the monitoring of seepage and erosion processes in dikes and earth dams. *Modern monitoring solutions of dams and dikes*, 33-41.

Ramteke, R.S. (2013). Geophysical investigations for solving seepage problems. *Journal of Indian Geophysical Union, 17*(2), 187-194.

Reddi, L. N., & Bonala, M. V. (1998). *Filtration and drainage in geotechnical/geoenvironmental engineering: Proceedings of sessions of Geo-Congress 98*. Reston, VA: American Society of Civil Engineers.

Richards, K. S., & Reddy, K. R. (2007). Critical appraisal of piping phenomena in earth dams. *Bulletin of Engineering Geology and the Environment, 66*(4), 381-402.

Rinehart, R. V., Parekh, M. L., Rittgers, J. B., Mooney, M. A., & Revil, A. (2012, February). Preliminary implementation of geophysical techniques to monitor embankment dam filter cracking at the laboratory scale. In *Proceedings of the 6th Annual International Conference on Software Engineering (ICSE)*.

Sakti, S. (2009). *Incorporating knowledge sources into statistical speech recognition*. New York: Springer.

Samouëlian, A., Cousin, I., Tabbagh, A., Bruand, A., & Richard, G. (2005). Electrical resistivity survey in soil science: A review. *Soil and Tillage Research, 83*(2), 173-193.

Schrott, L., & Sass, O. (2008). Application of field geophysics in geomorphology: Advances and limitations exemplified by case studies. *Geomorphology, 93*(1-2), 55-73.

Sjödahl, P., Dahlin, T., Johansson, S., & Loke, M. (2008). Resistivity monitoring for leakage and internal erosion detection at Hällby embankment dam. *Journal of Applied Geophysics, 65*(3-4), 155-164.

Sjödahl, P., Dahlin, T., & Johansson, S. (2005). Using resistivity measurements for dam safety evaluation at Enemossen tailings dam in southern Sweden. *Environmental Geology, 49*(2), 267-273.

Sjödahl, P., Dahlin, T., & Johansson, S. (2010). Using the resistivity method for leakage detection in a blind test at the Røssvatn embankment dam test facility in Norway. *Bulletin of Engineering Geology and the Environment, 69*(4), 643-658.

Smith, M. (2006). *Dam risk analysis using Bayesian networks*. ECI Conference on Geohazards. Engineering Conferences International (ECI), New York.

Tanajewski, D., & Bakuła, M. (2016). Application of Ground Penetrating Radar Surveys and GPS Surveys for Monitoring the Condition of Levees and Dykes. *Acta Geophysica, 64*(4).

Turner, G., Ingham, M., Bibby, H., & Keys, H. (2011). Resistivity monitoring of the tephra barrier at Crater Lake, Mount Ruapehu, New Zealand. *Journal of Applied Geophysics, 73*(3), 243-250.

USBR (1983). *Safety evaluation of existing dams: A manual for the safety evaluation of embankment and concrete dams*. Denver, CO: U.S. Bureau of Reclamation.

USBR (2011), *Reclamation Managing Water in the West.* Design Standards No. 13, Embankment dams, Chapter 8: Seepage. U.S. Bureau of Reclamation.

Xu, Y., Zhang, L., & Jia, J. (2011). Diagnosis of embankment dam distresses using Bayesian networks. Part II. Diagnosis of a specific distressed dam. *Canadian Geotechnical Journal, 48*(11), 1645-1657.

Zhang, L., Xu, Y., Jia, J., & Zhao, C. (2011). Diagnosis of embankment dam distresses using Bayesian networks. Part I. Global-level characteristics based on a dam distress database. *Canadian Geotechnical Journal, 48*(11), 1630-1644.

Zhao, M., Wang, H., Sun, X., & Zhang, Y. (2011). Comparison between the Isotope Tracking Method and Resistivity Tomography of Earth Rock-Fill Dam Seepage Detection. *Engineering, 03*(04), 389-399.

Zhu, P., Leng, Y., Dhillon, B. S., & Bin, G. (2008). Reliability Analysis of a Seepage Monitoring System Based on Distributed Optical Fiber Sensing. *2008 International Conference on Intelligent Computation Technology and Automation (ICICTA)*.